An Investigation Into the Significance of Dissipation in Statistical Mechanics

A thesis submitted for the degree of Doctor of Philosophy of
The Australian National University

November 2016

Charlotte Frances Petersen

Research School of Chemistry
Australian National University

Statement of Originality

I hereby declare that this submission is my own work. To the best of my knowledge and belief this thesis contains no material previously published or written by another person, except where due acknowledgement has been made in the text of the thesis. This work has not been submitted previously, in whole or in part, to qualify for any other academic award.

....

Charlotte Petersen Date

Acknowledgements

First I would like to thank my supervisors Dr Stephen Williams and Prof Denis Evans, without who this work would of course not have been possible. Your support, guidance and enthusiasm was greatly appreciated. You both exposed me to so much science outside of my own project.

I would also like to thank Prof Debra Searles and the other members of her group for the many interesting discussions.

Thanks to those who have helped me through this PhD, including the RSC community, particularly those always ready for a chat over tea. Thanks must go to the rest of the computational chemistry groups for taking an interest in my work. I would like to thank the friends who helped to proof read this thesis, Caitlin, Giles and Michael.

Finally, I would like to thank all of my friends and family, who have supported me through many years of study. In particular, my parents for their continued love and support and Michael, for constant encouragement and belief in me.

Abstract

The dissipation function is a key quantity in nonequilibrium statistical mechanics. It was originally derived for use in the Evans-Searles Fluctuation Theorem, which quantitatively describes thermal fluctuations in nonequilibrium systems. It is now the subject of a number of other exact results, including the Dissipation Theorem, describing the evolution of a system in time, and the Relaxation Theorem, proving the ubiquitous phenomena of relaxation to equilibrium. The aim of this work is to study the significance of the dissipation function, and examine a number of exact results for which it is the argument.

First, we investigate a simple system relaxing towards equilibrium, and use this as a medium to investigate the role of the dissipation function in relaxation. The initial system has a non-uniform density distribution. We demonstrate some of the existing significant exact results in nonequilibrium statistical mechanics. By modifying the initial conditions of our system we are able to observe both monotonic and non-monotonic relaxation towards equilibrium.

A direct result of the Evans-Searles Fluctuation Theorem is the Nonequilibrium Partition Identity (NPI), an ensemble average involving the dissipation function. While the derivation is straightforward, calculation of this quantity is anything but. The statistics of the average are difficult to work with because its value is extremely dependent on rare events. It is often observed to converge with high accuracy to a value less than expected. We investigate the mechanism for this asymmetric bias and provide alternatives to calculating the full ensemble average that display better statistics. While the NPI is derived exactly for transient systems it is expected that it will hold in steady state systems as well. We show that this is not true, regardless of the statistics of the calculation.

A new exact result involving the dissipation function, the Instantaneous Fluctuation Theorem, is derived and demonstrated computationally. This new theorem has the same form as previous fluctuation theorems, but provides information about the instantaneous value of phase functions, rather than path integrals. We extend this work by deriving an approximate form of the theorem for steady state systems, and examine the validity of the assumptions used.

Contents

Nomenclature

$\Omega_{ss,t}$	Integrated steady state dissipation function
$\bar{\Omega}_{ss,t}$	Time averaged steady state dissipation function
α	Thermostat multiplier
CDF	Cumulative Distribution Function
DFT	Discrete Fourier Transform
ES-FT	Evans Searles Fluctuation Theorem
$\mathbf{F}$	Force
$f(\mathbf{\Gamma})$	Phase space density
S^t	Time evolution operator
FCC	Face-Centered Cubic
FT	Fluctuation Theorem
$\dot{\gamma}$	Strain rate
Γ	Phase space position
JE	Jarzynski Equality
k_B	Boltzmann's constant
KE	Kinetic Energy
Λ	Phase space expansion factor
LHS	Left Hand Side
m	Particle mass
M^T	Time reversal map
NPI	Nonequilibrium Partition Identity
$\Omega(\mathbf{\Gamma})$	Instantaneous dissipation function

$\bar{\Omega}_t$	Time averaged dissipation function
$\Omega_t(\mathbf{\Gamma})$	Integrated dissipation function
p	Probability
Pr	Probability distribution
$\mathbf{p}$	Momentum
$\mathbf{q}$	Position
Φ	Potential
RHS	Right Hand Side
T	Temperature
Θ	Heaviside step function
WCA	Weeks-Chandler-Andersen
x	x component of position
y	y component of position

Chapter 1

Introduction

The Second Law of Thermodynamics predicts irreversible macroscopic behaviour. However, Newton's equations of motion, describing the behaviour of individual particles, are time reversible. If a trajectory satisfies the equations of motion, then the antitrajectory, where all of the momenta are reversed, also satisfies the equations of motion. If you run a movie of particles in motion backwards, the dynamics would still satisfy Newton's equations. In contrast, by observing the motion of particles you can often tell which direction time is running. For example, it is obvious if time is running backwards when observing a game of snooker. The question of how macroscopic irreversibility is derived from reversible microscopic behaviour was unsolved for over 100 years, and is referred to as Loschmidt's Paradox[1, 2].

Statistical mechanics is used to understand macroscopic behaviour from microscopic equations of motion. It considers ensembles, where every ensemble member has a different microstate, but the same macrostate. The microstate is determined by the position and momentum of each particle in the system, while the macrostate is given by parameters such as the temperature, energy, pressure or volume of the system. The time reversible equations of motion are then used to study the evolution of each of the ensemble members, and the average behaviour of the ensemble can give us macroscopically relevant information.

Boltzmann's H-theorem was an attempt at proving the Second Law of Thermodynamics using statistical mechanics[3]. However, Loschmidt objected to the derivation on the grounds that if a phase space trajectory satisfies the equations of motion, then its antitrajectory must also satisfy the equations of motion. "Apparently, if the instantaneous velocities of all the elements of any given system are reversed, the total course of the incidents must generally be reversed for each given system"[1, 4]. So, if the initial phase space distribution is even in the momenta, the Boltzmann H-function could not decrease monotonically as required by Boltzmann's H-theorem[4].

This problem has been avoided in the past by noting that the Second Law of Thermodynamics is only applicable in the large system size limit. Boltzmann stated that "as soon as one looks at bodies of such small dimension that they contain only a few molecules, the validity of this theorem [the Second Law of Thermodynamics] must cease"[5, 6]. Maxwell also commented on the range of applicability of the Second Law of Thermodynamics. "Hence the second law of thermodynamics is continually being violated and that to a considerable

extent in any sufficiently small group of molecules belonging to any real body. As the number of molecules in the group is increased, the deviations from the mean of the whole become smaller and less frequent; and when the number is increased till the group includes a sensible portion of the body, the probability of a measurable variation from the mean occurring in a finite number of years becomes so small that it may be regarded as practically an impossibility"[7, 8, 9].

The derivation of the Evans-Searles Fluctuation Theorem (ES-FT) resolves Loschmidt's Paradox by describing how irreversibility develops in a system governed by time-reversible equations of motion. It explicitly considers bundles of trajectories and their conjugate antitrajectory bundles[10]. Seemingly contrary to Loschmidt's objection, the existence of antitrajectories is essential to the derivation of time irreversible behaviour, however it is necessary to consider the probability of these conjugate trajectory bundles, rather than merely their existence. The paradox of time reversible equations of motion leading to time irreversible behaviour is resolved by assuming causality, events in the future are caused by events in the past, rather than the other way around. This breaks the time symmetry of the system. The Evans-Searles Fluctuation Theorem describes how a system can be reversible for short observation times, but can become irreversible for longer times[10]. This irreversibility grows with the observation time and system size.

The ES-FT is an exact result in nonequilibrium statistical mechanics, giving quantitative information about a system[11, 4, 12]. It gives the probability of particular fluctuations in a system, determined by the value of the dissipation function, a quantity defined for use in the ES-FT. The theorem quantifies the probability of Second Law violating trajectories. As the observation time increases, fluctuations in one direction become overwhelmingly more probable, and irreversible behaviour is recovered. This theorem has been demonstrated in computer simulations[13, 14] and experiments[15, 16].

The argument of the ES-FT is the dissipation function. This is, in general, a dimensionless dissipated energy[10]. It was derived to simplify the Evans-Searles Fluctuation Theorem and it takes the form of a path integral, that is, it is a function of the path a given trajectory takes through phase space. The dissipation function can be thought of as a measure of the irreversibility of a trajectory. The ES-FT gives the probability of the dissipation function taking on opposite values. The dissipation function is odd under time reversal, so the value of the dissipation function for a trajectory is the negative of its value for the corresponding antitrajectory. Thus, the fluctuation theorem gives the probability of particular sets of trajectories relative to the probability of their antitrajectories.

In addition to the Evans-Searles Fluctuation Theorem the dissipation function is the argument of a number of more recent exact results in nonequilibrium statistical mechanics. Derived directly from the ES-FT, the Second Law Inequality makes the irreversible behaviour expected explicit[12]. Another result, the Dissipation Theorem describes how a system will evolve with time[17, 18]. It gives the time evolving distribution of the system and the time evolving average of arbitrary phase functions, in terms of the dissipation function. This shows how the dissipation function plays a central role in nonlinear response theory. One of the most significant results involving the dissipation function is the proof of relaxation to equilibrium in systems satisfying a number of reasonable constraints. This is known as the

Relaxation Theorem[19, 20], and provides the form of the equilibrium distribution, as well as proving that this distribution is the unique dissipationless time-independent state. Any other distribution relaxes to the equilibrium distribution.

The prominence of the dissipation function in all of these important results demonstrates its significance to nonequilibrium statistical mechanics. The primary purpose of this thesis is to examine the role of the dissipation function in these exact results. We will do this using theoretical and computational methods.

We will start by applying the most significant results involving the dissipation function to a system relaxing towards equilibrium. We use a system relaxing from a non-uniform density distribution initially, which is simple to study because no field is applied during the relaxation. As well as using the dissipation function to monitor the relaxation, we can also study it intuitively by following the density distribution function. Both monotonic and non-monotonic relaxation will be investigated.

We will then move onto another exact result involving the dissipation function, which has been more problematic to demonstrate in simulation and experiment. This result is known as the Nonequilibrium Partition Identity (NPI), and is derived directly from the ES-FT[21]. A range of approaches are used to investigate the difficulty in calculating this exact result. We extend this work to the less studied steady state NPI, where we begin by using similar approaches to determine its value.

Finally, we introduce a new exact result in nonequilibrium statistical mechanics, which has the dissipation function as its argument. This Instantaneous Fluctuation Theorem provides different information to previous fluctuation relations. We also derive an approximate steady state form, and investigate its validity.

Chapter 2

Theoretical Background: The Dissipation Function

The dissipation function is relevant to nonequilibrium systems, and is the measure of the irreversibility of a process. It was defined to simplify the Evans-Searles Fluctuation Theorem, which will be discussed in this chapter when we give the definition of the dissipation function. While being defined for use in this specific theorem, it appears in many other exact results for nonequilibrium systems, such as the Dissipation Theorem, the Relaxation Theorem and the Second Law Inequality. It is central to the modern study of nonequilibrium statistical mechanics.

2.1 Equilibrium Ensemble

A fundamental concept in statistical mechanics is that of an ensemble[22], first conceived by Boltzmann[23] and described succinctly by Maxwell. "I have found it convenient, instead of considering one system of material particles, to consider a large number of systems similar to each other in all respects, except the initial circumstances of the motion, which are supposed to vary from system to system, the total energy being the same in all"[7]. That is, a set of systems which all share the same macrostate, but have different microstates. The macrostate is typically specified through the values of the temperature or the energy, the pressure or the volume, and the number of particles or the chemical potential. In this thesis we will only consider systems with a fixed volume and number of particles. For each macrostate there are many possible microstates. Each of these can be specified at a given time by their phase space position, that is, the position and momenta of every particle. Each microstate in an ensemble is referred to as an ensemble member. A system is a set of initial microstates, defined by some macrostate.

Feynman defined equilibrium as the state where “all the fast things have happened but the slow things have not”[24]. There are no macroscopic changes in the system and there are no net macroscopic flows of energy or matter. A system with no applied external forces will spontaneously relax towards equilibrium. Equilibrium can be defined as a state preserved

by the dynamics, in which trajectories and their antitrajectories are equally likely to occur. However, the study of relaxation to this state is difficult, and is clearly not possible for systems with deterministic equations of motion (since if the system was initially out of equilibrium, it will always return to that state under time reversal). For the purpose of this thesis we will define equilibrium as the point when the measured properties of the system have ceased to change.

If the equilibrium system is isolated, such that the energy of the system is fixed, it is said to be in a microcanonical distribution. All possible microstates in this distribution have the same probability. Alternatively, the equilibrium system may be in contact with a heat bath, such that the temperature of the system is fixed. The heat bath is a reservoir much larger than the system of interest, such that the system of interest does not change the temperature of the heat bath. It adds or removes heat from the system, so that the temperature may be kept constant. This equilibrium distribution is called a canonical ensemble, and is described by the Boltzmann distribution[25]. The probability of a particular microstate in this distribution is determined from its energy,

$$f(\mathbf{\Gamma}) = \frac{e^{-\frac{H(\mathbf{\Gamma})}{k_B T}}}{\int d\mathbf{\Gamma} e^{-\frac{H(\mathbf{\Gamma})}{k_B T}}} \tag{2.1}$$

where $\mathbf{\Gamma}$ is the phase space position specifying all momenta and positions of every particle, $f(\mathbf{\Gamma})$ is the phase space density, $H(\mathbf{\Gamma})$ is the energy of state $\mathbf{\Gamma}$, k_B is Boltzmann's constant and T is the temperature of the system.

We can relate the temperature to the kinetic energy, KE, using the Equipartition Theorem. It is the idea that in equilibrium, energy is distributed equally among all degrees of freedom[25]. For an ideal gas there are no configurational components, so it predicts that the kinetic energy of each particle is given by $3k_BT/2$, meaning that the total kinetic energy is given by

$$KE = \sum_{i}^{N} \frac{1}{2m} \mathbf{p}_i \cdot \mathbf{p}_i = \frac{3N}{2} k_B T \tag{2.2}$$

where $\mathbf{p}_i$ is the momentum of particle i and m is the particle mass. This is for a three dimensional system. For systems that do not contain polyatomic particles this is a suitable equation for the kinetic temperature.

The ergodic hypothesis, postulated by Boltzmann, states that ensemble averages in the system are equal to time averages[26]. In an ergodic system, a trajectory starting anywhere in the distribution samples all of phase space in the distribution. It does not become trapped in some sub-region of phase space. This is a useful property for computer simulations, where analysis based on ensemble averages is often applied to data obtained from time averages. It is also a necessary condition used in the derivation of many of the exact results we will discuss.

2.2 Equations of Motion and Thermostats

In this thesis we will restrict our studies to a deterministic classical mechanical description. A microstate, or position in phase space, uniquely determines the path the system will take from that point as it evolves with time. This path is called a trajectory, and is made up of the phase space position of every point along this path. The trajectory is determined by propagating the initial phase space position forward in time using Newton's equations of motion,

$$\begin{aligned} \dot{\mathbf{q}}_i &= \frac{\mathbf{p}_i}{m}, \\ \dot{\mathbf{p}}_i &= -\frac{\partial \Phi}{\partial \mathbf{q}_i} \equiv \mathbf{F}_i \end{aligned} \tag{2.3}$$

where $\mathbf{q}_i$ is the position of each particle i, $\mathbf{p}_i$ is the momentum, Φ is the potential and $\mathbf{F}_i$ is the force on each particle. This is due to the interparticle forces. If the system with these equations of motion satisfies the conditions of ergodicity and temporal correlation decay, it will relax to the microcanonical distribution in equilibrium[19].

These equations of motion are time reversible. If the equations of motion are applied to a particular point in phase space, $\mathbf{\Gamma}$ for a time t, a new point in phase space, $S^t\mathbf{\Gamma}$ is reached. S^t is the time evolution operator. Time reversibility means that a mapping exists such that if it is applied to $S^t\mathbf{\Gamma}$, and we then run the equations of motion forwards for a time t, the map of the original phase space position is reached. That is, $S^t M^T S^t \mathbf{\Gamma} = M^T \mathbf{\Gamma}$, where M^T is the time reversal map. For Newton's equations of motion this time reversal map is simply reversing all the momenta of the system, $M^T(\mathbf{q}, \mathbf{p}) = (\mathbf{q}, -\mathbf{p})$. This procedure is equivalent to running the equations of motion backwards in time from the point $S^t\mathbf{\Gamma}$.

We can design equations of motion that keep the system at a constant temperature using a mathematical formalism called a thermostat[27]. This acts like a heat bath in the system, but is unphysical. However, the equations of motion are time reversible.

$$\begin{aligned} \dot{\mathbf{q}}_i &= \frac{\mathbf{p}_i}{m}, \\ \dot{\mathbf{p}}_i &= \mathbf{F}_i - \alpha S_i \mathbf{p}_i \end{aligned} \tag{2.4}$$

where α is the thermostat multiplier and S_i is the switch which controls whether the thermostat is turned on for each particle. This allows the artificial thermostat to be placed a long distance from the system of interest. So, $S_i = 0$ except when particle i is in the reservoir, then $S_i = 1$. Since the system of interest is physically separated from the details of the thermostatting mechanism its artificial nature is irrelevant[28]. However, it has been observed that separating the thermostated particles from the system of interest is not necessary for most applications relevant to this thesis[29]. In this thesis we shall apply the thermostat to all particles, so S_i is always equal to unity.

The thermostat multiplier is determined by the constants of the system. In this thesis we will use an isokinetic thermostat[30], where the form of the thermostat multiplier is derived

to keep the kinetic energy of the system constant. The kinetic energy is given by

$$KE = \sum_i^N \frac{1}{2m} \mathbf{p}_i \cdot \mathbf{p}_i. \tag{2.5}$$

Let us say

$$K_i = \frac{1}{2m} \mathbf{p}_i \cdot \mathbf{p}_i. \tag{2.6}$$

Now, the change in the kinetic energy is given by

$$\frac{\partial KE}{\partial t} = \sum_i^N \frac{\partial \mathbf{p}_i}{\partial t} \cdot \frac{\partial K_i}{\partial \mathbf{p}_i} \tag{2.7}$$

$$= \sum_i^N \dot{\mathbf{p}}_i \cdot \frac{\mathbf{p}_i}{m}. \tag{2.8}$$

Using the equations of motion we have

$$\frac{\partial KE}{\partial t} = \sum_i^N (\mathbf{F}_i - \alpha \mathbf{p}_i) \cdot \frac{\mathbf{p}_i}{m}. \tag{2.9}$$

For the kinetic energy to be constant, the derivative will be zero. This gives us

$$\alpha = \frac{\sum_i^N \mathbf{F}_i \cdot \mathbf{p}_i}{\sum_i^N \mathbf{p}_i \cdot \mathbf{p}_i} \tag{2.10}$$

as the form of the thermostat multiplier. The equations of motion will now keep the kinetic temperature of the system constant[27].

2.3 Nonequilibrium Systems

The dissipation function must be studied in nonequilibrium systems, since it is zero in equilibrium[19]. A nonequilibrium system could be generated by starting a system in some nonequilibrium distribution, and allowing it to relax. In this case the equations of motion would be the same as above, given by Eq. (2.3) for an isoenergetic system, or in Eq. (2.4) for an isokinetic system.

Another method to generate a nonequilibrium system is to apply an external field. A system in contact with a heat bath, but subject to an external force can be described by the equations of motion

$$\dot{\mathbf{q}}_i = \frac{\mathbf{p}_i}{m} + \mathbf{C}_i \cdot \mathbf{F}_e, \tag{2.11}$$

$$\dot{\mathbf{p}}_i = \mathbf{F}_i + \mathbf{D}_i \cdot \mathbf{F}_e - \alpha S_i \mathbf{p}_i \tag{2.12}$$

where $\mathbf{F}_e$ is the external force and $\mathbf{C}_i$ and $\mathbf{D}_i$ determine how it couples to the position and momenta equations of motion respectively. This system will not approach an equilibrium. If the thermostat was not applied, and the external field adds energy to the system, it would

heat up without bound. Applying a thermostat to this system will allow it to approach a steady state. The thermostat removes heat from the system that is added by the external field. Steady states are some of the easiest nonequilibrium systems to study experimentally because they are constant in time.

There are many possible driven nonequilibrium systems to chose from. For convenience we will choose ones that can be easily modeled theoretically and computationally. Details of these systems are given below.

2.3.1 Couette Flow

Planar couette flow is a physically realistic and computationally convenient system to study. This system can be thought of as a fluid sheared between two plates, where we are only concerned with the fluid in the interior of the system, far from the plates. It corresponds to how the shear viscosity is measured in a rheometer. In the simulation of the system, there are no walls, the shearing occurs in an infinite system. The shear flow can be described with SLLOD equations of motion[27]. These equations of motion apply a gradient in the x-velocities of the particles, dependent on their y-position in the system, and is equivalent to boundary driven flow[31]. They effectively allow us to rewrite a boundary condition into the equations of motion, as if it was an external field. The infinite shearing is facilitated with periodic boundary conditions that shear with the system. These are discussed further in Section 3.1.5.1.

The SLLOD equations of motion for couette flow are given by

$$\dot{\mathbf{q}}_i = \frac{\mathbf{p}_i}{m} + \mathbf{i}\dot{\gamma}\Theta(t)y_i, \tag{2.13}$$

$$\dot{\mathbf{p}}_i = \mathbf{F}_i - \mathbf{i}\dot{\gamma}\Theta(t)p_{yi} - \alpha\mathbf{p}_i \tag{2.14}$$

where $\dot{\gamma}$ is the strain rate applied to the system, y_i is the y-component of the position of the i-th particle and p_{yi} is the y-component of the momenta of that particle. $\Theta(t)$ is the Heaviside step function, used to turn the shear on at time $t = 0$. These equations of motion are equivalent to

$$\ddot{\mathbf{q}}_i = \frac{\mathbf{F}_i}{m} + \mathbf{i}\dot{\gamma}\delta(t)y_i - \alpha(\dot{\mathbf{q}}_i - \mathbf{i}\dot{\gamma}y_i) \tag{2.15}$$

where $\delta(t)$ is the Dirac-delta function. This shows that the SLLOD equations of motion are equivalent to an initial condition on the acceleration of the particles depending on their y position.

We will use an isokinetic thermostat with this system. Its form is derived in the same way as the field free case above, by setting the change in the kinetic energy with time to zero,

$$\frac{\partial KE}{\partial t} = \sum_i^N \dot{\mathbf{p}}_i \cdot \frac{\mathbf{p}_i}{m} = 0. \tag{2.16}$$

Using the SLLOD equations of motion gives us a thermostat multiplier of

$$\alpha = \frac{\sum_i^N \mathbf{F}_i \cdot \mathbf{p}_i}{\sum_i^N \mathbf{p}_i \cdot \mathbf{p}_i} - \frac{\dot{\gamma} \sum_i^N p_{yi} p_{xi}}{\sum_i^N \mathbf{p}_i \cdot \mathbf{p}_i} \tag{2.17}$$

once the shear has been turned on. Before time $t = 0$ the thermostat multiplier is the same as for the field free equations of motion.

2.3.2 Colour Conductivity

Another possible method to perturb a system from equilibrium, in a way that is easy to study, is to apply a colour field to the system[27]. That is, a perturbation to the potential in the equations of motion of the particles. This acts like an external force applied to the system, where the force is the derivative of the potential perturbation. Each particle is assigned to one of two colours such that there are an equal number of particles of each colour. The potential perturbation for each colour is the same magnitude, applied in the opposite direction. This can be represented in the equations of motion as

$$\dot{\mathbf{q}}_i = \frac{\mathbf{p}_i}{m}, \tag{2.18}$$

$$\dot{\mathbf{p}}_i = \mathbf{F}_i + c_i \mathbf{F}_e - \alpha \mathbf{p}_i \tag{2.19}$$

where $\mathbf{F}_e$ is the colour field and $c_i = (-1)^i$ is the colour label. The colour field has no effect on interparticle interactions. This system is similar to an electric field applied to charged particles, as done in an electrophoresis experiment, except that the particles interact with each other as if they are uncharged. This removes the need to model long range interactions, making this system possible to study computationally with periodic boundary conditions and a small number of particles. The force from the colour field, $\mathbf{F}_e$, may be position dependent.

We will consider an isokinetic system, so the thermostat multiplier is derived to keep the kinetic energy constant. Its form will depend on the exact form of the colour field applied. Derived in the same way as above we have

$$\alpha = \frac{\sum_i^N \mathbf{F}_i \cdot \mathbf{p}_i}{\sum_i^N \mathbf{p}_i \cdot \mathbf{p}_i} + \frac{\sum_i^N c_i \mathbf{F}_e \cdot \mathbf{p}_i}{\sum_i^N \mathbf{p}_i \cdot \mathbf{p}_i}. \tag{2.20}$$

2.4 The Fluctuation Theorem

The Evans Searles Fluctuation Theorem[11, 4, 12] allows us to calculate quantitative information about a nonequilibrium system. It gives the probability of Second Law violating trajectories in a system, over a specific time scale. This fluctuation theorem (FT) is applicable to small systems which are far from equilibrium, for short time scales. It shows how irreversibility increases as the system size increases, and reduces to the Second Law of Thermodynamics in the large system limit. It also provides a solution to the long standing paradox of how the Second Law of Thermodynamics, which specifies the direction the system will move, can arise from time reversible equations of motion.

2.4.1 Derivation of the Fluctuation Theorem

The fluctuation theorem is derived simply in the review article by Evans and Searles[4]. We will provide an outline of this derivation below.

A crucial result used to derive the ES-FT is the phase space continuity equation. Let $M(t)$ be the total proportion of ensemble members inside an arbitrary phase space volume V_Γ at time t. We can write this in terms of the phase space density, $f(\mathbf{\Gamma}, t)$ as

$$M(t) = \int_{V_\Gamma} d\mathbf{\Gamma} f(\mathbf{\Gamma}, t). \tag{2.21}$$

where $f(\mathbf{\Gamma}, t)$ is the phase space density at phase space position $\mathbf{\Gamma}$, in the distribution at time t. Now,

$$\frac{dM(t)}{dt} = \int_{V_\Gamma} d\mathbf{\Gamma} \frac{\partial f(\mathbf{\Gamma}, t)}{\partial t}. \tag{2.22}$$

We can also consider the ensemble members which are flowing out of the surface around the volume, $S_\mathbf{\Gamma}$. Since ensemble members are conserved, we know

$$\frac{dM(t)}{dt} = -\int_{S_\Gamma} d\mathbf{S}_\mathbf{\Gamma} f(\mathbf{\Gamma}, t)\dot{\mathbf{\Gamma}}(\mathbf{\Gamma}, t). \tag{2.23}$$

Using the Divergence Theorem

$$\frac{dM(t)}{dt} = -\int_{V_\Gamma} d\mathbf{\Gamma} \frac{\partial}{\partial \mathbf{\Gamma}} [\dot{\mathbf{\Gamma}} f(\mathbf{\Gamma}, t)], \tag{2.24}$$

and since the volume is arbitrary

$$\frac{\partial f(\mathbf{\Gamma}, t)}{\partial t} = -\frac{\partial}{\partial \mathbf{\Gamma}} \cdot [\dot{\mathbf{\Gamma}} f(\mathbf{\Gamma}, t)]. \tag{2.25}$$

This is the phase space continuity equation, also referred to as Liouville's Theorem. Using this result we can write the streaming derivative of the phase space density as

$$\frac{df(\mathbf{\Gamma}, t)}{dt} = \frac{\partial f}{\partial t} + \dot{\mathbf{\Gamma}} \cdot \frac{\partial f}{\partial \mathbf{\Gamma}} = -f \frac{\partial}{\partial \mathbf{\Gamma}} \cdot \dot{\mathbf{\Gamma}} \equiv -f\Lambda \tag{2.26}$$

where we define $\Lambda \equiv (\partial/\partial \mathbf{\Gamma}) \cdot \dot{\mathbf{\Gamma}}$ as the phase space expansion factor. The formal solution to this differential equation is

$$f(S^t\mathbf{\Gamma}, t) = \exp\left[-\int_0^t ds \Lambda(S^s\mathbf{\Gamma})\right] f(\mathbf{\Gamma}, 0) \tag{2.27}$$

where $f(S^t\mathbf{\Gamma}, t)$ is the streaming density. Here S^t is the time evolution operator. It propagates the phase space position $\mathbf{\Gamma}$ forwards by a time of t, using the equations of motion.

Consider a volume element of size $\delta V_\mathbf{\Gamma}(\mathbf{\Gamma}, 0)$ centered about the point $\mathbf{\Gamma}$. A comoving phase volume centered around the point $S^t\mathbf{\Gamma}$ will have the same number of ensemble members

by construction. This allows us to write

$$\frac{\delta V_{\mathbf{\Gamma}}(\mathbf{\Gamma},0)}{\delta V_{\mathbf{\Gamma}}(S^t\mathbf{\Gamma},t)} = \frac{f(S^t\mathbf{\Gamma},t)}{f(\mathbf{\Gamma},0)} \tag{2.28}$$

$$= \exp\left[-\int_0^t ds\Lambda(S^s\mathbf{\Gamma})\right] \tag{2.29}$$

where we have used Eq. (2.26), the phase space continuity equation. The comoving volume element, $\delta V_{\mathbf{\Gamma}}(S^t\mathbf{\Gamma},t)$, is the volume of the same ensemble members in $\delta V_{\mathbf{\Gamma}}(\mathbf{\Gamma},0)$, after they have evolved for a length of time t.

The fluctuation theorem considers conjugate sets of trajectory and antitrajectory bundles. A bundle of trajectories is generated by taking all of the ensemble members within some volume $\delta V_{\mathbf{\Gamma}}(\mathbf{\Gamma},0)$ and propagating them forward in time. Since our equations of motion are time reversible, for every trajectory there is an antitrajectory. The antitrajectory is generated by applying a time reversal mapping to the final phase space position of the trajectory, then propagating this phase space position forward in time for length t[32]. This is equivalent to running the equations of motion backwards in time from the final point reached in the trajectory. For the trajectory of length t that begins from the point $\mathbf{\Gamma}$ we will denote the initial point of the antitrajectory as $\mathbf{\Gamma}^* \equiv M^T S^t\mathbf{\Gamma}$, where M^T is the time reversal mapping. The equations of motion must be time reversible[33, 34]. For the colour field equations of motion $M^T(\mathbf{q},\mathbf{p},Fe) = (\mathbf{q},-\mathbf{p},Fe)$ and for SLLOD equations of motion $M^T(\mathbf{q},\mathbf{p},\dot\gamma) = (\mathbf{q},-\mathbf{p},-\dot\gamma)$. The antitrajectory bundle is the set which contains all trajectories initiating from the time reversed map of the volume element $\delta V_{\mathbf{\Gamma}}(S^t\mathbf{\Gamma},t)$. We can write the probability of a bundle of trajectories relative to the conjugate set of antitrajectories as

$$\frac{p(\delta V_{\mathbf{\Gamma}}(\mathbf{\Gamma},0))}{p(\delta V_{\mathbf{\Gamma}}(\mathbf{\Gamma}^*,0))} = \frac{f(\mathbf{\Gamma},0)\delta V_{\mathbf{\Gamma}}(\mathbf{\Gamma},0)}{f(\mathbf{\Gamma}^*,0)\delta V_{\mathbf{\Gamma}}(\mathbf{\Gamma}^*,0)}. \tag{2.30}$$

We will assume the distribution is even in the momenta. As such, $f(\mathbf{\Gamma}^*,0) = f(M^T S^t\mathbf{\Gamma},0) = f(S^t\mathbf{\Gamma},0)$. The volume element at the start of the antitrajectory is equal to the volume element at the end of the trajectory, $\delta V_{\mathbf{\Gamma}}(S^t\mathbf{\Gamma},t) = \delta V_{\mathbf{\Gamma}}(\mathbf{\Gamma}^*,0)$. Using Eq. (2.29) we can now write

$$\frac{p(\delta V_{\mathbf{\Gamma}}(\mathbf{\Gamma},0))}{p(\delta V_{\mathbf{\Gamma}}(\mathbf{\Gamma}^*,0))} = \frac{f(\mathbf{\Gamma},0)}{f(S^t\mathbf{\Gamma},0)}\exp\left[-\int_0^t ds\Lambda(S^s\mathbf{\Gamma})\right]. \tag{2.31}$$

We can now finally introduce the dissipation function, defined to simplify this equation.

$$\int_0^t ds\Omega(S^s\mathbf{\Gamma}) \equiv \ln\left(\frac{f(\mathbf{\Gamma},0)}{f(S^t\mathbf{\Gamma},0)}\right) - \int_0^t ds\Lambda(S^s\mathbf{\Gamma}) \equiv \Omega_t(\mathbf{\Gamma}) \tag{2.32}$$

where $\Omega_t(\mathbf{\Gamma})$ is the integrated dissipation function and $\Omega(\mathbf{\Gamma})$ is the instantaneous dissipation function. This allows us to rewrite Eq. (2.31) as

$$\frac{p(\delta V_{\mathbf{\Gamma}}(\mathbf{\Gamma},0))}{p(\delta V_{\mathbf{\Gamma}}(\mathbf{\Gamma}^*,0))} = \exp[\Omega_t(\mathbf{\Gamma})]. \tag{2.33}$$

Since we have not yet specified how the trajectory volumes are defined, we may choose volumes such that the value of the dissipation function for trajectories inside a volume is

A. That is, choose $\delta V_{\mathbf{\Gamma}}(\mathbf{\Gamma}, 0; \Omega_t(\mathbf{\Gamma}) = A \pm \delta A)$. The dissipation function is odd under time reversal, so trajectories in the conjugate set will have a value of $-A$ for the dissipation function. We now have

$$\ln\left[\frac{p(\Omega_t = A \pm \delta A)}{p(\Omega_t = -A \pm \delta A)}\right] = A. \tag{2.34}$$

For sufficiently small δA we can replace the probability with a probability distribution,

$$\ln\left[\frac{Pr(\Omega_t = A)}{Pr(\Omega_t = -A)}\right] = A. \tag{2.35}$$

This is the Evans-Searles Fluctuation Theorem. Implicit in this derivation is the assumption that if $f(\mathbf{\Gamma}, 0) \neq 0$ then $f(\mathbf{\Gamma}^*, 0) \neq 0$. This property is called ergodic consistency, and is necessary to avoid dividing by zero. We also assume causality by comparing the volumes at time zero rather than at time t, thus breaking the time reversal symmetry. This is the solution to the paradox of irreversible behavior being derived from time-reversible equations of motion.

We can see that the fluctuation theorem gives the probability of negative values of the dissipation function, relative to the probability of positive values.

The dissipation function can be thought of as a measure of the irreversibility of a trajectory. It is a function of the initial distribution of the system, and the phase space positions along the trajectory. In this way, it is a path integral. The form of the dissipation function is dependent on the system in question, but it often takes on a simple physical quantity[35, 36]. In many cases it is the dissipative flux.

It is common to refer to the time average of the dissipation function, defined by

$$\bar{\Omega}_t \equiv \frac{1}{t}\Omega_t. \tag{2.36}$$

The ES-FT using the time averaged dissipation function is given by

$$\ln\left[\frac{Pr(\bar{\Omega}_t = A)}{Pr(\bar{\Omega}_t = -A)}\right] = At. \tag{2.37}$$

This form is sometimes more convenient, and makes the time dependence explicit.

The integrated dissipation function is extensive in observation time t and system size. As either is increased, it becomes exponentially more likely that positive values of the dissipation function will be observed. In the large system or long time limit, only positive values of the dissipation function will be observed. This is consistent with the Second Law of Thermodynamics. We have predicted irreversible behaviour from time reversible equations of motion.

This theorem has been demonstrated extensively computationally[35, 14, 37, 38, 39, 13] and experimentally[15, 40, 41, 42, 43, 16].

2.5 The Second Law Inequality

The ES-FT can be used directly to derive an expression equivalent to the Second Law Inequality[12]. We can write the ensemble average of the dissipation function as

$$\begin{aligned}
\langle \Omega_t \rangle &= \int_{-\infty}^{\infty} APr(\Omega_t = A) dA && (2.38)\\
&= \int_{0}^{\infty} (APr(\Omega_t = A) - APr(\Omega_t = -A)) dA && (2.39)\\
&= \int_{0}^{\infty} APr(\Omega_t = A)(1 - \exp[-A]) dA && (2.40)\\
&= \langle \Omega_t (1 - \exp[-\Omega_t]) \rangle_{\Omega_t > 0} \times \int_{0}^{\infty} Pr(\Omega_t = A) dA && (2.41)
\end{aligned}$$

where $\langle \cdots \rangle_{\Omega_t > 0}$ denotes an ensemble average over fluctuations in which the dissipation function is positive. Since the exponential term is always less than unity, and an integral of probabilities must always be positive, we have

$$\langle \Omega_t \rangle \geq 0 \quad \forall \quad t > 0. \tag{2.42}$$

While the instantaneous dissipation function can be negative, the ensemble average of the integrated dissipation function cannot be negative. This statement is the Second Law Inequality, and demonstrates clearly the nonreversible behaviour.

2.6 Nonequilibrium Partition Identity

The Nonequilibrium Partition Identity, formerly known as the Kawasaki normalization factor, is the phase space average of the exponential of the negative dissipation function. It was first derived for thermostatted systems by Morriss and Evans[31]. Its value can be derived trivially from the ES-FT[21]. Starting by writing the average as an integral we have

$$\langle \exp[-\Omega_t] \rangle = \int_{-\infty}^{\infty} dA Pr(\Omega_t = A) \exp[-A] \tag{2.43}$$

and then applying the ES-FT to the integrand gives us

$$\begin{aligned}
\langle \exp[-\Omega_t] \rangle &= \int_{-\infty}^{\infty} dA Pr(\Omega_t = -A) && (2.44)\\
&= \int_{-\infty}^{\infty} dA Pr(\Omega_t = A) = 1. && (2.45)
\end{aligned}$$

This quantity is a good check of computational and experimental accuracy and sampling size. If the form of the dissipation function is not correct, the Nonequilibrium Partition Identity will not have a value of unity. If the sample size is not large enough, the average will not equal unity. The NPI is slow to converge, and displays non-Gaussian statistics. This makes it appear to converge to a value of less than unity in most instances, which made it difficult to demonstrate initially[32]. It has now been demonstrated experimentally[21] and

has had considerable interest recently[44, 45, 46, 47, 48, 49, 50].

The NPI is closely related to summing rules from other fluctuation theorems, such as the Jarzynski equality[51, 52, 53, 54, 55, 56, 57].

2.6.1 Partial Range NPI

As an attempt to improve the statistics of the NPI a new form of it was derived, where not all values of the dissipation function are included in the average[44]. From the expression for the NPI, Eq. (2.43), we can use the ES-FT to replace the integrand for the negative range of the interval. This reduces the NPI to an integral over positive values of the dissipation function,

$$\int_0^\infty dA(1+\exp[-A])Pr(\Omega_t = A) = 1. \tag{2.46}$$

Here we have used the fluctuation theorem to map the negative half of the probability distribution to the positive half. The value of this average is still equal to unity. However, since the fluctuation theorem is effectively being used to convert this average over the positive values of the dissipation function to an average of all the values, it is not a good test of a computational or experimental system. It tends to hold even if the distribution of dissipation function values does not satisfy the FT, and so is not sensitive to errors in the system or how it is modeled.

2.7 T-mixing

T-mixing, or Transient mixing, is a condition used to characterize nonequilibrium systems[58, 59]. A system is said to be T-mixing if ensemble averages of the transient time correlation function of the form $\langle B(S^s\mathbf{\Gamma})\Omega(\mathbf{\Gamma})\rangle = \int d\mathbf{\Gamma} B(S^s\mathbf{\Gamma})\Omega(\mathbf{\Gamma})f(\mathbf{\Gamma},0)$ go to zero at long times, sufficiently quickly that the time integral of this expression converges to a constant finite value as the integration time goes to infinity.

$$\int_0^\infty ds\, \langle B(S^s\mathbf{\Gamma})\Omega(\mathbf{\Gamma})\rangle = L_0 \tag{2.47}$$

where $B(\mathbf{\Gamma})$ is any arbitrary phase function that is sufficiently smooth and L_0 is real and finite. The system undergoes a transient that begins at time zero. That is, the system is out of equilibrium initially but begins to move towards it at time 0.

This condition means that correlations between the dissipation function and other phase functions decay with time. T-mixing is a useful condition which we will utilize occasionally in this thesis.

2.8 Steady State Fluctuation Theorem

The ES-FT is exact for systems where the initial distribution and dynamics are known. It can typically be applied to systems starting from some known distribution, and relaxing towards equilibrium. This is called a transient system. The initial known distribution is

often an equilibrium distribution for a system under different conditions than the dynamics being applied. For example, initially the system could be in equilibrium at one temperature, so the distribution is known, but then dynamics are applied corresponding to a different temperature, and the system undergoes a transient as it relaxes towards the new equilibrium.

We can also study systems that start in a known distribution, and undergo a transient towards a steady state, rather than an equilibrium. This occurs when we use driven dynamics, with the heat removed by a thermostat.

Using the transient fluctuation theorem we are not able to study systems where the distribution is not known initially. However, at long times, when the system is in a steady state, the initial distribution becomes irrelevant. The distribution in a steady state is unknown for most systems. We can investigate these systems using the Steady State Fluctuation Theorem, an asymptotic result[60, 61, 62, 11]. This can be derived intuitively[10, 40, 4] by writing the integrated dissipation function as a sum of transient and steady state parts,

$$\Omega_t = \int_0^\tau ds\Omega(s) + \int_\tau^t ds\Omega(s) \tag{2.48}$$

where the system is in equilibrium at time 0, and the dissipation function is defined from this point. Here the time τ is an arbitrary cutoff, a time at which the system is considered to be in the steady state. We can define a steady state dissipation function as $\Omega_{ss,t} = \int_\tau^t ds\Omega(s)$ and and use it to approximate the value of the transient dissipation function, $\Omega_t \approx \Omega_{ss,t} + \mathcal{O}(\tau)$. The error is of order τ, a constant with respect to t. Substituting this into the transient fluctuation theorem, and considering the limit as time, t, goes to infinity we have

$$\lim_{t\to\infty} \frac{1}{t} \ln\left[\frac{Pr(\bar{\Omega}_{ss,t} = A)}{Pr(\bar{\Omega}_{ss,t} = -A)}\right] = A + \frac{1}{t}\mathcal{O}(\tau) \tag{2.49}$$

$$= A \tag{2.50}$$

where $\bar{\Omega}_{ss,t} = \frac{1}{t}\Omega_{ss,t}$.

An alternative derivation is provided in Searles et. al.[34]. In this paper the applicability of the Steady State Fluctuation Theorem is also discussed, and they show it is applicable near and far from equilibrium. The existence of a steady state fluctuation relation is a consequence of T-mixing, ergodic consistency and time reversibility[63, 64].

This form of the fluctuation theorem has been demonstrated computationally[65, 66, 61, 62, 12] and experimentally[40, 42]. It can be easier to work with this form of the fluctuation theorem experimentally because steady state systems are more easily experimentally accessible than transient ones, since they are constant in time. The result has even been demonstrated with a single steady state trajectory[41].

2.9 The Dissipation Theorem

The dissipation function is also the argument in another useful result, known as the Dissipation Theorem[17, 18]. We will outline the derivation of this result below.

From solving the differential equation for the streaming version of the phase space con-

tinuity equation, Eq. (2.26), we have

$$f(S^t\mathbf{\Gamma},t) = \exp\left[-\int_0^t d\tau\Lambda(S^\tau\mathbf{\Gamma})\right] f(\mathbf{\Gamma},0). \tag{2.51}$$

Rewriting the definition of the dissipation function, Eq. (2.32),

$$f(\mathbf{\Gamma},0) = f(S^t\mathbf{\Gamma},0)\exp\left[\int_0^t d\tau(\Omega(S^\tau\mathbf{\Gamma}) + \Lambda(S^\tau\mathbf{\Gamma}))\right]. \tag{2.52}$$

Substituting this into Eq. (2.51) gives

$$f(S^t\mathbf{\Gamma},t) = \exp\left[\int_0^t d\tau\Omega(S^\tau\mathbf{\Gamma})\right] f(S^t\mathbf{\Gamma},0)\forall\mathbf{\Gamma}. \tag{2.53}$$

Recognising that $S^t\mathbf{\Gamma}$ is a dummy variable we can write

$$f(\mathbf{\Gamma},t) = \exp\left[\int_0^t d\tau\Omega(S^{\tau-t}\mathbf{\Gamma})\right] f(\mathbf{\Gamma},0) \tag{2.54}$$

which after a change of variables becomes

$$f(\mathbf{\Gamma},t) = \exp\left[-\int_0^{-t} ds\Omega(S^s\mathbf{\Gamma})\right] f(\mathbf{\Gamma},0). \tag{2.55}$$

This result gives the transient distribution of a system in terms of the initial distribution and the value of the dissipation function.

We can use this result to derive an expression relating nonequilibrium averages to equilibrium expressions and time correlation functions. Starting with the average of an arbitrary phase function at time t,

$$\langle B(t)\rangle_{Fe,f(\mathbf{\Gamma},0)} = \int d\mathbf{\Gamma}B(\mathbf{\Gamma})f(\mathbf{\Gamma},t). \tag{2.56}$$

The subscript on the ensemble average denotes that it is taken in an initial distribution with any value for **Fe**, the external field. Substituting the Dissipation Theorem, Eq. (2.55) into this equation, we get

$$\langle B(t)\rangle_{Fe,f(\mathbf{\Gamma},0)} = \int d\mathbf{\Gamma}B(\mathbf{\Gamma})\exp\left[-\int_0^{-t} d\tau\Omega(S^\tau\mathbf{\Gamma})\right] f(\mathbf{\Gamma},0). \tag{2.57}$$

Taking the derivative of this equation with respect to time, and using Eq. (2.55) gives u

$$\frac{d\langle B(t)\rangle_{Fe,f(\mathbf{\Gamma},0)}}{dt} = \int d\mathbf{\Gamma}B(\mathbf{\Gamma})\Omega(S^{-t}\mathbf{\Gamma})f(\mathbf{\Gamma},t). \tag{2.58}$$

Let $S^{-t}\mathbf{\Gamma} = \mathbf{\Gamma}'$,

$$\frac{d\left\langle B(t)\right\rangle_{Fe,f(\mathbf{\Gamma},0)}}{dt} = \int d\mathbf{\Gamma}' B(S^t\mathbf{\Gamma}')\Omega(\mathbf{\Gamma}')f(S^t\mathbf{\Gamma}',t)\exp\left[\int_0^t \Lambda(S^s\Gamma')ds\right] \quad (2.59)$$

$$= \int d\mathbf{\Gamma}' B(S^t\mathbf{\Gamma}')\Omega(\mathbf{\Gamma}')f(\mathbf{\Gamma}',0) \quad (2.60)$$

$$= \left\langle \Omega(\mathbf{\Gamma}')B(S^t\mathbf{\Gamma}')\right\rangle_{Fe,f(\mathbf{\Gamma}',0)}. \quad (2.61)$$

Reintegrating this equation gives us the other useful form of the Dissipation Theorem (relabelling Γ' as Γ),

$$\left\langle B(t)\right\rangle_{Fe,f(\mathbf{\Gamma},0)} = \left\langle B(0)\right\rangle_{f(\mathbf{\Gamma},0)} + \int_0^t ds\left\langle \Omega(\mathbf{\Gamma})B(S^s\mathbf{\Gamma})\right\rangle_{Fe,f(\mathbf{\Gamma},0)}. \quad (2.62)$$

This is an exact result and is valid arbitrarily far form equilibrium. It has been successfully demonstrated computationally by Reid et. al.[38]. It is a very general form of the transient time correlation function, giving the nonlinear response of the system. If the Dissipation Theorem is linearised the Green-Kubo[67, 68] expression for linear response is recovered.

The presence of the dissipation function in this nonequilibrium result demonstrates how central it is to nonequilibrium statistical mechanics. While it was originally defined as a measure of the irreversibility of a system, it is also important in describing how a system will respond to a nonequilibrium perturbation.

2.10 The Relaxation Theorem

The dissipation function, along with the Second Law Inequality, can be used to prove relaxation to equilibrium. We will go through the derivation for the microcanonical case below[20]. The derivation for the canonical case, of an ergodic Hamiltonian system in contact with a heat bath, is given in [19]. For this derivation we assume that the system is T-mixing.

We start with the uniform distribution

$$f(\mathbf{\Gamma}) = \frac{\delta(H_0(\mathbf{\Gamma}) - E)\delta(\mathbf{p}_s)}{\int d\mathbf{\Gamma}\delta(H_0(\mathbf{\Gamma}) - E)\delta(\mathbf{p}_s)} \quad (2.63)$$

where $\mathbf{p}_s = \sum_i \mathbf{p}_i$. It is understood that the delta function represents an infinitesimally thin shell of energies, such that the ostensible dimension of phase space is not altered. We will show that this is the equilibrium distribution for a microcanonical system, which satisfies Newton's equations of motion, Eq. (2.3). From the definition of the dissipation function, Eq. (2.32), we have

$$\exp[\Omega_t(\mathbf{\Gamma})] = \frac{f(\mathbf{\Gamma},0)}{f(S^t\mathbf{\Gamma},0)} \quad (2.64)$$

since the phase space expansion factor, $\Lambda \equiv (\partial/\partial\mathbf{\Gamma})\cdot\dot{\mathbf{\Gamma}} = 0$, for Newton's equations of motion. So,

$$\delta(H_0(S^t\mathbf{\Gamma}) - E)\delta(\mathbf{p}_s)\exp[\Omega_t(\mathbf{\Gamma})] = \delta(H_0(\mathbf{\Gamma}) - E)\delta(\mathbf{p}_s). \quad (2.65)$$

We can integrate both sides to get rid of the delta functions, and we are left with

$$\int d\mathbf{\Gamma}\delta(H_0(S^t\mathbf{\Gamma}) - E)\delta(\mathbf{p}_s)\exp[\Omega_t(\mathbf{\Gamma})] = \int d\mathbf{\Gamma}\delta(H_0(\mathbf{\Gamma}) - E)\delta(\mathbf{p}_s), \tag{2.66}$$

$$\exp[\Omega_t(\mathbf{\Gamma})] = 1, \tag{2.67}$$

$$\Omega_t(\mathbf{\Gamma}) = 0 \tag{2.68}$$

for all phase space positions, $\mathbf{\Gamma}$, in the uniform distribution. So, there is no dissipation anywhere in phase space for a uniform distribution. From the ES-FT, this result means that every set of trajectories and antitrajectories are equally likely to occur. Forward and reverse motion is completely indistinguishable in the uniform distribution.

From this result we can say that $\Omega(S^t\mathbf{\Gamma}) = 0$. Using this in the Dissipation Theorem, Eq. (2.55), so that $\int_0^{-t} ds\Omega(S^s\mathbf{\Gamma}) = 0$, we have

$$f(\mathbf{\Gamma}, t) = f(\mathbf{\Gamma}, 0). \tag{2.69}$$

The uniform distribution is preserved by the dynamics.

We can now consider a deviation from the uniform distribution,

$$f(\mathbf{\Gamma}, 0) = \frac{\delta(H_0(\mathbf{\Gamma}) - E)\delta(\mathbf{p}_s)\exp[-g(\mathbf{\Gamma})]}{\int d\mathbf{\Gamma}\delta(H_0(\mathbf{\Gamma}) - E)\delta(\mathbf{p}_s)\exp[-g(\mathbf{\Gamma})]} \tag{2.70}$$

where g is an arbitrary phase function, which is real and even in the momentum. The deviation is placed as an exponent to ensure that the distribution function is always positive. We can recalculate the integrated dissipation function and find that

$$\Omega_t(\mathbf{\Gamma}) = \ln\left[\frac{\exp[-g(\mathbf{\Gamma})]}{\exp[-g(S^t\mathbf{\Gamma})]}\right], \tag{2.71}$$

$$= g(S^t\mathbf{\Gamma}) - g(\mathbf{\Gamma}) \equiv \Delta g(\mathbf{\Gamma}, t) = \int_0^t ds\Omega(S^s\mathbf{\Gamma}). \tag{2.72}$$

So,

$$\int_0^{-t} ds\Omega(S^s\mathbf{\Gamma}) = g(S^{-t}\mathbf{\Gamma}) - g(\mathbf{\Gamma}) = \Delta g(\mathbf{\Gamma}, -t) \tag{2.73}$$

and from the Dissipation Theorem, Eq. (2.55),

$$f(\mathbf{\Gamma}, t) = \exp[-\Delta g(\mathbf{\Gamma}, -t)]f(\mathbf{\Gamma}, 0). \tag{2.74}$$

Unless g is a constant of the motion the distribution is not preserved. This proves that for an ergodic system, the uniform distribution is the unique time independent, dissipationless state. As such we will call it the equilibrium distribution function. This result is known from ergodic theory, which says that a mixing, ergodic, autonomous Hamiltonian system will eventually relax towards the microcanonical distribution[69]. The distribution coincides with the dissipationless distribution found with the relaxation theorem.

The Second Law Inequality states that the average dissipation is greater than or equal to zero, Eq. (2.42). When the initial distribution is perturbed from the uniform distribution

this becomes

$$\langle \Delta g(\mathbf{\Gamma}, t\rangle \geq 0. \tag{2.75}$$

For an initial distribution that differs from the uniform one, there is non-zero dissipation, so on average this dissipation is positive. This is true for arbitrary g, provided it is an even function of the momentum.

The Dissipation Theorem allows us to relate averages in the initial distribution to a correlation function, Eq. (2.62). Selecting the phase function g, this gives us

$$\left\langle g(S^t\mathbf{\Gamma})\right\rangle_{f(\mathbf{\Gamma},0)} - \left\langle g(\mathbf{\Gamma})\right\rangle_{f(\mathbf{\Gamma},0)} = \int_0^t ds\, \left\langle \Omega(\mathbf{\Gamma}) g(S^s\mathbf{\Gamma})\right\rangle_{f(\mathbf{\Gamma},0)}. \tag{2.76}$$

We know $\Omega_t = \Delta g(\mathbf{\Gamma}, t)$, so $\Omega(S^t\mathbf{\Gamma}) = \dot{g}(S^t\mathbf{\Gamma})$. Now we have

$$\left\langle g(S^t\mathbf{\Gamma})\right\rangle_{f(\mathbf{\Gamma},0)} - \left\langle g(\mathbf{\Gamma})\right\rangle_{f(\mathbf{\Gamma},0)} = \int_0^t ds\, \left\langle \dot{g}(\mathbf{\Gamma}) g(S^s\mathbf{\Gamma})\right\rangle_{f(\mathbf{\Gamma},0)}. \tag{2.77}$$

If we assume the correlations decay after a sufficiently long time, t_c, since the system is T-mixing,

$$\begin{aligned}
\left\langle g(S^t\mathbf{\Gamma})\right\rangle_{f(\mathbf{\Gamma},0)} &= \left\langle g(\mathbf{\Gamma})\right\rangle_{f(\mathbf{\Gamma},0)} + \int_0^{t_c} ds\, \left\langle \dot{g}(\mathbf{\Gamma}) g(S^s\Gamma)\right\rangle_{f(\mathbf{\Gamma},0)} \\
&\quad + \int_{t_c}^t ds\, \left\langle \dot{g}(\mathbf{\Gamma})\right\rangle_{f(\mathbf{\Gamma},0)} \left\langle g(S^s\mathbf{\Gamma})\right\rangle_{f(\mathbf{\Gamma},0)} \qquad (2.78) \\
&= \left\langle g(\mathbf{\Gamma})\right\rangle_{f(\mathbf{\Gamma},0)} + \int_0^{t_c} ds\, \left\langle \dot{g}(\mathbf{\Gamma}) g(S^s\mathbf{\Gamma})\right\rangle_{f(\mathbf{\Gamma},0)} \qquad (2.79)
\end{aligned}$$

for $t > t_c$, since $\left\langle \dot{g}(\mathbf{\Gamma})\right\rangle_{f(\mathbf{\Gamma},0)} = 0$ because g is even in the momentum, implying that $\dot{g}$ is odd in the momentum. Now from the Dissipation Theorem, Eq. (2.62), we have

$$\left\langle g(S^t\mathbf{\Gamma})\right\rangle_{f(\mathbf{\Gamma},0)} = \left\langle g(S^{t_c}\mathbf{\Gamma})\right\rangle_{f(\mathbf{\Gamma},0)}. \tag{2.80}$$

Therefore,

$$\lim_{t\to\infty} \frac{d}{dt} \left\langle g(S^t\mathbf{\Gamma})\right\rangle_{f(\mathbf{\Gamma},0)} = 0. \tag{2.81}$$

At sufficiently long times there is no dissipation, so the system has reached its unique equilibrium state. Thus, systems under Newton's equations of motion will relax to the uniform distribution, provided temporal correlations decay and the system is ergodic.

Unlike the ergodic theory proof, this approach can also be applied to a canonical system. In this system, the Boltzmann distribution is the unique dissipationless state, which is preserved under the dynamics. As in the microcanonical case, if the system satisfies a number of conditions, such as decay of temporal correlations and ergodicity, Evans et. al.[19] show that any nonequilibrium distribution relaxes to this equilibrium distribution.

This relaxation towards equilibrium need not be monotonic in the decay of the phase average dissipation function. Relaxation towards equilibrium has been previously addressed with the Boltzmann H-theorem[3], however this implies that uniform gasses have a monotonic relaxation. It is only applicable to dilute gases. The Relaxation Theorem allows for

much more complex behaviour, like what is seen in physically realistic systems[38]. The initial ensemble response is always towards equilibrium.

For this system any given distribution can be written as a deviation from the Boltzmann distribution,

$$f(\mathbf{\Gamma}) = \frac{\delta(KE_{th} - KE)e^{-\frac{H(\mathbf{\Gamma})}{k_B T} - g(\mathbf{\Gamma})}}{\int d\mathbf{\Gamma}\delta(KE_{th} - KE)e^{-\frac{H(\mathbf{\Gamma})}{k_B T} - g(\mathbf{\Gamma})}} \tag{2.82}$$

where the deviation function is given by $g(\mathbf{\Gamma})$.

2.10.1 Conformal Relaxation

In the special case where the deviation in Eq. (2.82) decays conformally, the dissipation function will relax monotonically[19]. This means that the deviation function (for the distribution as it relaxes with time) can be written as

$$g(\mathbf{\Gamma}) = c(t)\varrho(\mathbf{\Gamma}) \tag{2.83}$$

where $\varrho(\mathbf{\Gamma})$ is constant in time, and $c(t)$ is dependent only on the time, t. So, the deviation function is a multiple of $\varrho(\mathbf{\Gamma})$. Exact conformal relaxation is not possible from the initial time, however the system can approach this behaviour asymptotically.

2.11 Covariant Dissipation Function

The covariant dissipation function can be used to convert a dissipation function defined from a particular distribution to one defined from a different distribution. This is done using the time symmetry of trajectories and antitrajectories. Evans et. al.[70] show that the dissipation function defined from the time evolving phase space distribution has a simple relationship with the dissipation function defined with respect to the initial distribution. The dissipation function, defined from a time t_1 and integrated from the initial phase space point $S^{t_1}\mathbf{\Gamma}$ at time t_1 to time $t_1 + \tau$ is defined by

$$\Omega_\tau(S^{t_1}\mathbf{\Gamma}, t_1) \equiv \ln\left(\frac{f(S^{t_1}\mathbf{\Gamma}, t_1)}{f(S^{t_1+\tau}\mathbf{\Gamma}, t_1)}\right) - \int_{t_1}^{t_1+\tau} ds\Lambda(S^s\mathbf{\Gamma}). \tag{2.84}$$

This is equivalent to a dissipation function defined from the initial time,

$$\Omega_\tau(S^{t_1}\mathbf{\Gamma}, t_1) = \Omega_{2t_1+\tau}(\mathbf{\Gamma}, 0). \tag{2.85}$$

This covariant dissipation function is not local in time, it includes a time t_1 before the interval under consideration, and a time t_1 after it. From this relationship an exact steady state fluctuation theorem can be derived, however it is also not local in time. It is the standard transient Evans-Searles Fluctuation Theorem, evaluated over the symmetrically extended time range. This proves that there is no exact time local, steady state form of the ES-FT.

2.12 Other Fluctuation Relations

The Evans-Searles fluctuation theorem is one of many such relations applicable to non-equilibrium statistical mechanics. Here we provide a very brief overview of a selection of these results, and how they relate to the ES-FT. A key division among these relations is between those that apply to deterministic systems and those that are applicable to stochastic systems. The ES-FT was derived for deterministic systems, as was another very general result, the Crooks fluctuation theorem[71, 72]. The work in this thesis has been done considering purely a deterministic approach.

Fluctuation relations of a similar kind have been derived for systems which exhibit stochastic dynamics.

2.12.1 Crooks Fluctuation Theorem

The Crooks fluctuation theorem is like the ES-FT in that it derives irreversible behaviour from reversible microscopic equations of motion. It's form is similar to that of the ES-FT discussed above, except instead of considering probabilities of trajectories characterized by their dissipation function, it deals with sets of trajectories described by the work[10]. The Crooks FT is given by

$$\frac{p_f(W=C)}{p_r(W=-C)} = \exp[\beta(C-\Delta F)] \tag{2.86}$$

where W is the work done by a trajectory which starts in state A and ends in state B and ΔF is the difference between these two states. A key difference between this relation and the ES-FT is that the probability distributions used for the forward and reverse trajectories are not the same. The probability of forward trajectories, $p_f(W=C)$, is the probability of trajectories which move from state A to state B whose work is equal to C. The probability of reverse trajectories, $p_r(W=-C)$, is the probability of trajectories which move from state B to state A having a value of the work of $-C$. In this process both the initial and final states must be in equilibrium, so the distribution functions are known.

This relationship is similar to the classical thermodynamic result that the work needed to traverse between two states quasistatically is equal to the free energy difference between those states. However, the Crooks FT provides much more detail, and gives microscopic quantitative information about non-equilibrium systems. For quasistatic processes, the classical thermodynamic result is recovered.

Similar to the non-equilibrium partition identity for the ES-FT, the Crooks FT has an identity for the phase space average of the exponential of the work. This is given by

$$\exp[-\beta\Delta F] = \langle \exp[-\beta W] \rangle_f \tag{2.87}$$

where the subscript f denotes that this ensemble average is taken over forward trajectories from state A to B. While the result can be directly derived from the Crooks FT, it had been previously discovered, and is know as the Jarzynski equality[73, 74]. The relationship allows the free energy difference between two states to be calculated from non-equilibrium trajectories between these states. This is a major advance over traditional thermodynamics,

where this quantity would have to be measured by constructing quasitatic trajectories, which are always in equilibrium. The Crooks fluctuation theorem, as well as the Jarzynski equality, have been applied to many experimental systems[51, 75].

2.12.2 Stochastic Fluctuation Theorems

Stochastic dynamics are not time reversible, and incorporate some element of randomness. They are typically used when the system of interest involves large molecules or colloids in a solvent whose degrees of freedom aren't considered explicitly. This requires a separation of timescale between the system of interest and the heat bath. One example is the Langevin equation, which was initially constructed to describe Brownian motion. The derivation of the Evans-Searles FT and many of the theorems derived from it, discussed earlier in this chapter, rely on time reversibility. However, both the ES-FT and the Crooks FT have been shown to be applicable to systems with stochastic dynamics[76, 66, 37, 40]. There are many fluctuation theorems of the same form which have been derived for stochastic systems[77]. Some work specific to driven Langevin dynamics was done by Sekimoto[78] to show that classical thermodynamic quantities such as heat and work could be calculated for individual trajectories. In fact, the derivation of many of these fluctuation theorems has been unified[47], and its form is very general[79]. These results form part of a field known as stochastic thermodynamics[80].

Stochastic thermodynamics could be particularly useful for describing the non-equilibrium behaviour of systems which are too complex to model easily with deterministic equations of motion, such as biological systems and molecular machines[81]. Experimentally these theorems have been applied to colloidal systems, such as with a moving optical trap[15, 41], a stationary trap with an applied field[82, 83] and under a non-harmonic potential created by a laser and a fixed repulsive surface[84]. Stochastic fluctuation theorems also have application to other quite varied systems, such as electric circuits[42, 85] and gravitational wave detectors[86], which can be effectively described with Langevin dynamics.

One key advantage of stochastic dynamics over deterministic dynamics is that it is comparatively straightforward to apply their fluctuation theorems to non-equilibrium steady states. The stochastic approach has some disadvantages, such as making different assumptions to the ES-FT. For example, when working with the Langevin equation, it is necessary to assume that the noise is not affected by the driving[47].

Chapter 3

Computer Simulation Techniques

The work in this thesis was largely undertaken using computer simulations. This chapter will provide an overview of the techniques employed. Molecular dynamics was used to model the behavior of each system, and the properties of interest were calculated in ensembles of trajectories. The Weeks-Chandler-Andersen potential[87] was used to model particle interactions in a simple manner. Artificial thermostats were used in the simulations to allow a wide range of systems to be modeled[27]. We use modifications to the equations of motion to allow us to generate desired initial conditions, such as modifying the equations to include perturbations to the potential. Simple driven shear flow systems were modeled using the SLLOD[27] equations of motion. All simulations are run in two dimensions to save on computational expense.

All of the code was written in C++. The simulations were run on local desktop computers, as well as at the NCI supercomputer facility. The code used in this thesis was based off existing molecular dynamics code, which was modified extensively for each different system studied.

The methodology used to analyse the results differs for each system being studied. In most cases the results are in terms of probabilities, calculated from frequency histograms generated with the simulations. In the first part of this thesis, studying the relaxation of a density gradient, the results include the position dependent density of the system. To analyse these results we used a least squares fit of the density data to monitor the relaxation, as well as a discrete Fourier decomposition of this data in more complex systems.

3.1 Molecular Dynamics

Molecular dynamics is a tool for propagating Newton's equations of motion in a computational system[88, 89]. An example of the equations of motion used in a computer simulation are given in Section 2.2, Eq. (2.3). The motion of the particles in the system depends on the position and momentum of each particle. The force on each particle can be calculated from the particles positions, allowing us to integrate the equations of motion and simulate trajectories.

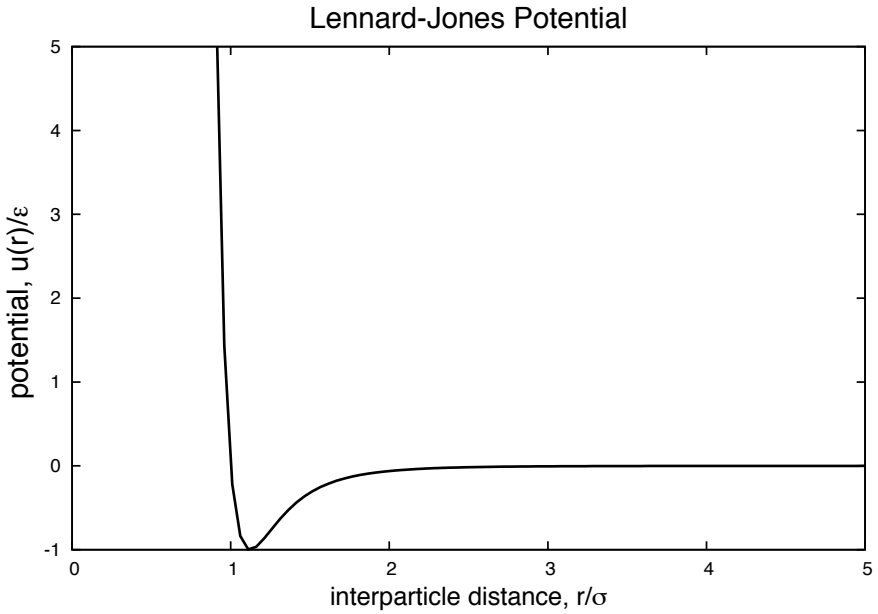

Figure 3.1: The Lennard-Jones potential, plotted without units as r/σ against $u(r)/\varepsilon$.

3.1.1 Force Calculations

The force on each particle, $\mathbf{F}_i$, depends on the positions of every particle in the system and is given in terms of the pair forces, the derivative of the potential between two particles. The interactions between two particles can be modeled using the Lennard-Jones potential[90, 91], given by

$$u(r) = 4\varepsilon \left[\left(\frac{\sigma}{r}\right)^{12} - \left(\frac{\sigma}{r}\right)^{6} \right] \tag{3.1}$$

where r is the interparticle distance, ε is the depth of the well and σ is the distance at which the potential passes through zero. This function is plotted in Figure 3.1. It is a reasonable approximation of the potential between two argon atoms.

The effect of non-additive interactions are not included[92, 93]. This is a very commonly used potential[94], even though it has been shown that the selected exponents 6 and 12 do not fit the experimental data best[95, 96]. Alternative potentials that include three body interactions and fit experimental data better have been developed[97], however adding three body interactions increases the complexity and computer time required.

To simplify our simulations we use a truncated form of the Lennard-Jones potential, the Weeks-Chandler-Andersen(WCA) potential[87, 27]. The potential is truncated at the minimum, so it is cutoff at the distance $r_c = 2^{1/6}\sigma$, and shifted up by ε so that the potential is continuous, and zero at the cutoff. By truncating the potential at the minimum its derivative is also continuous. This potential includes only the repulsive short range interactions, leading to faster computer simulations by ignoring long range attractive interactions. Only two body interactions are considered.

3.1.2 Integration Method

The equations of motion can be approximately solved numerically using iterative methods. This work uses the fourth order Runge-Kutta method[98], which has the advantage of being self starting[27].

The algorithm takes the phase space position of the system at some given point, and uses the calculated force on each of the particles to progress the equations of motion forward by one time step. The accuracy of the calculation is dependent on the length of time step used. It uses a trial step at the midpoint of the time step interval. The smaller the time step, the more reversible the numerical integration of the equations of motion will be.

A thermostat, which was discussed in Section 2.2, can be included. The equations of motion can then be solved using the same method as above, including the thermostat term.

The thermostat used in this thesis is designed to keep the kinetic energy constant. However, errors are introduced in the numerical simulations, due to both rounding and discretisation. Respectively, the size of these errors are dependent on word-length and time step used in the simulation. Because of these errors, it is possible for the value of the kinetic energy to drift, since the thermostat is keeping it constant, rather than at a specific value. To rectify this problem we can add a proportional correction factor to the value of α[99, 100].

$$\alpha = \frac{\sum_i \mathbf{F}_i \cdot \mathbf{p}_i}{\sum_i \mathbf{p}_i \cdot \mathbf{p}_i} + \frac{0.02}{2Ndt}\left(\left(\sum_i \mathbf{p}_i \cdot \mathbf{p}_i\right) - (2N-3)k_BT\right) \tag{3.2}$$

where dt is the time step length. If the value of the kinetic energy calculated from the simulation is equal to the value determined with the input temperature, this correction factor is zero and has no effect. If the kinetic energy has drifted, the correction factor will change α so that it moves the kinetic energy towards the value specified by the input temperature. In our two dimensional system the kinetic energy of the system is given by $(2N-3)k_BT$ from the Equipartition Theorem, since both components of the momenta are fixed, as well as the total kinetic energy.

The other imposed condition on the system is that the total momentum is equal to zero. This should be preserved by the equations of motion, however it may also drift due to rounding error.

An applied field that is not applied symmetrically in both directions can result in non-zero total momentum. This can be fixed by readjusting the momentum depending on the forces applied to the system, effectively moving the reference frame of the simulation.

To keep the momentum zero we will rezero each component of the total momentum every time step. This is done by calculating the total value of each component of the momenta, dividing it by the total number of particles in the system, and subtracting this amount from that component of each particle's momentum.

3.1.3 Periodic Boundary Conditions

In order to approximately simulate the behaviour of a bulk fluid, using a reasonable amount of computer time, we conduct our simulation with periodic boundary conditions. This allows

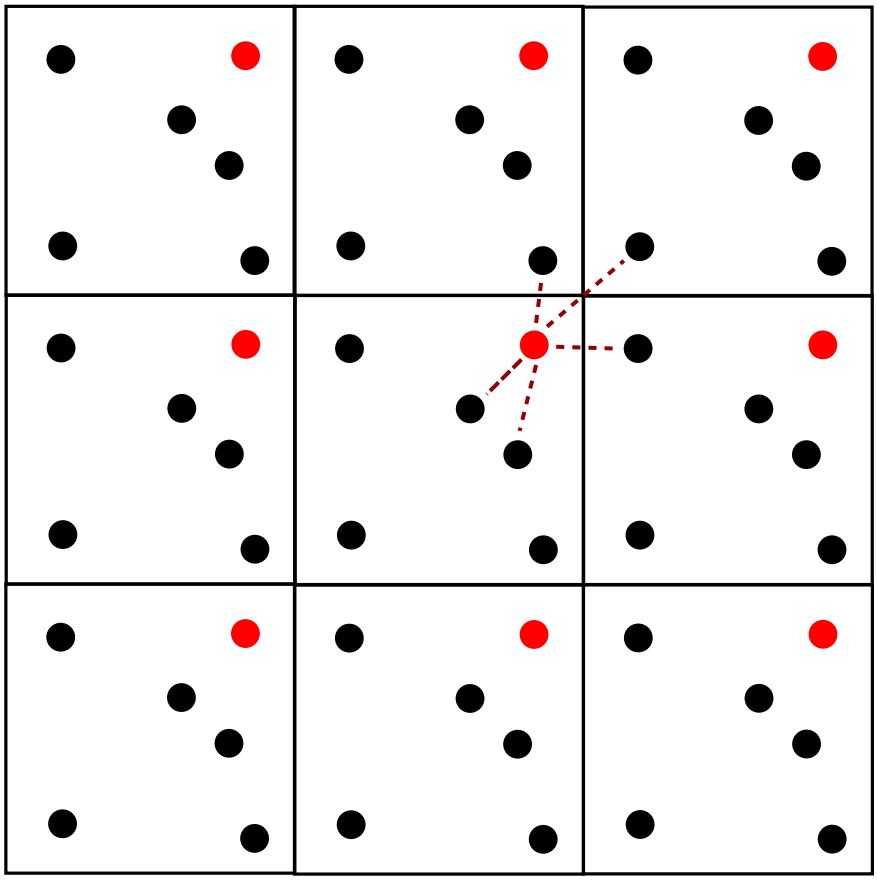

Figure 3.2: Illustration of periodic boundary conditions. The nearest neighbours of the red particle in the central unit cell are connected to it with dotted lines.

us to simulate a small number of particles without having to be concerned with the effects of boundaries.

We use orthogonal periodic boundary conditions[27], where one cubic cell which contains all the simulated particles of the system is surrounded by an infinite array of identical cells. This initial cell is called the primitive cell. Now when considering interactions between particles, the force on a given particle is calculated from the interaction with the image of each other particle that is closest to it. The interactions may be within the primitive cell, or between neighbouring cells. Each particle interacts with all other particles that are within the cutoff distance of the potential function. If a particle leaves the primitive cell, it is replaced by an image of itself entering from the adjacent cell.

These periodic boundary conditions can just as easily be applied to two dimensional systems, where a square is surrounded by an infinite array of identical squares. This situation is illustrated in Figure 3.2.

3.1.4 Initial Conditions

To run molecular dynamics simulations, the initial position and momentum of each particle need to be known. We initially assign these values so that the particles are not overlapping,

and the kinetic energy of the system matches the input temperature for the simulation.

3.1.4.1 Position

It is convenient to set up the particles in a regular lattice initially[101]. Generally in a liquid system, the choice of lattice is arbitrary, since it will relax to equilibrium independently of the initial positions. However, if the liquid system is near its freezing point, it is important to select initial positions that are not metastable if an equilibrium system is desired. In this thesis the particle positions were initiated in a FCC lattice.

3.1.4.2 Momenta

The simulations in this thesis will be in an isokinetic ensemble. In this case, the initial momenta need to be selected such that the system has the desired kinetic temperature. This is done by assigning each component of the velocity of each particle randomly, according to a Gaussian distribution. The kinetic energy of the system with these randomly assigned momenta is calculated, and then each component is rescaled to give the correct value of the kinetic temperature.

Since the assigned initial positions are fixed, it is important that the momenta are assigned randomly, as this will allow for simulations in the same macrostate but which generate different trajectories.

3.1.4.3 Equilibrium

All of the simulations in this thesis begin in an equilibrium state. This state is achieved by starting with the initial positions and momenta given above, and integrating the equations of motion for a sufficiently long time. To generate an ensemble of trajectories starting in the equilibrium distribution, each trajectory must start from a different initial position. These positions are generated by running the simulation in equilibrium for a time long enough that the phase space position is uncorrelated from the last sampled point. This is repeated in series for the number of ensemble members required.

When the ensemble is generated through multiple simulations run on different computers (i.e. cores of a super computer) a different seed is used for the random number generator when assigning the initial momenta. This ensures the sets of ensemble members calculated on each computer are unique.

3.1.5 SLLOD

Planer couette flow, described in Section 2.3.1, is a convenient and interesting nonequilibrium system to study computationally. The equations of motion given in Eq. (2.13) and (2.14) can be used in the simulation, however different periodic boundary conditions are needed.

3.1.5.1 Lees-Edwards Periodic Boundary Conditions

Since the system is shearing, the periodic boundary conditions need to move with the system[102]. This can be thought of as the unit cells sliding past one another, illustrated in

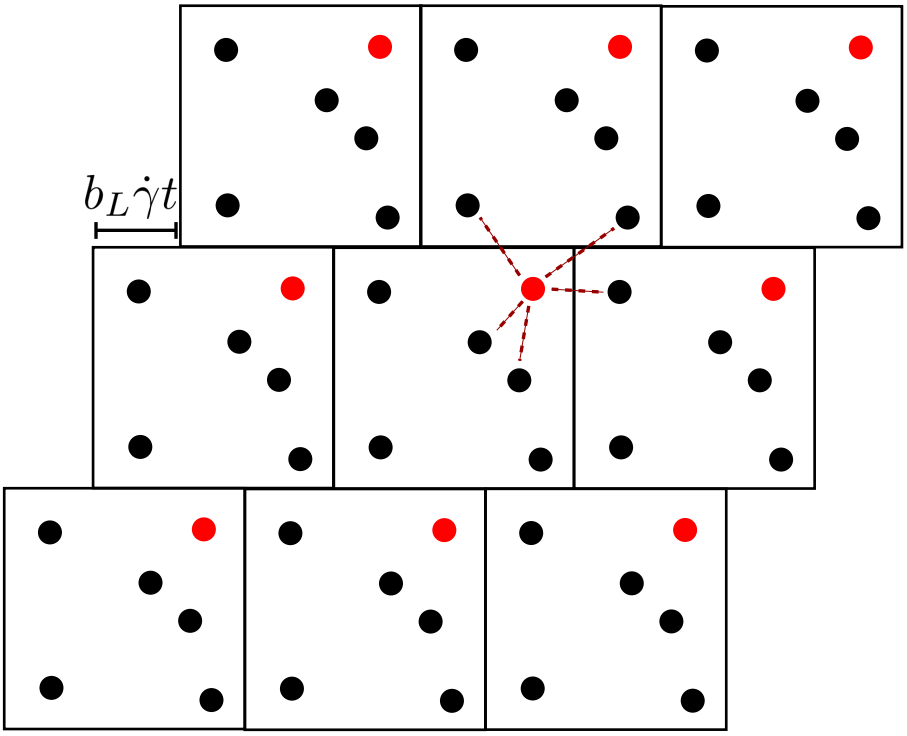

Figure 3.3: Lees-Edwards periodic boundary conditions, shown in a sliding brick representation. The nearest neighbors of the red particle in the central unit cell are connected to it with dashed lines. The lattice cell offset is dependent on the amount of time the simulation has been running for, t and the length of the unit cell, b_L.

Figure 3.3.

The rate at which the unit cells move relative to one another is determined by the strain rate, $\dot{\gamma}$. This sliding brick system is equivalent to shearing (deforming) the unit cell, then remapping the boundaries of the unit cell to include a convenient set of particles. This remapping is done once every cycle, equivalent to the time it takes for one unit cell to move into the original position of the neighbouring cell in the sliding brick method. While the remapping is not theoretically necessary, it is required in practice due to the size limit of numbers that can be stored in the computer simulation.

The system being simulated changes slightly as the sliding bricks move relative to one another. That is, the system is not that same when the adjacent unit cells are offset as when they are aligned. Each particle's own periodic image is in a different relative location in each of these cases. The shifting of the boundary conditions puts a strain on the system which results in a non-zero stress[103]. This causes the simulation to be non-autonomous. That is, it depends explicitly on time, as the periodic boundary conditions depend explicitly on the time since the system began shearing.

This effect is only noticeable for very small system sizes. Once the system is big enough that a particle's own periodic image has no effect on it, the simulation behaves as if it is autonomous.

One way to negate some of the effects of the non-autonomous simulation is to consider the

lattice cell offset as a phase space variable, and average over an extended phase space[104]. That is, each trajectory can be initiated with a random value for the initial offset. This method has been used to calculate the viscosity of a system[105], which converges to the bulk viscosity more quickly than simulations using other methods[106].

3.1.6 Code Functionality Verification

As a check to see if the molecular dynamics simulation is working as expected we can calculate the change in energy of the system in two different ways. First, we can calculate the value of the energy directly, and compute its change over some length of the simulation. That is, we calculate the sum of the kinetic energy and the potential energy from the configuration and interparticle potential function. If an external field is applied to the system this also needs to be included in the potential energy calculation.

We can also calculate the change in energy of the system as the energy removed by the thermostat. The change in energy with time is given by

$$\begin{aligned}
\dot{H}_0 &= \left(\frac{\partial}{\partial t}\sum_{i=1}^{N}\frac{\mathbf{p}_i\cdot\mathbf{p}_i}{2m}\right)+\dot{\mathbf{\Phi}} \qquad (3.3)\\
&= \sum_{i=1}^{N}\frac{\dot{\mathbf{p}}_i\cdot\mathbf{p}_i}{m}-\mathbf{F}_i\cdot\dot{\mathbf{q}}_i\\
&= \sum_{i=1}^{N}\frac{(\mathbf{F}_i-\alpha\mathbf{p}_i)\cdot\mathbf{p}_i}{m}-\mathbf{F}_i\cdot\frac{\mathbf{p}_i}{m}\\
&= -\alpha\sum_{i=1}^{N}\frac{\mathbf{p}_i\cdot\mathbf{p}_i}{m}\\
&= -\alpha(2N-3)k_BT.
\end{aligned}$$

The change in H_0 can be calculated during the same Runge-Kutta integration process used to integrate the equations of motion. We can compare this value to that calculated from the change in H_0 directly to ensure that the simulation is conserving energy. Many coding problems will cause the simulation to not conserve energy, and so this check will detect them.

3.1.7 Reduced units

In order to make our simulations as general as possible, we run them in reduced units[101]. That is, all parameters are expressed in terms of more fundamental units, allowing equivalent simulations to be mapped to a range of physical systems. All quantities in the thesis will be written in units of distance, given by σ from the Lennard-Jones potential, energy, given by ε from the Lennard-Jones potential, and the particle mass, m. The dimensionless parameters are given below.

$x^* =$	x/σ	distance
$\Phi^* =$	Φ/ε	energy
$T^* =$	$k_B T/\varepsilon$	temperature
$t^* =$	$t\sqrt{\varepsilon/m\sigma^2}$	time
$\mathbf{v}^* =$	$\mathbf{v}\sqrt{m/\varepsilon}$	velocity
$\mathbf{p}^* =$	$\mathbf{p}\sqrt{1/\varepsilon m} = \mathbf{v}^*$	momentum
$\mathbf{F}^* =$	$\mathbf{F}\sigma/\varepsilon$	force

The * will be omitted in this thesis when referring to these quantities in the simulations.

3.2 Monte Carlo

As an alternative to generating particular distributions by allowing the simulation to come to equilibrium with a molecular dynamics simulation, we can select the configurations using the Metropolis Monte Carlo process[107]. A Monte Carlo algorithm starts with a given configuration, modifies it, and then accepts the modified result according to some rule. Appropriately selected, this acceptance criteria allows us to generate configurations from an equilibrium distribution[89].

For the Metropolis method the acceptance criteria is based on the energy of the configuration, as well as the equation describing the desired phase space distribution. If the modified configuration, l, has a lower energy than the configuration before it, i, the change is accepted. For a Boltzmann distribution, if the energy is increased, then the probability that the change will be accepted is equal to

$$p = \exp[\beta(\Phi(l) - \Phi(i))] \tag{3.4}$$

where $\Phi(l)$ is the potential energy of the modified state and $\Phi(i)$ is the potential energy of the previous state. This is calculated using the interparticle potential. This acceptance criteria is designed to preserve the equilibrium distribution. The configurations generated will converge to the Boltzmann distribution.

To accept the moves according to the given probability in Eq. (3.4) we select a random number from a uniform distribution spanning $[0, 1]$. If the random number is less than p than the move will be accepted. Otherwise the move is not accepted, and the previous position is used again. It is important to make sure that the random number generator used correctly samples the uniform distribution[101].

The modified configuration can be generated by moving one or more of the particle positions. The larger the change, the lower the probability that the move will be accepted, and so the lower the acceptance ratio. The acceptance ratio is the ratio between accepted moves and total moves tried. Larger accepted moves will sample the distribution more quickly. The most efficient acceptance ratio will differ with each program, but a ratio of 20% has been found to be quite efficient for a Lennard-Jones system[108]. In this thesis the moves will consist of moving one particle for each trial, selected at random. This ensures that the sampling of phase space will be ergodic[101].

Any starting configuration may be used for the Monte Carlo simulation. We will start with an FCC lattice. To properly sample the Boltzmann distribution the configuration must relax first. That is, the Monte Carlo process must be carried out for some time until the configurations are correctly sampling the Boltzmann distribution. To get independent configurations, a sufficient number of trials must be conducted between each configuration used.

3.3 Data Analysis

3.3.1 Frequency Histograms

As the ES-FT is written in terms of relative probabilities of the dissipation function, we need a method for calculating these in simulations. This is typically done by approximating the relative probabilities with relative frequencies.

The value of the dissipation function can be calculated for any trajectory. We can simulate an ensemble of trajectories, and calculate the value of the dissipation function for each one. For each value calculated we assign it to a histogram bin. The histogram is built up as we conduct the simulation. When enough trajectories are included, the relative frequencies become a good approximation to the relative probabilities of dissipation function values.

3.3.2 Fourier Transform

In this thesis we will be analysing the density distribution throughout a system. The density of the system is sampled over M different x-positions across the system. That is, the system is cut into M slices, and the average density is calculated in each slice. The density distribution of a function can be analysed using a discrete Fourier transform (DFT)[109]. This takes a series of data points and fits them to a sum of trigonometric functions. The number of functions is equal to the number of data points in the series. This allows the function to be fit to the data points exactly.

Our data points, $D_m(x_m)$, are fit to the function

$$D_m(x_m) = \frac{1}{M} \sum_{j=0}^{M-1} A_j e^{i2\pi jm/M} \tag{3.5}$$

which is written in terms of complex sinusoids,

$$e^{i2\pi jm/M} = \cos(2\pi jm/M) + i \sin(2\pi jm/M) \tag{3.6}$$

where M is the total number of data points. The coefficient of each of these sinusoids, A_j, is a complex number. Since all of our data points are real numbers, the real part of A_j will give the coefficient of the cosine functions and the imaginary part will give the coefficient of the sine functions. Each value of j corresponds to the coefficient for a sinusoid with different

frequency. To calculate the value of each coefficient from the data points we use the equation

$$A_j = \sum_{m=0}^{M-1} D_m(x_m) e^{-i2\pi jm/M}. \tag{3.7}$$

The values for j span from 0 to $M-1$. While there will be one complex coefficient, A_j, calculated for each data point, all the data points are real numbers, so we have $A_{M-j} = A_j^*$. Here, A_j^* denotes the complex conjugate of A_j. We can see that $A_{M/2}$ must be real valued, as its complex conjugate is equal to itself. We also know that A_0 is real, as $\sin(0) = 0$. The rest of the DFT is completely specified by $M/2 - 1$ complex coefficients.

Chapter 4

Dissipation in Monotonic and Non-monotonic Relaxation to Equilibrium

Relaxation to equilibrium is an essential phenomena in physics because the equilibrium state has many useful properties which make it easy to study. For instance, thermodynamics is only applicable in equilibrium. However, relaxation to equilibrium is an inherently nonequilibrium process, making it more difficult to study. The dissipation function has been shown to be a very useful tool in studying nonequilibrium systems[34, 59], and can be used in the Evans-Searles Fluctuation Theorem[11, 63], the Relaxation Theorem[19], the Second Law Inequality[12] and the Dissipation Theorem[17, 18] to monitor relaxation to equilibrium. This has been done computationally using a model of an optically trapped particle, in a system which relaxes non-monotonically towards equilibrium[38]. We will extend this area by computationally studying the relaxation process in a simpler field free system, and look at monotonic as well as non-monotonic relaxation scenarios. We will study the relaxation process using the dissipation function, as well as other more intuitive measures.

A particularly interesting feature of the Relaxation Theorem and Second Law Inequality is that they allow for non-monotonic relaxation. However, systems often relax monotonically. We will endeavor to construct a system which clearly displays non-monotonic relaxation.

4.1 Initial Conditions

A simple system for studying the relaxation process is a system of particles that begins with a non-uniform density distribution. We will model the relaxation of this system with molecular dynamics using a 2-dimensional fluid of WCA[87] particles with periodic boundary conditions[27]. The equations of motion are solved with a time step length of 0.001. The system begins in equilibrium with an applied perturbation to the potential. This non-uniform perturbation in the potential results in a density gradient across the system. This initial distribution can be generated using either Monte Carlo or molecular dynamics. Because the

system is in equilibrium initially the distribution function is known, which is a condition for calculating the form of the dissipation function. A number of different perturbations were used to study different relaxation processes.

4.2 Discrete Potential Step Perturbation

The first potential perturbation considered to generate the density gradient was a potential step.

$$H = H_0 + \sum_{i=1}^{N} U_{p,i} \tag{4.1}$$

$$U_{p,i} = h_0(1 - \Theta(x_i - b_L/2)) \tag{4.2}$$

where H is the energy of the system, H_0 is the internal energy, $U_{p,i}$ is the potential perturbation on each particle, Θ is the Heaviside step function and b_L is the periodic box length. The potential of all the particles on the left side of the box is perturbed by the step height, h_0. Since the derivative of the Heaviside step function is not finite, the force due to it would be an impulse in the equations of motion, and so it is easier to generate the initial distribution using the Monte Carlo method, described in Section 3.2. The added energy penalty for particles on the left side of the box will result in less moves being accepted that increase the density on the left side, resulting in a non-uniform density gradient. The system is in an equilibrium distribution.

4.2.1 Simulation Details

The simulation includes 256 particles with a density of 0.6 in a periodic box. The box length is determined from the density and number of particles. The temperature is set to 1.0 and the strength of the applied potential perturbation is set to $h_0 = 0.5$. An equilibrium state was reached by running the simulation for 10^7 trials from the initial FCC positions. From this point 10^8 trials (moves) were conducted to sample the distribution and calculate the density profile. The phase space position is sampled every 5,000th move.

4.2.2 Density Profile

The density of this equilibrium system will not be uniform because of this potential perturbation applied to the particles. We can study the density profile of the system by dividing our periodic box into slices and calculating an average density for each slice. The periodic box is split into 100 slices. The density as a function of position in the system is plotted in Figure 4.1.

We can see that the potential perturbation has caused a lower average density on the left hand side of the periodic box. It has also introduced significant fluctuations in density throughout the length of the system.

As an aside, we can predict the density profile of the system with the potential perturbation from equilibrium correlations of the density in a system with no potential perturbation.

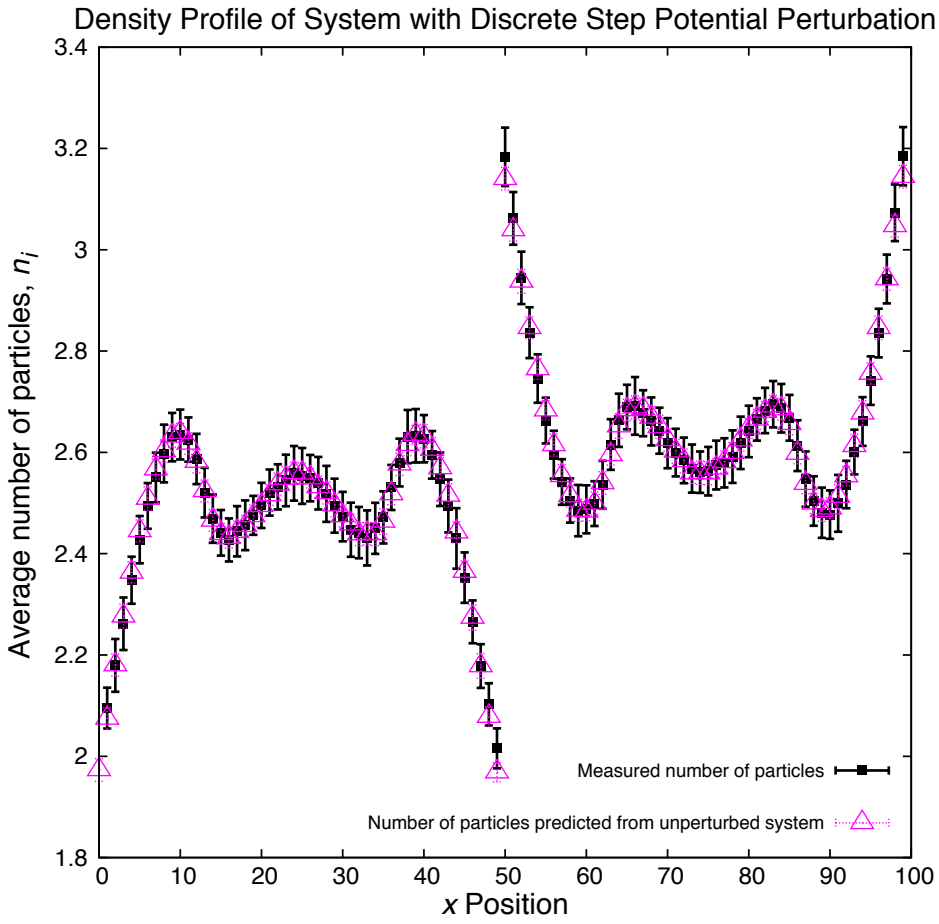

Figure 4.1: Average distribution of particles in the perturbed system as a function of x position, shown as black squares. The pink triangles show the predicted distribution from computer simulations of an unperturbed system, the RHS of Eq. (4.8). The x position is given as a percentage of the box length.

This kind of approach has been used in the past to predict properties of liquids from their density distribution under applied potential perturbations[110].

Let us divide up our periodic box into M slices, and let n_i be the number of particles in slice i. Now,

$$\langle n_i \rangle_\lambda = \int d\mathbf{\Gamma} f(\mathbf{\Gamma}, \lambda) n_i(\mathbf{\Gamma}) \tag{4.3}$$

where λ determines whether the potential perturbation is included in the equations of motion. For $\lambda = 0$ no perturbation is included, for $\lambda = 1$ the perturbation is the Heaviside step function with an amplitude of h_0 described in Eq. (4.2). Our equilibrium system is described by the Boltzmann distribution so,

$$\langle n_i \rangle_\lambda = \frac{\int d\mathbf{\Gamma} \exp[-\beta H(\mathbf{\Gamma}, \lambda)] n_i(\mathbf{\Gamma})}{\int d\mathbf{\Gamma} \exp[-\beta H(\mathbf{\Gamma}, \lambda)]}. \tag{4.4}$$

The energy of the system, H, can be split up into the energy from particles and particle interactions, H_0, and the energy due to the potential perturbation, $h(\mathbf{\Gamma})$,

$$H(\mathbf{\Gamma}, \lambda) = H_0(\mathbf{\Gamma}) + \lambda h(\mathbf{\Gamma}). \tag{4.5}$$

We can write the energy due to the perturbation as $h(\mathbf{\Gamma}) = h_0 \sum_{i=1}^{N} 1 - \Theta(x_i - b_L/2) = h_0 n_L$, where n_L is the number of particles on the left side of the box. Taking the derivative of Eq. (4.4) with respect to λ we have

$$\begin{aligned}
\frac{\partial \langle n_i \rangle_\lambda}{\partial \lambda} &= \frac{\int d\mathbf{\Gamma} - \beta h(\mathbf{\Gamma}) \exp[-\beta H(\mathbf{\Gamma}, \lambda)] n_i(\mathbf{\Gamma})}{\int d\mathbf{\Gamma} \exp[-\beta H(\mathbf{\Gamma}, \lambda)]} \\
&\quad - \frac{(\int d\mathbf{\Gamma} - \beta h(\mathbf{\Gamma}) \exp[-\beta H(\mathbf{\Gamma}, \lambda)]) \times (\int d\mathbf{\Gamma} n_i(\mathbf{\Gamma}) \exp[-\beta H(\mathbf{\Gamma}, \lambda)])}{(\int d\mathbf{\Gamma} \exp[-\beta H(\mathbf{\Gamma}, \lambda)])^2} \\
&= -\beta(\langle h n_i \rangle - \langle n_i \rangle \langle h \rangle) \\
&= -\beta h_0(\langle n_L n_i \rangle - \langle n_i \rangle \langle n_L \rangle).
\end{aligned} \tag{4.6}$$

To first order we have

$$\begin{aligned}
\langle n_i \rangle_1 - \langle n_i \rangle_0 &= \left. \frac{\partial \langle n_i \rangle_\lambda}{\partial \lambda} \right|_{\lambda=0} (1 - 0) \\
&= -\beta h_0(\langle n_L n_i \rangle_0 - \langle n_i \rangle_0 \langle n_L \rangle_0).
\end{aligned} \tag{4.7}$$

The subscripts of 0 here indicate that these averages are taken in the system with no perturbing potential. This allows us to write the average number of particles at each position in the perturbed system, in terms of correlation functions in the unperturbed system,

$$\langle n_i \rangle_1 = \langle n_i \rangle_0 - \beta h_0(\langle n_L n_i \rangle_0 - \langle n_i \rangle_0 \langle n_L \rangle_0). \tag{4.8}$$

The RHS of this equation was calculated using computer simulations and is included in the Figure 4.1, as a function of x position in the system. We can see that the density calculated from the unperturbed equilibrium system is within the error bars of the directly calculated density in the perturbed system.

4.2.3 Derivation of Dissipation Function

The dissipation function is helpful in studying the relaxation process. It is needed in the Relaxation Theorem[19] and the Dissipation Theorem[17, 18], both of which are applicable to systems relaxing to equilibrium. The form of the dissipation function for our system can be derived from its definition[10]

$$\Omega_t \equiv \ln\left(\frac{f(\mathbf{\Gamma},0)}{f(S^t\mathbf{\Gamma},0)}\right) - \int_0^t \Lambda(S^s\mathbf{\Gamma})ds, \tag{4.9}$$

where Ω_t is the integrated dissipation function, $f(\mathbf{\Gamma},0)$ is the phase space density of phase space position $\mathbf{\Gamma}$ at time 0, S^t is the natural time evolution operator and Λ is the phase space expansion factor. No perturbation is applied to the dynamics during the trajectory so the phase space expansion factor is determined by the thermostatted dynamics of the system. It is not affected by the initial perturbation, and so is given by its usual expression from the equations of motion, Eq. (2.4),

$$\Lambda = \beta\dot{H}_0$$

where $\beta = 1/k_BT$, k_B is Boltzmann's constant and $\dot{H}_0$ is the change in energy of the system, not including the energy from the potential step perturbation applied to generate the initial distribution. The initial canonical distribution is given by

$$f(\mathbf{\Gamma},0) = \frac{\exp[-\beta H(\mathbf{\Gamma})]}{\int d\mathbf{\Gamma}\exp[-\beta H(\mathbf{\Gamma})]} \tag{4.10}$$

where $H(\mathbf{\Gamma}) = H_0(\mathbf{\Gamma}) + h(\mathbf{\Gamma})$. Now the dissipation function is given by

$$\begin{aligned}
\Omega_t &= \ln\left(\frac{\exp\left[-\beta(H_0(\mathbf{\Gamma})+h(\mathbf{\Gamma}))\right]}{\exp\left[-\beta(H_0(S^t\mathbf{\Gamma})+h(S^t\mathbf{\Gamma}))\right]}\right) - \int_0^t \beta\dot{H}_0(\mathbf{\Gamma}(s))ds && (4.11)\\
&= \beta(h(S^t\mathbf{\Gamma}) - h(\mathbf{\Gamma})) && (4.12)\\
&= \beta h_0(n_L(S^t\mathbf{\Gamma}) - n_L(\mathbf{\Gamma})). && (4.13)
\end{aligned}$$

The integrated dissipation function is not continuous, since its value is determined by the number of particles on the left side of the system at the final and initial times, and there are a finite number of particles in the system. This means that its derivative, the instantaneous dissipation function will involve delta functions whenever a particle crosses from the right to the left, or vise versa. The Dissipation Theorem and Relaxation Theorem will be difficult to apply to a system with such a complicated form of the instantaneous dissipation function, making this seemingly simple system not an ideal candidate to study relaxation. A system with a continuous and smooth perturbing potential would be a more suitable choice.

4.3 Sine Potential Perturbation - Colour Field

For simplicity, the first continuous perturbation used was a sine curve as a function of x position.

$$U_{p,i} = \frac{a}{2} \sin\left(\frac{2\pi x_i}{b_L}\right) \tag{4.14}$$

where a determines the strength of the applied perturbation. Using a smooth continuous perturbation function is necessary for the resulting form of the dissipation function to be easy to work with. We studied a gentle relaxation process by using a colour field, applying a different perturbation to different particles in the system. Since the potential is smooth the initial distribution can be generated with molecular dynamics. The equations of motion used to set up the initial distribution are

$$\dot{\mathbf{q}}_i(t) = \frac{\mathbf{p}_i}{m}, \tag{4.15}$$

$$\dot{\mathbf{p}}_i(t) = \mathbf{F}_i(t) - \alpha p_{yi}\mathbf{j} + c_i\mathbf{F}_{p,i} - \mu, \tag{4.16}$$

$$\alpha = \frac{F_y \cdot p_y}{p_y \cdot p_y}, \tag{4.17}$$

$$\mu = \left(\sum_{i=0}^{N} c_i \mathbf{F}_{p,i}\right)/N, \tag{4.18}$$

$$\mathbf{F}_{p,i} = -\frac{\partial U_{p,i}}{\partial x}\mathbf{i} = -\frac{a\pi}{b_L}\cos\left(\frac{2\pi x_i}{b_L}\right)\mathbf{i}, \tag{4.19}$$

where $c_i = (-1)^i$ is the switch to control the colour of each particle. By using the colour field to set up the initial distribution, both colours of particles will have a density gradient across the system, but the total density distribution will be relatively uniform, allowing for gentle relaxation.

The term μ is added to keep the total momenta of the system zero. The applied colour field may exert more force to the system as a whole to one direction or another, depending on the position of the particles. This term effectively moves the reference frame of the simulation with the system.

Once the initial distribution has been set up, the system is allowed to undergo field free relaxation, with an isokinetic thermostat. The equations of motion are the same as for the setup, but c_i is zero. The thermostat is only applied in the y direction so that it does not interfere with the relaxation of the density gradient in the x direction in an unphysical way.

4.3.1 Density Profile

We can visualize the initial distribution of the system by creating a histogram of the x positions of the particles from a number of repetitions of the simulation. An ensemble of 10^6 trajectories was used. From this we can calculate the average particle density in each part of the system, shown in Figure 4.2. The strength of the perturbing potential was determined by $a = 2.5$.

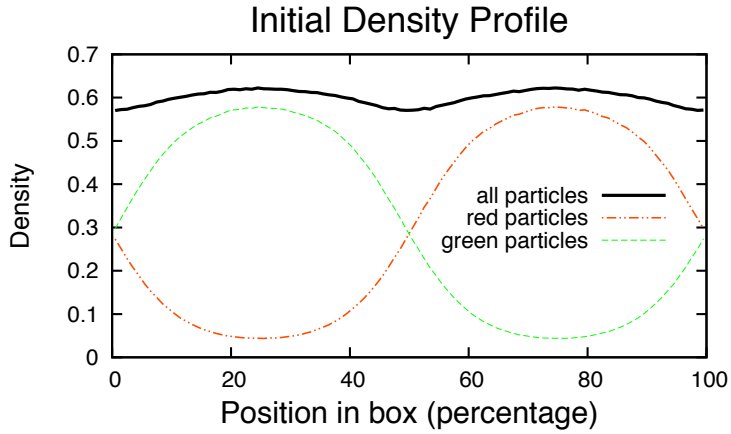

Figure 4.2: Average density in the system as a function of x position. A sine potential perturbation was applied to the equations of motion of the particles to generate this distribution, seen in Eq. (4.19) with $a = 2.5$.

4.3.2 Derivation of Dissipation Function

From the equations of motion for the relaxing system and the initial distribution we can derive the form of the dissipation function in the same way as was done for the discrete potential step system. From Eq. (4.12) we have

$$\Omega_t = \beta(h(S^t\mathbf{\Gamma}) - h(\mathbf{\Gamma})). \tag{4.20}$$

For this system the potential due to the perturbation is

$$h(S^t\mathbf{\Gamma}) = \sum_{i=1}^{N} c_i \frac{a}{2} \sin\left(\frac{2\pi x_i(t)}{b_L}\right) \tag{4.21}$$

where $x_i(t)$ is the x coordinate of particle i at time t. The dissipation function is now given by

$$\Omega_t = \beta\frac{a}{2}\left(\sum_{i=1}^{N} c_i \sin\left(\frac{2\pi x_i(t)}{b_L}\right) - \sum_{i=1}^{N} c_i \sin\left(\frac{2\pi x_i(0)}{b_L}\right)\right). \tag{4.22}$$

The streaming derivative of this gives us the instantaneous dissipation function

$$\Omega(S^t\mathbf{\Gamma}) = \frac{\beta a\pi}{mb_L}\left(\sum_{i=1}^{N} c_i p_{x_i}(t) \cos\left[\frac{2\pi x_i(t)}{b_L}\right]\right) \tag{4.23}$$

where p_{x_i} is the x component of the momenta of particle i and m is the particle mass. We can monitor the relaxation process with the dissipation function, and expect the integrated dissipation function to obey the Second Law Inequality.

4.3.3 Relaxation

From our initial distribution generated with the perturbed equations of motion we can set c_i to zero for all values of i to study field free relaxation. We can monitor the density distribution as the system relaxes. An ensemble of 10^6 trajectories was simulated for 5×10^4 time steps over the relaxation process. A sample of density profiles of the system at different points in time are shown in Figure 4.3. We can see that the total density relaxes to a uniform distribution quickly. The distributions of each colour appear to relax to sine curves, whose amplitude decreases with time.

To quantify our study of the relaxation process we can preform a least squares fit[111] of these density distribution graphs to a sine curve of fundamental wavelength. That is, we fit the difference between the colour density and the average colour density, as a function of position, to the equation

$$D = A \sin\left(\frac{2\pi x}{b_L}\right) \tag{4.24}$$

to give the amplitude of the sine wave, A, which is plotted against time in Figure 4.4. We used the density of the green particles, where $c_i = -1$. The average colour density is given by $\rho/2$. As expected, the density approaches a uniform distribution as the relaxation time approaches infinity.

We can also monitor the relaxation of the system by calculating the value of the instantaneous dissipation function throughout the relaxation process, seen in Figure 4.5. Initially the average value of the dissipation function is zero because the distribution is even in the momenta, since it is an equilibrium distribution under the potential perturbation. The integral of the instantaneous dissipation function approaches its equilibrium value monotonically. We know from the Relaxation Theorem that if the deviation function in the distribution relaxes conformally then the average dissipation function relaxes monotonically[19], as discussed in Section 2.10.1. The density distribution graphs in Figure 4.3 appear to relax conformally, so this monotonic behaviour of the dissipation function is expected. We can also observe from Figure 4.5 that since the average of the instantaneous dissipation function is always positive, the average integrated dissipation function is always greater than zero, satisfying the Second Law Inequality.

The Dissipation Theorem, described in Section 2.9, relates a phase function's average value to its transient correlation function with the instantaneous dissipation function. We can demonstrate the Dissipation Theorem in this system, using the instantaneous dissipation function as the argument. From Eq. (2.62) the Dissipation Theorem becomes

$$\langle \Omega(S^t \mathbf{\Gamma}) \rangle = \int_0^t \langle \Omega(\mathbf{\Gamma}) \Omega(S^s \mathbf{\Gamma}) \rangle ds. \tag{4.25}$$

The RHS of Eq. (4.25) is included in Figure (4.5) and a close agreement is seen between the average of the dissipation function and the integral of the correlation function, demonstrating the Dissipation Theorem in this relaxing system.

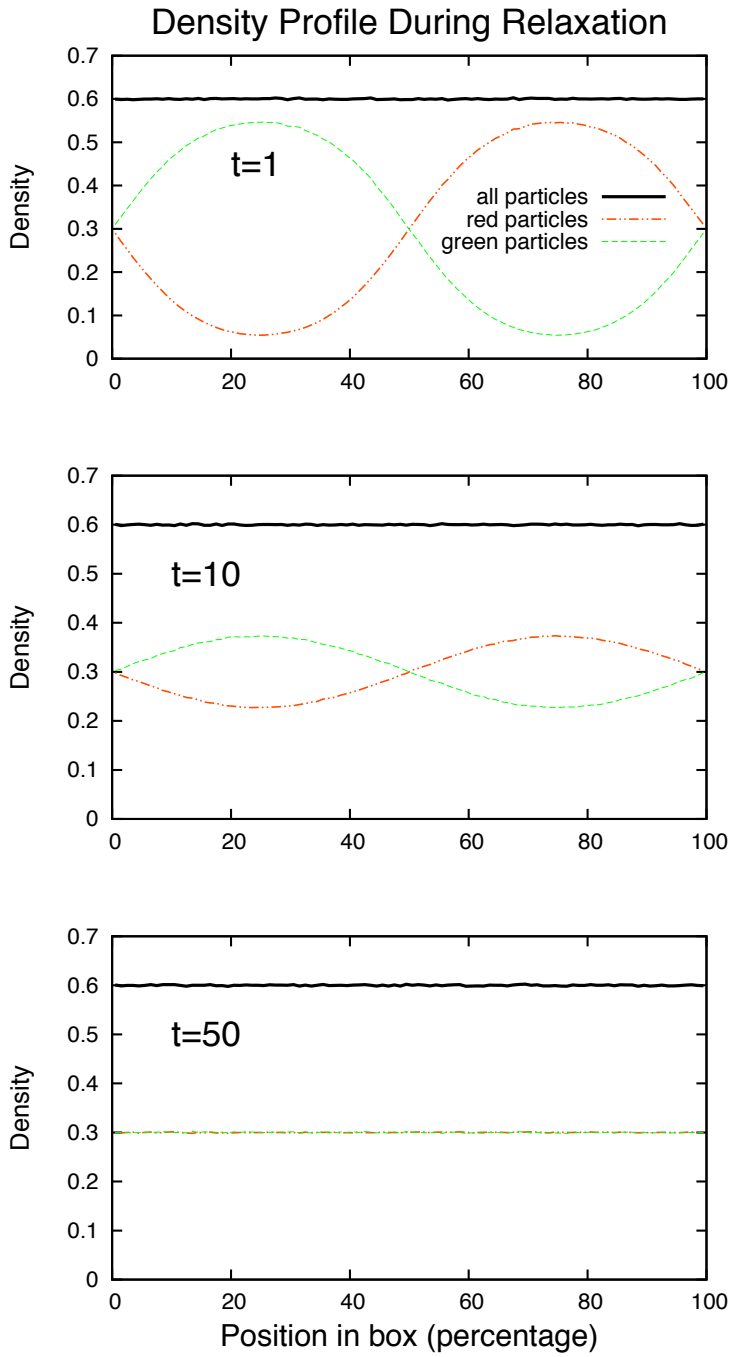

Figure 4.3: A sample of density profiles as the system relaxes. The density profile of both colours is shown (in red and green), as well as the total density profile in black.

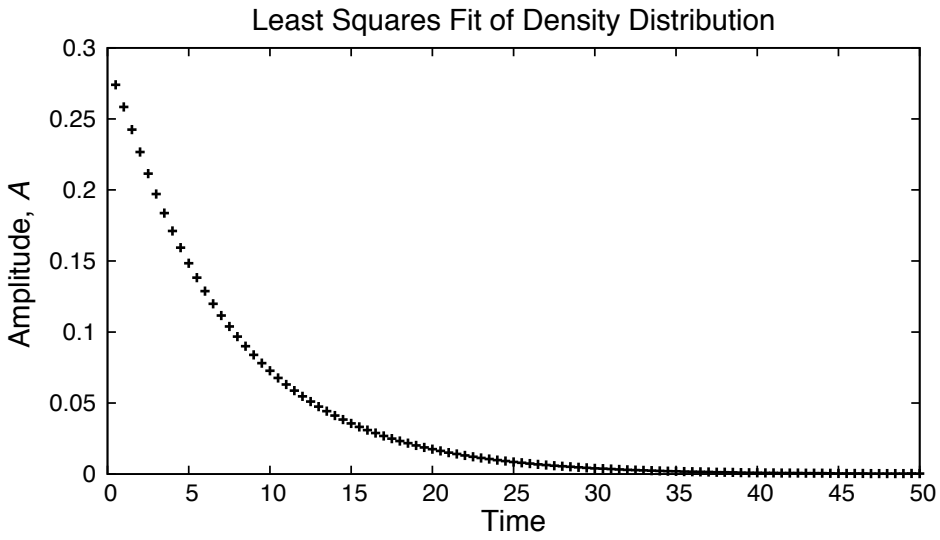

Figure 4.4: Least squares fit of the density distributions of the green particles to a sine curve with wavelength equal to the box length. The amplitude of the least squares fit is plotted against time as the system relaxes.

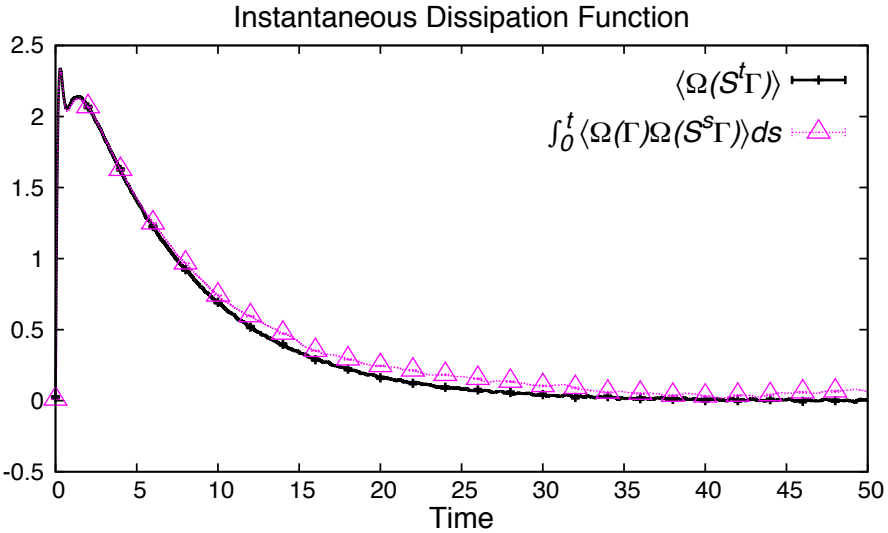

Figure 4.5: Average value of the instantaneous dissipation function, shown as black ticks, calculated along the relaxation process. The integral of the autocorrelation function of the dissipation function is included as pink triangles to demonstrate the Dissipation Theorem. Note that the error bars cannot be seen on this scale.

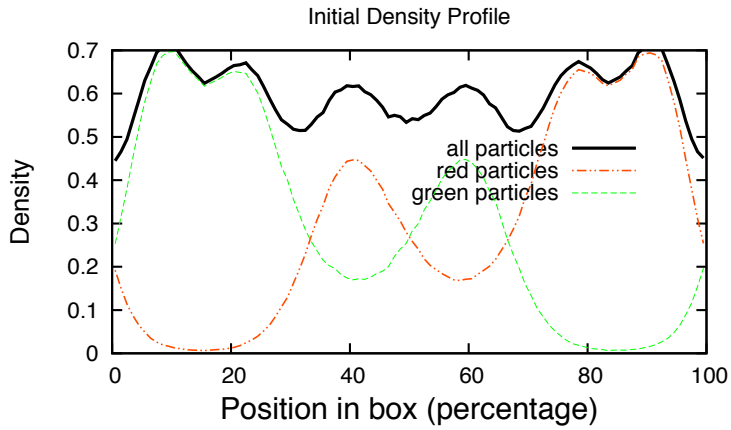

Figure 4.6: Distribution generated by perturbing the equations of motion with a potential equal to the sum of two sine curves, Eq. (4.26). The total density distribution is shown in black, and the two colours shown in red and green.

4.4 More Complex Potential Perturbation - Colour Field

To look at more complex relaxation a sum of two sine functions was used as the perturbation on the potential to generate the initial distribution.

$$U_{p,i} = \frac{a}{2}\left(\sin\left(\frac{2\pi x_i}{b_L}\right) + \sin\left(\frac{4\pi x_i}{b_L}\right)\right). \tag{4.26}$$

The equations of motion used were the same as in Eqs. (4.15)-(4.18) but with the force due to the perturbation given by

$$\mathbf{F}_{p,i} = -\frac{a\pi}{b_L}\left(\cos\left(\frac{2\pi x_i}{b_L}\right) + 2\cos\left(\frac{4\pi x_i}{b_L}\right)\right)\mathbf{i}. \tag{4.27}$$

4.4.1 Density Profile

The initial distribution can be seen in Figure 4.6. The strength of the perturbation is given by $a = 2.5$. We can see that the distribution of each colour is more complex, and the total density distribution is far from uniform.

4.4.2 Dissipation Function

The integrated dissipation function is the same as in Eq. (4.20) with the new form of $\mathbf{F}_{p,i}(x)$. This leads to

$$\begin{aligned}\Omega_t &= \beta\frac{a}{2}\left(\sum_{i=1}^{N} c_i\left(\sin\left(\frac{2\pi x_i(t)}{b_L}\right) + \sin\left(\frac{4\pi x_i(t)}{b_L}\right)\right)\right) \\ &\quad -\beta\frac{a}{2}\left(\sum_{i=1}^{N} c_i\left(\sin\left(\frac{2\pi x_i(0)}{b_L}\right) + \sin\left(\frac{4\pi x_i(0)}{b_L}\right)\right)\right).\end{aligned} \tag{4.28}$$

The instantaneous dissipation function is given by the streaming derivative,

$$\Omega(S^t\mathbf{\Gamma}) = \frac{\beta a\pi}{mb_L}\left(\sum_{i=1}^{N} c_i p_{x_i}(t)\left(\cos\left[\frac{2\pi x_i(t)}{b_L}\right] + 2\cos\left[\frac{4\pi x_i(t)}{b_L}\right]\right)\right). \tag{4.29}$$

4.4.3 Relaxation

We let the system relax from the initial distribution in the same way as above. An ensemble of 10^6 trajectories was simulated for 5×10^4 time steps. Examples of the density distributions throughout the relaxation process are shown in Figure 4.7, and the dissipation function is plotted in Figure 4.8. We can see that the total density relaxes quickly to a uniform distribution, while the density of each colour remains fairly complex, before apparently relaxing to a sine curve of fundamental period. This sine curve then decays conformally. At long time both colours relax to a uniform distribution. Again the instantaneous dissipation function starts at zero, before increasing rapidly and then decaying monotonically.

In order to quantitatively monitor the relaxation we do a least squares fit of the green particles density distribution to the sum of two sine waves. The density distribution function at each time is fit to an equation of the form

$$D = A_1 \sin\left(\frac{2\pi x}{b_L}\right) + A_2 \sin\left(\frac{4\pi x}{b_L}\right). \tag{4.30}$$

The parameters, A_1 and A_2 are plotted against time in Figure 4.9. We can see that the shorter period component decays faster. We fit each series in Figure 4.9 to an exponential function, which gave the equations of best fit $A_1 = 0.225\exp[-0.142t]$ and $A_2 = 0.259\exp[-0.574t]$. The amplitude of the second harmonic decays four times as fast as the amplitude of the fundamental. This is what is expected from the solution to the diffusion equations[112].

4.5 Approximate Square Wave Potential Perturbation - Colour Field

To study a system similar to what would be generated by applying a colour potential step perturbation to the equations of motion we can perturb the potentials of each colour with an approximate square wave. This was done using a finite number of terms of the Fourier decomposition of a square wave,

$$U_{p,i} = \frac{4a}{\pi}\sum_{n=1,3,5\ldots}^{11}\left(\frac{1}{n}\sin\left(\frac{2\pi n x_i}{b_L}\right)\right) \tag{4.31}$$

which is displayed graphically in Figure 4.10.

The force due to the perturbation is given by

$$\mathbf{F}_{p,i} = -\frac{8a}{b_L}\sum_{n=1,3,5\ldots}^{11}\left(\cos\left(\frac{2\pi n x_i}{b_L}\right)\right)\mathbf{i}. \tag{4.32}$$

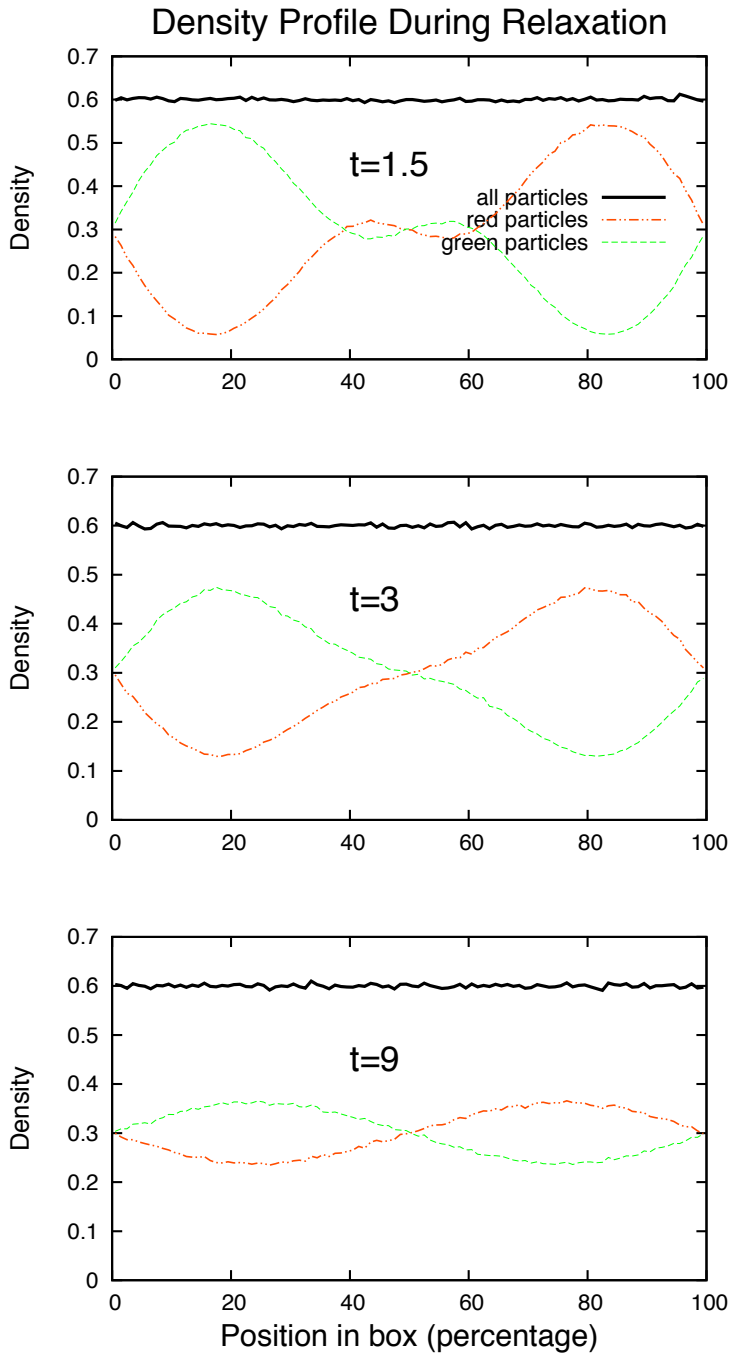

Figure 4.7: Relaxation of the system from a distribution generated by a perturbation that was the sum of two sine curves. Density distributions of each colour, as well as the total density are shown for a selection of times along the relaxation process.

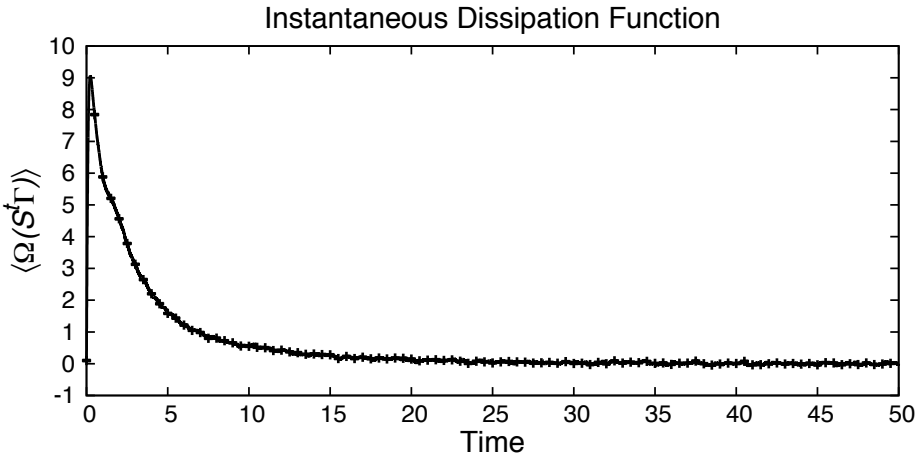

Figure 4.8: The instantaneous dissipation function calculated throughout the relaxation process. Initially the system was in the distribution generated by allowing it to come to equilibrium with the equations of motion perturbed by the potential in Eq. (4.26).

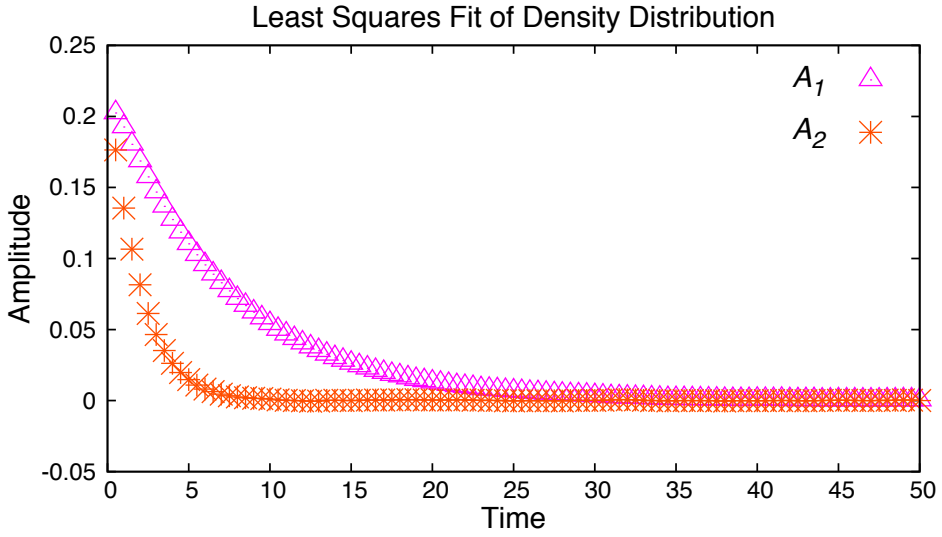

Figure 4.9: A least squares fit of the density distribution of the green particles to the sum of two sine curves, Eq. (4.30). Both amplitudes are plotted, where A_1 is the amplitude of the sine curve of fundamental wavelength, and A_2 is the amplitude of the shorter wavelength component.

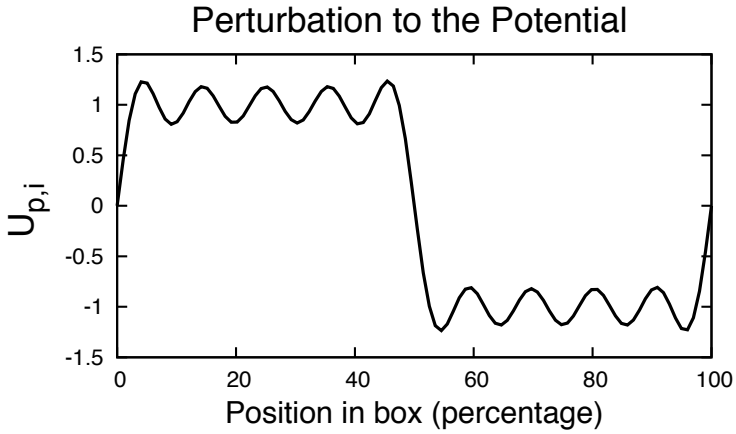

Figure 4.10: Approximate square wave used to perturb the equations of motion to generate the initial distribution (here the amplitude is determined by $a = 1$).

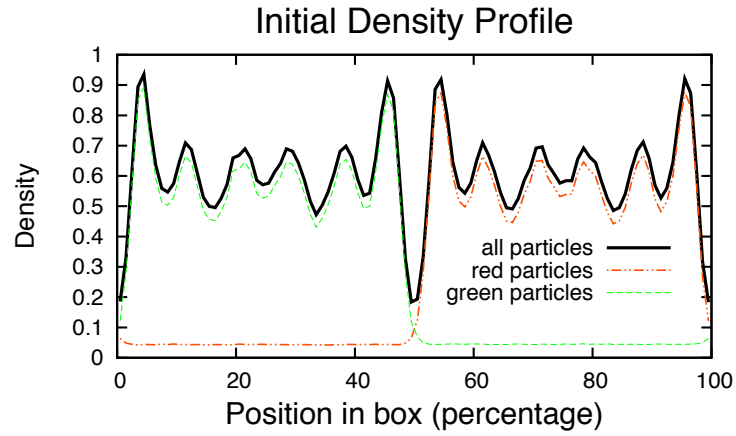

Figure 4.11: Initial density profile distribution of the system generated from the approximate square wave. The total density is in black, and each colour is shown in red and green.

4.5.1 Density Profile

A graph of the initial density distribution generated using the approximate square wave potential perturbation is shown in Figure 4.11. The two colours are almost completely separated on each side of the box, with a non-uniform density on each side. The simulation was carried out with the amplitude of the perturbation determined by $a = 2.5$ in Eq. (4.32) and an ensemble of 10^4 trajectories was used.

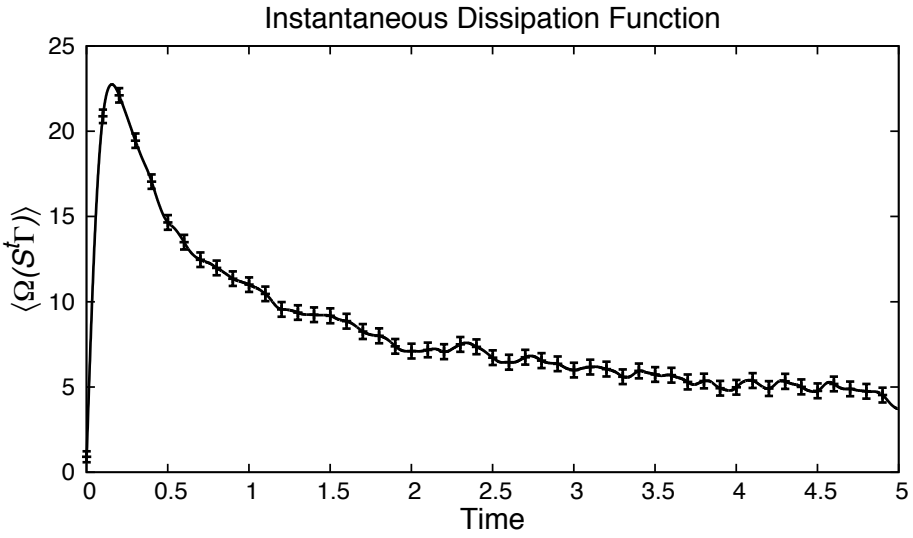

Figure 4.12: The ensemble average of the instantaneous dissipation function calculated as the system relaxes from a non-uniform initial density generated using an approximate square wave applied to each colour.

4.5.2 Dissipation Function

The dissipation function is derived in the same way as described above, leading to an instantaneous dissipation function of

$$\Omega(S^t\mathbf{\Gamma}) = \frac{8\beta a}{mb_L}\left(\sum_{i=1}^{N} c_i p_{x_i}(t)\left(\sum_{n=1,3,5\ldots}^{11}\cos\left(\frac{2\pi n x}{b_L}\right)\right)\right). \tag{4.33}$$

4.5.3 Relaxation

The path integral of the dissipation function again approaches its equilibrium value monotonically, seen in Figure 4.12.

A sample of density distribution profiles from the relaxation process are shown in Figure 4.13. We can see that the total density relaxes to a uniform distribution before the distribution of individual colours appears to relax to sine curves of fundamental wavelength.

As the density distributions are more complicated, the easiest way to monitor them quantitatively is to preform a discrete Fourier transform on each distribution, and then plot each component with time. The discrete Fourier transform fits the density distribution to an equation of the form

$$D = \sum_{i=1}^{M} A_i \sin\left(\frac{2i\pi x}{b_L}\right) + B_i \cos\left(\frac{2i\pi x}{b_L}\right). \tag{4.34}$$

An overview of discrete Fourier transforms and how these components, A_i and B_i, are calculated is presented in Section 3.3.2. A selection of the components are shown in Figure 4.14. We can see that the higher frequencies generally decay faster than the lower ones.

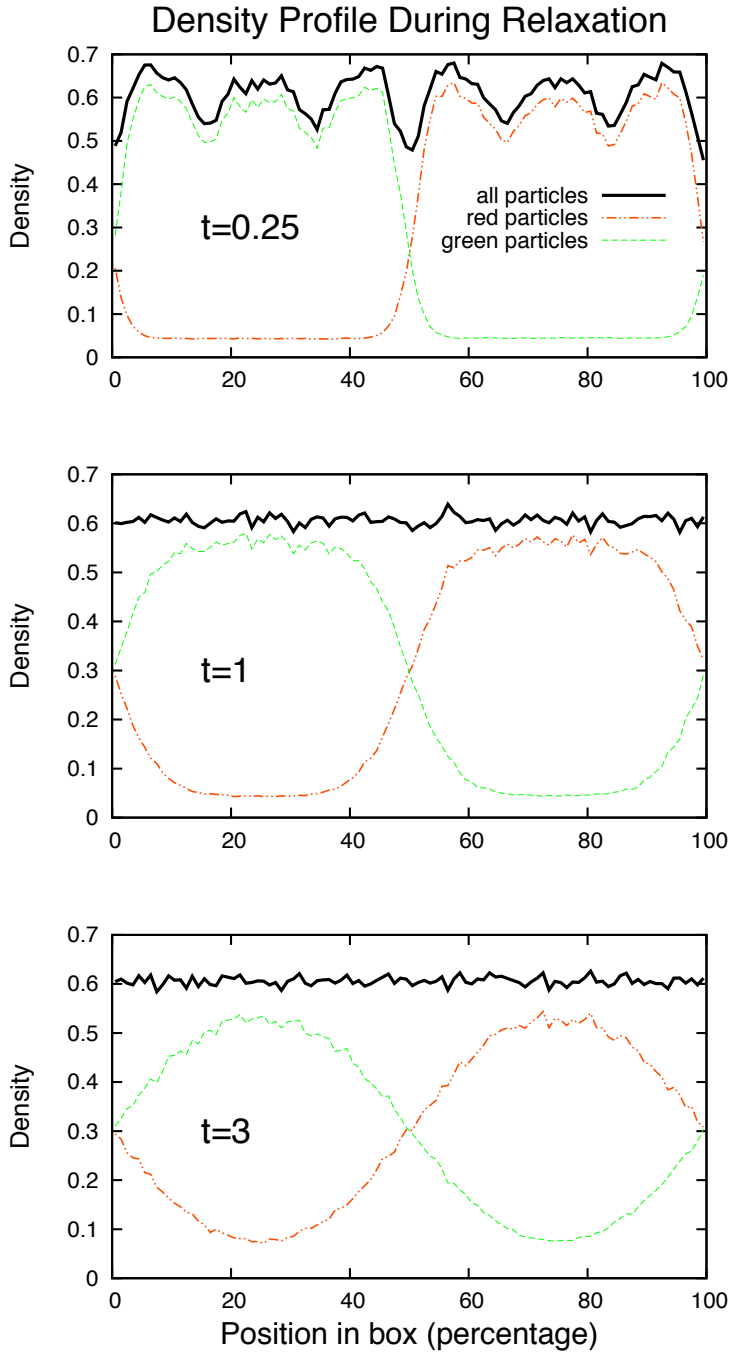

Figure 4.13: A sample of density distributions along the relaxation process.

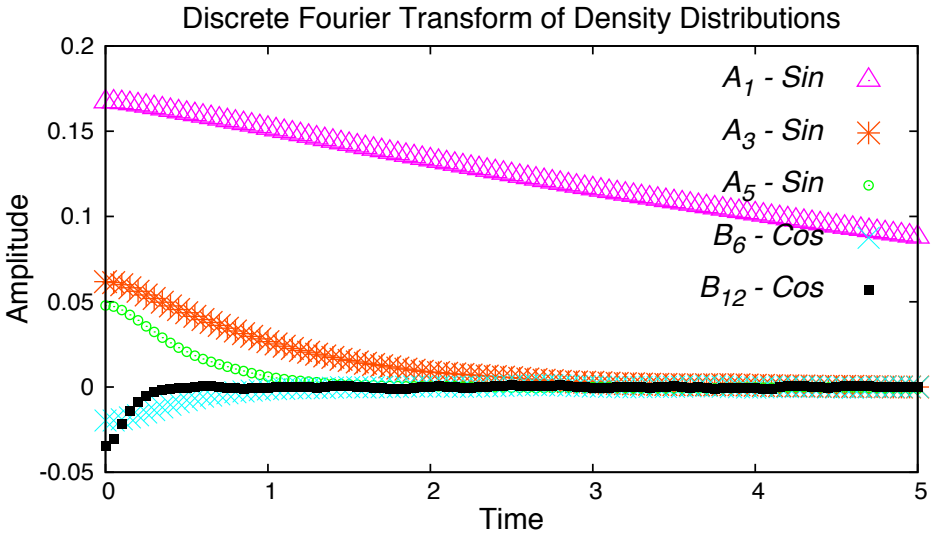

Figure 4.14: A selection of the most significant components from the discrete Fourier transform of the density distribution as the system relaxes.

4.6 Approximate Square Wave Potential Perturbation Applied to All Particles

To study a more dramatic relaxation process we used the same approximate square wave perturbation, but applied it to every particle. That is, we use the form of $\mathbf{F}_p$ given in Eq. (4.32) and Figure 4.10 but let $c_i = 1$ for all particles in the equations of motion, Eqs. (4.15)-(4.18).

4.6.1 Density Profile

This non-colour field perturbation results in a large density gradient across the system, and a very non-uniform initial distribution, seen in Figure 4.15. The size of the perturbation is determined by $a = 2.5$.

4.6.2 Dissipation Function

The dissipation function has the same form given by Eq. (4.33), but with $c_i = 1$ for all particles.

4.6.3 Non-Monotonic Relaxation

The relaxation of the density distribution in time is fairly complex, seen in Figure 4.16, and we will again use a DFT to analyze it. A few key components can be seen in Figure 4.17. We can see that the relaxation process is complex, and that each component does not simply decay exponentially, and so can not be described by the diffusion equations. A particularly interesting component, the first sine component, A_1 is plotted separately in Figure 4.18. We can see that it displays non-monotonic relaxation, as the amplitude approaches zero, it

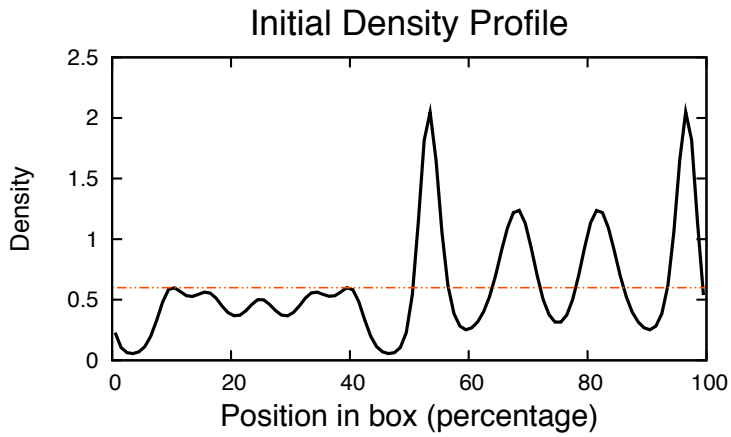

Figure 4.15: Initial density distribution generated by perturbing the equations of motion by an approximate square wave potential applied to every particle. The total density as a function of position is shown in black, and the red line shows the average density within the system.

"bounces", passing through zero a number of times before finally relaxing to it. This means that at times, the density is moving away from a uniform distribution.

Figure 4.19 displays the calculated instantaneous dissipation function of the system, which also shows complex relaxation. The points where the instantaneous dissipation function is zero correspond to the stationary points in the first component of the density distribution; there is instantaneously approximately no change in the distribution. While the instantaneous dissipation function is not always positive in this system, the integrated dissipation function, shown in Figure 4.20, is always greater than zero. This is consistent with the Second Law Inequality. We can also observe from this plot that the dissipation function approaches its equilibrium value non-monotonically.

We can use the dissipation function to demonstrate the Dissipation Theorem in this system, and again we see a good agreement between the average and the autocorrelation function, also plotted in Figure 4.19.

4.7 Conclusion

Field free relaxation was studied in systems relaxing from a non-uniform initial density, monitored using both density distributions and the dissipation function. When this density gradient was in coloured particles the density distribution decayed to a sine curve of fundamental wavelength, which then decayed conformally towards a uniform distribution. The dissipation function decayed towards its equilibrium value monotonically, consistent with the predictions of the Relaxation Theorem for a conformally relaxing system. When the system was initiated with a more dramatic density gradient non-conformal relaxation was seen in both the dissipation function and the Fourier components of the density distribution. At times, the system appeared to be moving away from a uniform density distribution. In both cases, the Second Law Inequality was satisfied, and the Dissipation Theorem demonstrated.

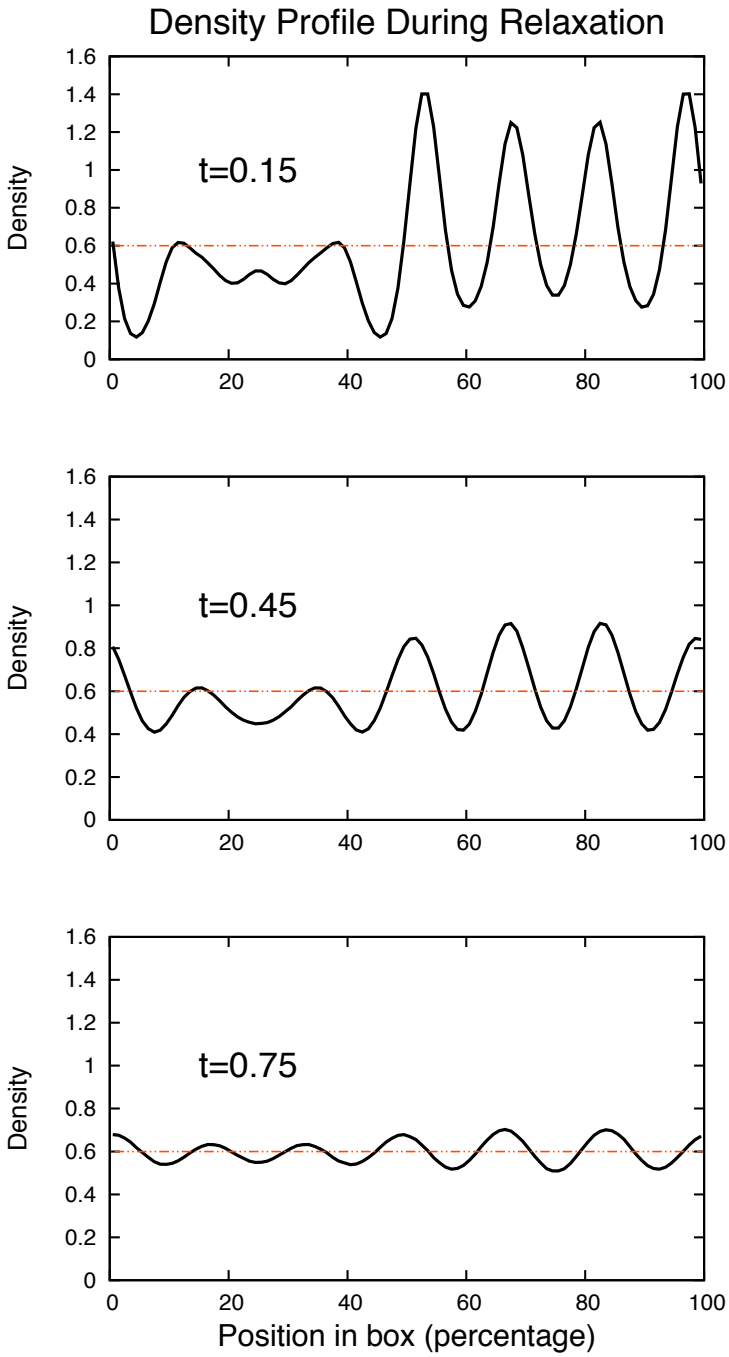

Figure 4.16: Density distributions of the system as it relaxes. Each plot is shown on the same scale for comparison.

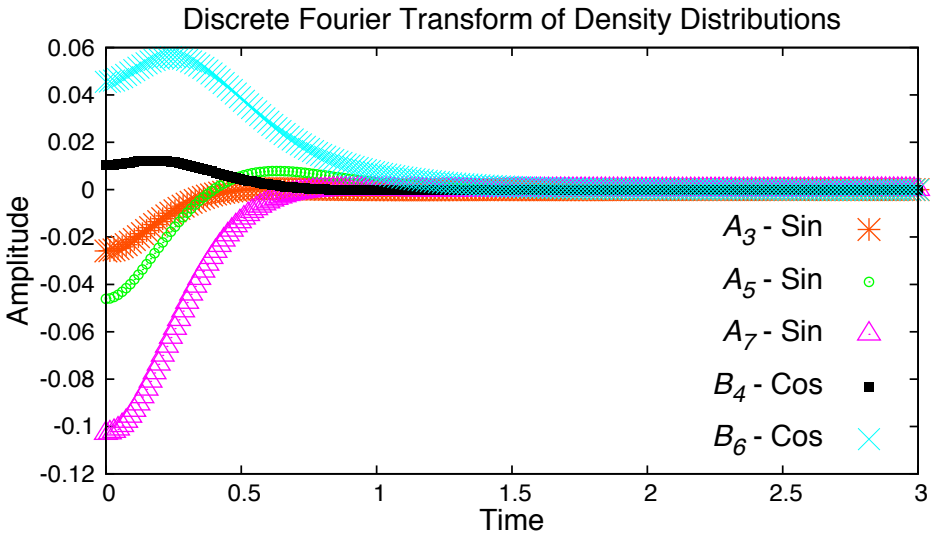

Figure 4.17: A selection of components of the discrete Fourier transform of the density distribution throughout the relaxation process.

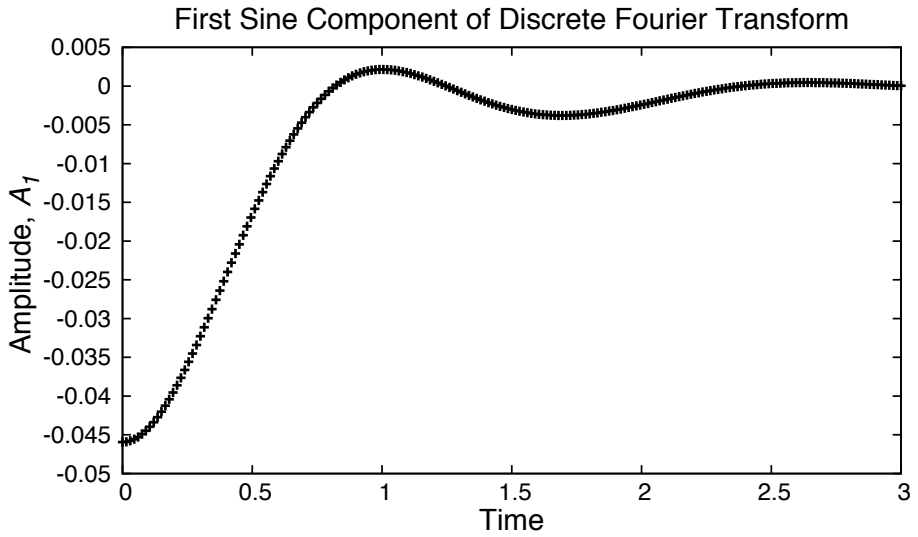

Figure 4.18: Amplitude of the first sine component of the discrete Fourier transform as the system relaxes with time.

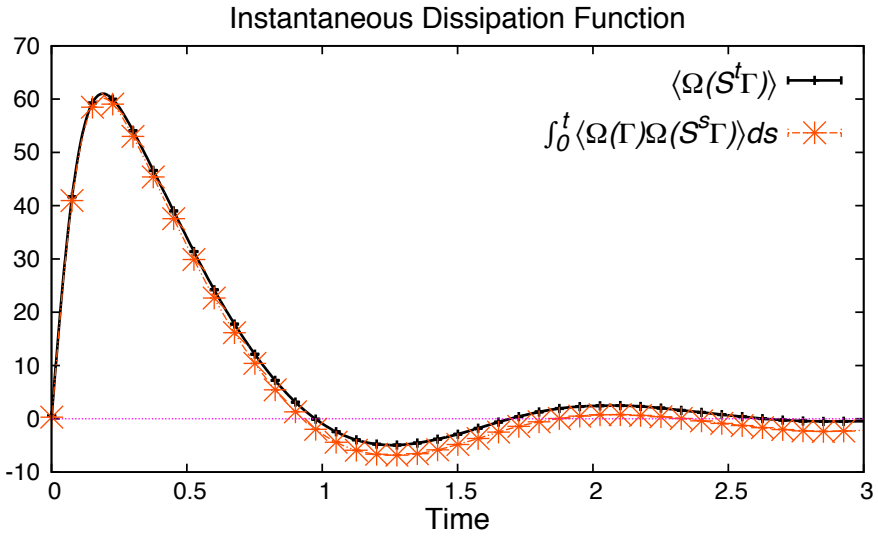

Figure 4.19: Value of the instantaneous dissipation function as the system relaxes towards equilibrium, seen in black. The form of the dissipation function is given in Eq. (4.33) with $c_i = 1$ for all particles. An average dissipation of zero is marked by the dotted pink line. The integral of the autocorrelation function, which is predicted by the Dissipation Theorem to be equal to the average of the dissipation function, is shown in orange crosses. Note the error bars cannot be seen on this scale.

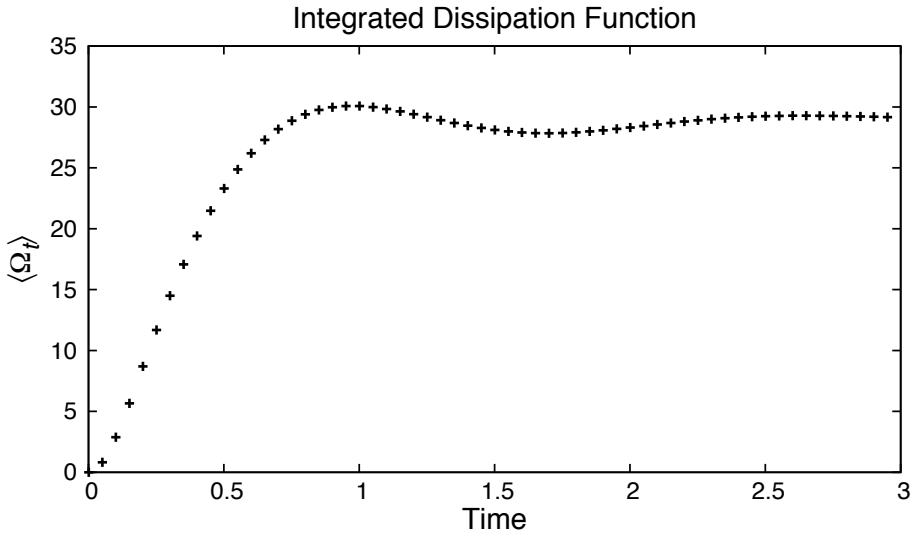

Figure 4.20: The ensemble average of the integrated dissipation function plotted over the relaxation process.

Chapter 5

Mechanism for Asymmetric Bias in the NPI

The Nonequilibrium Partition Identity (NPI) is an exact relationship in nonequilibrium statistical mechanics involving the dissipation function. It is a result of the Evans-Searles Fluctuation Theorem and its derivation is included above in Section 2.6. The NPI can be useful as a diagnostic tool in computer simulations and experiments. This is because its value is known for all systems, and is sensitive to errors in the measurement of the dissipation function[21]. It can also be used to determine if phase space sampling in an experiment has been sufficient. The NPI takes the form of an ensemble average of an exponential function,

$$\langle e^{-\bar{\Omega}_t t} \rangle = 1 \tag{5.1}$$

where $\bar{\Omega}_t$ is the time average of the dissipation function over a trajectory of length t. This average is slow to converge when the average of the exponent is not similar to the natural log of the average of the exponential function[44]. The NPI often appears to converge to a value lower than one[27].

Just as the NPI is derived from the ES-FT, the well known Jarzynski Equality(JE)[73, 74] can be derived from the Crooks Fluctuation Theorem[71, 72], another exact result in nonequilibrium statistical mechanics. The JE is mathematically the same as the NPI if it is written in terms of the purely irreversible work. Collectively the JE and NPI are known as summing rules or integral fluctuation theorems. There has been immense interest in these types of summing rules over the past 10-15 years[51, 52, 53, 54, 55, 56, 57, 44, 45, 46, 47, 48, 49, 50, 31, 32], however there has been no detailed analysis of how the rare events contribute to the ensemble average. We will conduct our analysis on the NPI, however it should be directly applicable to the JE.

In this chapter we will consider alternative descriptions of the ensemble average in question in the NPI, and analyse the rare events involved in calculating this average.

5.1 Alternative Derivation

The NPI exhibits vastly different behaviour when its value is derived assuming full ensemble averaging, when compared to approximating the distribution with a Dirac-delta function. Using the ES-FT we can prove that the NPI has a value of unity, where we assume infinite sampling of the distribution. However, we also expect that the mean of $\bar{\Omega}_t$ will be constant in t, while the standard deviation will scale with $1/\sqrt{t}$ for long enough durations. As such, at long times we can approximate the distribution of $\bar{\Omega}_t$ with a Dirac-delta distribution. Using this approximation the value of the NPI will be

$$\left\langle \exp[-\bar{\Omega}_t t] \right\rangle = \int_{-\infty}^{\infty} dA Pr(\bar{\Omega}_t = A) \exp[-At], \tag{5.2}$$

$$\int_{-\infty}^{\infty} dA \delta\left(A - \left\langle \bar{\Omega}_t \right\rangle\right) \exp[-At] = \exp\left[-\left\langle \bar{\Omega}_t \right\rangle t\right]. \tag{5.3}$$

This means that given enough time the measured NPI will be related to a transport coefficient. In the case of colour conductivity this will be the self-diffusion coefficient,

$$D = \frac{N-1}{N} \frac{1}{\beta\rho} \lim_{t\to\infty} \lim_{F_{ex}\to 0} \frac{\langle J(t) \rangle}{F_{ex}}, \tag{5.4}$$

where

$$\lim_{t\to\infty} \left\langle \bar{\Omega}_t \right\rangle = \beta \left\langle J(t) \right\rangle V F_{ex} \tag{5.5}$$

as the system approaches a steady state. So the value of the NPI is given by

$$\left\langle \exp[-\bar{\Omega}_t t] \right\rangle = \exp\left[-DF_{ex}^2 \beta^2 V \rho \frac{N}{N-1} t\right] \tag{5.6}$$

as the trajectory length goes to infinity and the field strength goes to zero. This is clearly not equal to the value of unity required by the ES-FT.

The reason for this discrepancy is because it is inappropriate to apply the fluctuation theorem to a distribution that can be described by a delta function. The definition of the dissipation function requires that the system is ergodically consistent, that is if $f(\Gamma, 0) \neq 0$ then $f(M^T S^t \Gamma, 0) = f(S^t \Gamma, 0) \neq 0$. This means that if there is a finite likelihood of observing a dissipation function value of $\bar{\Omega}_t = A$, then there must also be a non-zero probability of observing the value $\bar{\Omega}_t = -A$. While our system is ergodic in principle, since the value of the NPI can be calculated at the value given by the ES-FT with enough sampling, it may not be ergodic in practice. We may not be able to observe any antitrajectories for each trajectory observed given the time available to conduct simulations. In this chapter we will study systems where the value of the NPI is given by the Dirac-delta function approximation, systems where its value is given by the ES-FT, and the intermediate region where neither regime describes the system. Simulations that fall into the first category are studied in detail below is section 5.8.

5.2 Difficulty of Calculation

The NPI can be calculated for any system, experimental or computational, where the path integral of the dissipation function can be measured for an ensemble of trajectories. Practically, the ensemble average can be calculated by summing $e^{-\bar{\Omega}_t t}$ for each trajectory and dividing the sum by the total number of ensemble members. We can also calculate this average by writing it as an integral,

$$\langle e^{-\bar{\Omega}_t t} \rangle = \int_{-\infty}^{\infty} Pr(\bar{\Omega}_t = A) e^{-At} dA \tag{5.7}$$

where $Pr(\bar{\Omega}_t = A)$ is the probability distribution of the time averaged dissipation function. This form has the advantage that large values for the sum of $e^{-\bar{\Omega}_t t}$ don't need to be stored, as well as making difficulties in the calculation process easier to identify.

The probability distribution of the dissipation function can be approximated by a Gaussian distribution in low field systems. The Gaussian distribution that satisfies the fluctuation theorem has a variance twice the value of the mean[113]. This distribution will satisfy the NPI relationship by construction. To understand the calculation of the ensemble average using the integral in Eq. (2.43) we can use a Gaussian distribution, shown in Figure 5.1 as the solid line, as a substitute for the probability distribution of the dissipation function.

To calculate the integrand in Eq. (2.43) we multiply the probability distribution in Figure 5.1 by the exponential of the negative dissipation function value multiplied by time. This is plotted in Figure 5.2 as the solid line. We can see that distribution is peaked mostly on negative values of A, even though these values of the dissipation function are very unlikely. This is due to the large value of the exponential function at very negative values of A. The NPI is calculated by integrating the function shown in Figure 5.2.

The Gaussian distribution has no noise associated with it, resulting in a smooth distribution when it is multiplied by e^{-At}. However, in a real system we approximate the probability distribution using a frequency histogram, which we would expect to be noisy, particularly in the wings of the distribution.

We will calculate a histogram of dissipation function values using simulation results from a colour conductivity system where a colour field is applied to all particles. We will use a field strength of 0.71 and a trajectory length of 19,100 time steps. The other parameters are specified in Section 5.5. The value of the dissipation function was calculated for each of the 10^8 trials of the simulation completed. These were used to construct a frequency histogram, shown in Figure 5.1.

To calculate the integrand in Eq. (2.43) we multiply the dissipation function histogram by the exponential, e^{-At}. This is plotted in Figure 5.2 for each value of A. This graph is much noisier than the original probability distribution, especially around the values of A corresponding to the negative edge of the probability distribution. This will cause the value of the NPI to be noisy when it is calculated by integrating the function in Figure 5.2. We can also note that for sufficiently unlikely values of the dissipation function, no trajectories are observed in the simulation, and the integrand drops abruptly to zero. This occurs at $A = -0.718$ (one trajectory was measured at $A = -0.799$ but it is not shown on the scale

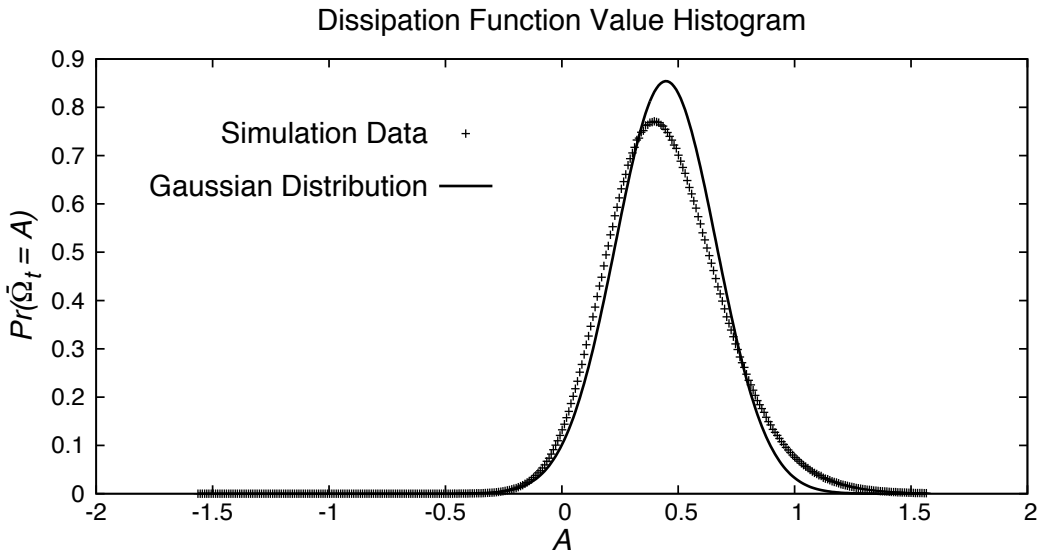

Figure 5.1: Histogram of the dissipation function calculated from a colour conductivity simulation. 10^8 trajectories with a duration of 19.1 were included in the histogram. The frequency of each value of A is divided by this total number of trajectories to give an approximate probability distribution, $Pr(\bar{\Omega}_t = A)$. A Gaussian distribution is also shown, with a mean fit to the simulation data.

used in Figure 5.2 due to restricted space). We can see from comparison with the Gaussian distribution example that a significant part of the integrand should be to the left of this point, none of which is included in the simulation results when the function is integrated over the full range of the distribution. It is for this reason that the NPI can appear to converge to a value less that unity. For a given number of trajectories in the simulation, the same portion of the distribution will typically be missed due to insufficient sampling.

To further demonstrate the difficulty in calculating the value of the NPI we will look at the results obtained from nonequilibrium molecular dynamics simulations, as we increase the length of the trajectory while keeping the amount of sampling fixed. This is presented in Figure 5.3, for a colour conductivity system with a field strength of $F_{ex} = 2$. The other parameters are specified in Section 5.5. The error bars included are two standard errors, estimated from 10 separate block averages. We can see that initially the value of the NPI is unity, and the error bars appear reasonable up to a trajectory duration of $t = 1.5$. At longer times the errors estimated from the block averages do not come close to including the expected value for the NPI of unity.

The displayed data is serially correlated because the same ensemble of trajectories was used initially for all values of the duration t. As the trajectory duration increases the rare events in the simulation become rarer, and also each make a larger contribution to the full ensemble average. A portion of the rare events have become so rare that they are completely unobservable, resulting in the NPI being consistently underestimated. As the trajectory length increases, the proportion of rare events which are unobservable increases, which decreases the value of the calculated average. This underestimation of the NPI is repeatable

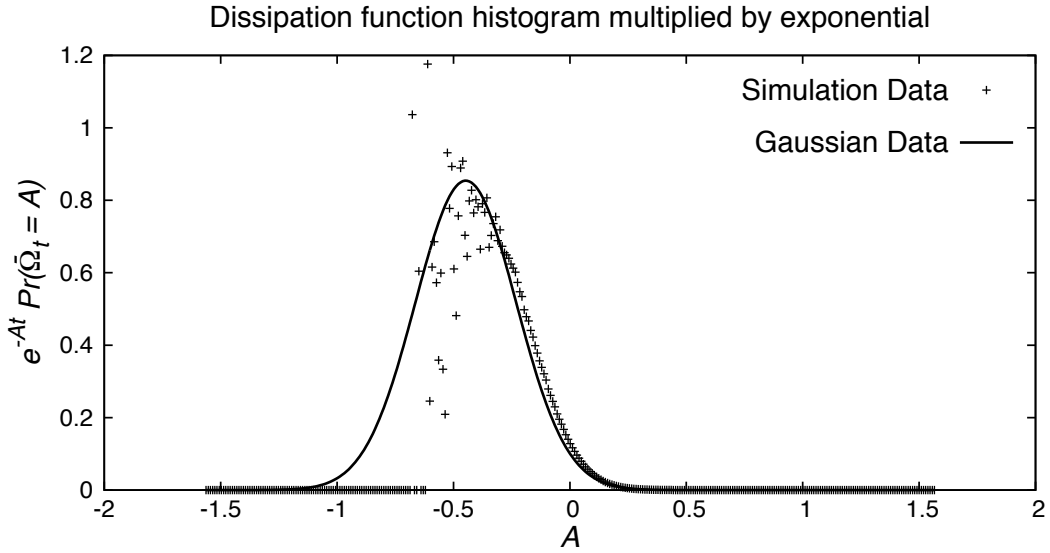

Figure 5.2: The probability distribution for the dissipation function, $Pr(\bar{\Omega}_t = A)$, multiplied by e^{-At}, against the value of the dissipation function, A. The crosses use real simulation data for the probability distribution. The solid line uses a Gaussian distribution for the probability distribution. This function is the integrand in Eq. (2.43).

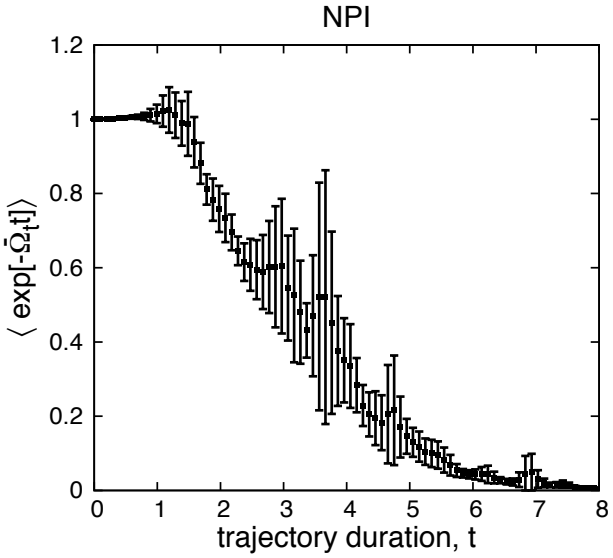

Figure 5.3: NPI calculated for an ensemble as the duration of the trajectory is increased.

between duplicates of the simulation, resulting in small error bars from the standard error analysis.

An interesting feature of Figure 5.3 is the correlation of error bar size with fluctuations in the height of each data point. When a data point happens to have a larger value for the average relative to the neighboring data points, the error bars are consistently larger for that point. This is due to an increased sampling of rare events, which raise both the height of the data point and the calculated standard error.

The NPI is a consequence of the ES-FT, so understanding the statistical fluctuations in the ES-FT is a good place to begin before tackling the more difficult case of the NPI. While the ES-FT is exact, it is written in terms of probabilities of certain events characterised by the dissipation function. To demonstrate the theorem computationally or experimentally it is necessary to approximate the relative probabilities using an estimator in which there are uncertainties. Determining the magnitude of the uncertainty is inherently difficult because the distribution of errors around the mean is not Gaussian.

The ES-FT is usually demonstrated in the literature[16, 43, 11, 4, 36, 42, 14, 114, 37, 66, 12, 40, 115, 15, 28] using its log form,

$$A = \frac{1}{t} \ln \left[\frac{Pr(\bar{\Omega}_t = A)}{Pr(\bar{\Omega}_t = -A)} \right] \tag{5.8}$$

and plotting $\frac{1}{t} \ln[Pr(\bar{\Omega}_t = A)/Pr(\bar{\Omega}_t = -A)]$ vs A with an expected slope of unity. Fluctuation relations involving functions other than the dissipation function have also been examined using this method[75, 84, 116]. We will establish how well we can expect to be able to demonstrate the ES-FT given a finite amount of sampling, and build upon these results in order to analyse the NPI.

5.3 Using the Fluctuation Theorem to Estimate Uncertainties in the Frequency Histogram

Demonstrating the ES-FT involves comparing the number of trajectories which have a dissipation function value of $\bar{\Omega}_t = A \pm \delta A$ to the number with the less likely value, $\bar{\Omega}_t = -A \pm \delta A$. Practically, we compare these values by comparing the relative heights of the corresponding bins of a frequency histogram. Often, the counts for the bins in the negative wing of the distribution will be dominated by noise. The error in the ratio of frequencies will be most significant when the negative bin has far fewer counts than the positive bin. To model the error in the bin height we need to know the expected height, which can be determined by mapping the positive side of the distribution to the negative side using the ES-FT itself. This will result in a distribution that is as noisy as the positive side of the original distribution. The expected value for each histogram bin is now given by

$$\lambda(A) = \begin{cases} \exp[At] n_m(-A) & \text{if } A < 0 \\ n_m(A) & \text{if } A \geq 0 \end{cases} \tag{5.9}$$

where $n_m(A)$ is the measured frequency of the histogram bin for $\bar{\Omega}_t = A \pm \delta A$. With the expected value of each bin height, we will be able to determine the expected distribution for each bin height.

In systems that have an approximately Gaussian distribution of dissipation function values, we can estimate the true height of the bin by replacing the distribution with a Gaussian distribution for the purpose of calculating the uncertainty. The mean of this distribution is set to the mean of the data. The variance of the Gaussian distribution that satisfies the ES-FT is twice the mean[113]. This would result in less noise in each expected bin height. For the rest of the analysis we will consider the more general case where a Gaussian approximation cannot be used.

5.4 Binomial Distribution

The binomial distribution gives the probability distribution for a biased coin toss experiment. That is, for a process with a fixed probability of success, r, performed W times, the probability of obtaining exactly k successes is given by the binomial distribution,

$$p_k(r, W) = \binom{W}{k} r^k (1-r)^{W-k}. \tag{5.10}$$

The height of each histogram bin in our system, $n(A)$, can be described by a binomial distribution where W is the total number of trajectories that have been simulated and $r = \lambda(A)/W$ is the probability of a trajectory falling within a particular histogram bin.

This distribution function is related to the frequency histogram used to demonstrate the ES-FT in the following way. There are a total of W trajectories computed, with the expectation value $\lambda(A)$ for the number of these trajectories found in the histogram bin $A \pm \delta A$. So the binomial distribution gives the probability of observing a value of k trajectories falling in the histogram bin given by $A \pm \delta A$. Note that the binomial distribution Eq. (5.10) is skewed and asymmetric, particularly for distributions with lower values for the average, λ. It is plotted for a selection of values of λ in Figure 5.4. The value used for the total number of trajectories is $W = 9 \times 10^7$, the value we will use in the simulations below.

To generate error bars from this distribution, which gives the probability of a given number of events, we need to use the cumulative probability distribution,

$$CDF_k(r, W) = \sum_{i=0}^{\lfloor k \rfloor} \binom{W}{k} r^k (1-r)^{W-k} \tag{5.11}$$

where k is the highest number of occurrences that the probability mass function is summed to and $\lfloor k \rfloor$ is the largest integer less than k. This distribution is plotted for a range of values of the mean in Figure 5.5.

To get error bars of certain confidence we can calculate the value of k required to give specific values of the CDF. For example, to include at least 95% of the distribution, the error bars would span from the value of $k = k_{0.025}$, the largest integer value satisfying $CDF_{k_{0.025}}(\lambda) \leq 0.025$ to the value of $k = k_{0.975}$, the smallest integer value satisfying

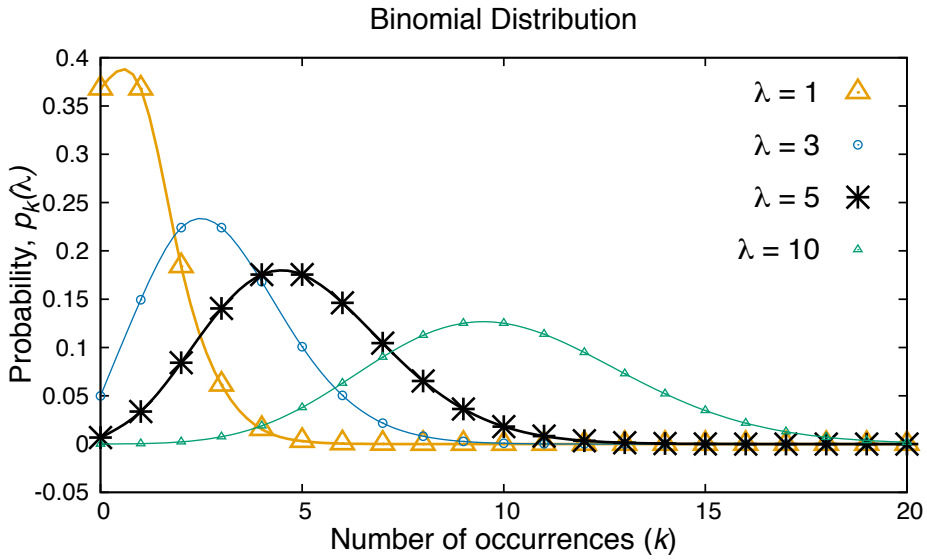

Figure 5.4: Binomial probability distribution function, given in Eq. (5.10), shown for a number of different values of the mean, λ. In all cases $W = 9 \times 10^7$.

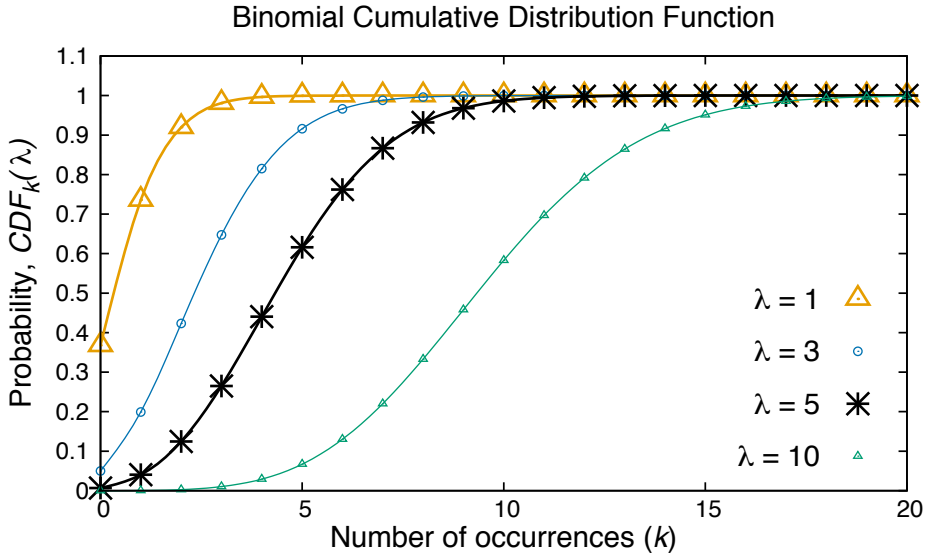

Figure 5.5: Binomial cumulative distribution function, Eq. (5.11), for various values of the mean. In all cases $W = 9 \times 10^7$.

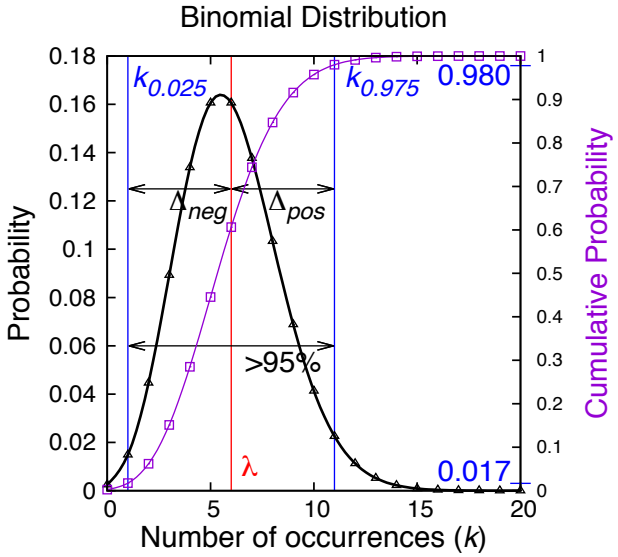

Figure 5.6: The binomial distribution function with $\lambda = 6$ and $W = 10^8$ (black triangles), overlaid with its cumulative distribution (purple squares). The size of error bars which would cover at least 47.5% of the distribution on each side of the median are shown.

$CDF_{k_{0.975}}(\lambda) \geq 0.975$. For the histogram bin associated with the variable A (e.g. recall Eq. (5.9)), we can label the positive and negative error bars as $\Delta_{pos}(A) = k_{0.975}(A) - \lambda(A)$ and $\Delta_{neg}(A) = \lambda(A) - k_{0.025}(A)$ respectively. In general we have

$$\Delta_{pos}(A) = k_{0.5+p/2}(A) - \lambda(A), \tag{5.12a}$$

$$\Delta_{neg}(A) = \lambda(A) - k_{0.5-p/2}(A) \tag{5.12b}$$

where p is the proportion of the histogram to be included in the error bars, and the value of k is determined using the CDF. These error bars may be asymmetric due the skew of the distribution. An example of how these error bars are calculated can be seen in Figure 5.6.

These error bars give the range of values that could be expected to be measured for each histogram bin. The average number of occurrences in the histogram bin will be different for each bin, and so will have a different corresponding binomial distribution. This means that the error bars will vary with each bin, in both size and symmetry. The binomial distribution is more skewed for smaller values of λ, resulting in relatively less symmetric error bars for less populated bins. We will only consider histogram bins where the error bars do not overlap with zero, to avoid dividing by zero. In these cases, the calculated error bars are roughly symmetric.

5.5 Numerical System

To illustrate the method we will use data from a model computational system. To generate a nonequilibrium system we will apply a colour field to all the particles in the system[4].

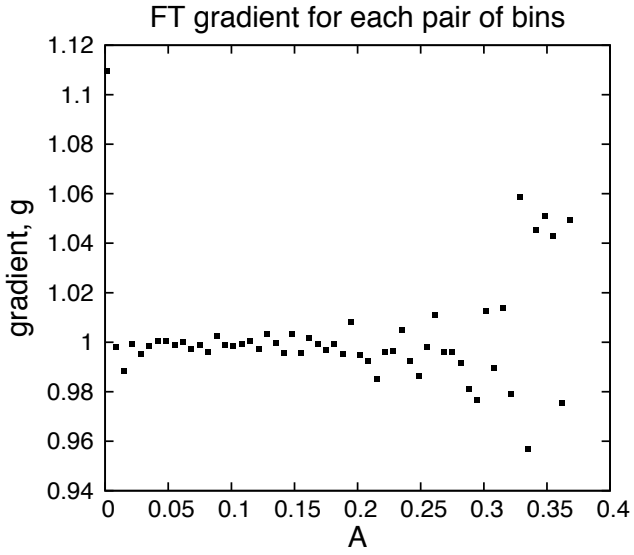

Figure 5.7: Gradient calculated from each pair of bins, given by Eq. (5.13). The histogram of dissipation function values was taken from the example computational system.

The equations of motion used are given in Section 2.3.2, Eq. (2.18) and (2.19). An isokinetic thermostat[27] is used, where the thermostat multiplier is given by Eq. (2.20). The system begins in an equilibrium canonical distribution. This was generated with an equilibrium molecular dynamics simulation, with starting points for the transient simulations taken every 2,000 time steps. This ensures the simulations are statistically independent. We use a two dimensional system of 8 particles (N=8) with a number density of $\rho = N\sigma^2/V = 0.6$. The trajectory duration is labelled t, with a time step length of 0.001. $W = 9 \times 10^7$ trials of the simulation were completed. The histogram bin width was initially 0.003, and only bins which contained data are included. We will initially use a field strength of F_{ex} =0.17 and a trajectory duration of 12. The form of the dissipation function for this system is well known[34], and given by $\Omega(t) = \beta F_{ex} \sum_{i=1}^{N} c_i \dot{x}_i(t)$.

5.6 Propagating Uncertainties to Demonstrate the Fluctuation Theorem

To demonstrate the fluctuation theorem we will take the approach of calculating the gradient of the LHS against the RHS, for each pair of histogram bins. That is,

$$g = \frac{1}{At} \ln \left[\frac{n_m(A)}{n_m(-A)} \right]. \tag{5.13}$$

For the fluctuation theorem to be satisfied, we would expect g to have a value of unity for each histogram bin. Using our example computational system g was calculated for each value of A, shown in Figure 5.7.

To calculate the total slope of the LHS of the fluctuation theorem against the RHS, we

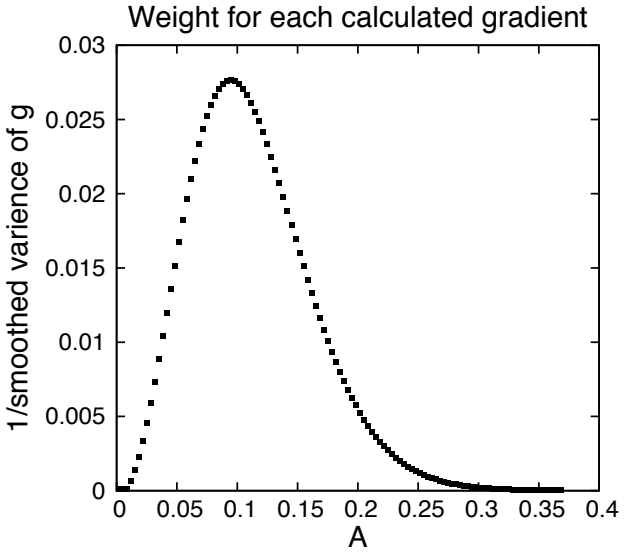

Figure 5.8: Inverse of the smoothed variance of each point, calculated from the binomial distribution describing each histogram bin's height in Eq. (5.16).

can construct a weighted average of the gradient calculated for each pair of histogram bins,

$$G = \frac{\sum_i^h g_i / \left\langle \Delta g_i^2 \right\rangle}{\sum_i^h 1 / \left\langle \Delta g_i^2 \right\rangle}. \tag{5.14}$$

Each point is weighted by the inverse variance, calculated from the variance of the binomial distribution for each histogram bin using the standard error propagation method,

$$\begin{aligned} \left\langle \Delta g_i^2 \right\rangle &= \left\langle \frac{\partial g}{\partial n(A)} \right\rangle^2 \left\langle \Delta n(A)^2 \right\rangle + \left\langle \frac{\partial g}{\partial n(-A)} \right\rangle^2 \left\langle \Delta n(-A)^2 \right\rangle \\ &= \frac{\left\langle \Delta n(A)^2 \right\rangle}{(At \left\langle n(A) \right\rangle)^2} + \frac{\left\langle \Delta n(-A)^2 \right\rangle}{(At \left\langle n(-A) \right\rangle)^2} \end{aligned} \tag{5.15}$$

to linear order. The variance of the binomial distribution is given by $\left\langle \Delta n(A)^2 \right\rangle = \lambda(A)(1 - \lambda(A)/W)$, giving us

$$\left\langle \Delta g_i^2 \right\rangle = \frac{1}{(At)^2} \left[\frac{1}{\lambda(A)} + \frac{1}{\lambda(-A)} - \frac{2}{W} \right]. \tag{5.16}$$

To weight each point we will smooth the calculated variance, so that each variance is replaced by the average of itself with 2 data points on each side. The inverse of this calculated variance is shown for each pair of histogram bins in Figure 5.8. Points close to the origin receive a low weight because small fluctuations in the height of these histogram bins have a large effect on the slope. Points in the wings of the distribution have a low weight because of the large variance in the histogram bin height relative to their average height.

The weighted average of the slope is plotted in Figure 5.9 as we increase the number of histogram bins included in the average. The average quickly converges to its expected value of unity as more data is added. While the calculated slopes for histogram bins in the wings

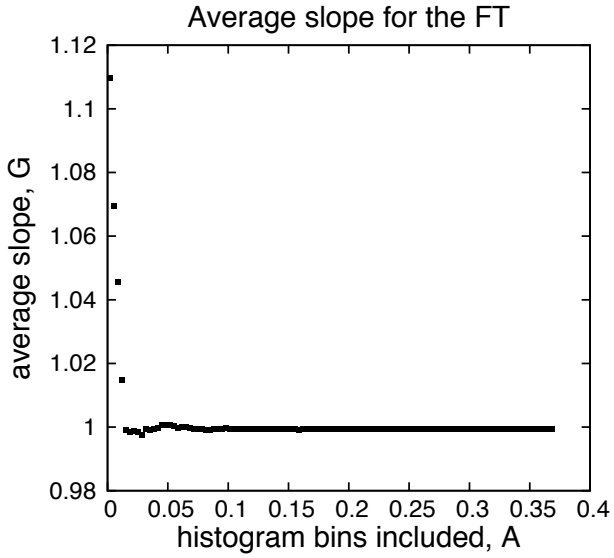

Figure 5.9: Slope of the ES-FT calculated as a weighted average of slopes calculated from each pair of histogram bins, given by Eq. (5.14). The average was calculated using all pairs of histogram bins up to the value of A given on the x-axis.

of the distribution are significantly noisier, this is not reflected in the final average because these points have low weights.

Propagating the variance from the binomial distribution into the variance for g does not take into account the asymmetry in the initial distribution for each bin height, or any asymmetry due to the small size of the histogram bin height relative to the expected range in this height in the bins near the wings of the distribution. To account for this, we can calculate the largest and smallest possible values for g, given that the height of each histogram bin is determined by a specific proportion of the binomial distribution in Eq. (5.12).

$$\Delta_{g+}(A) = \frac{1}{At} \ln \left[\frac{n(A) + \Delta_{pos}(A)}{n(-A) - \Delta_{neg}(-A)} \right] - 1, \tag{5.17a}$$

$$\Delta_{g-}(A) = 1 - \frac{1}{At} \ln \left[\frac{n(A) - \Delta_{neg}(A)}{n(-A) + \Delta_{pos}(-A)} \right]. \tag{5.17b}$$

In doing this we have not assumed that the errors are small enough to be accurately approximated as linear, as was done in Eq. (5.15). This range of possible values for g is plotted in Figure 5.10 for each pair of histogram bins in our example system. We can see that for large values of A the range is asymmetric. That is, the slope can land further from the expected value of unity on the positive side than on the negative side. We can propagate these asymmetric ranges to the weighted average of the slope, G, using the standard error propagating method, but applying it separately to the positive and negative range.

$$\Delta_{G+} = \sqrt{\sum_i^h \left(\frac{\partial G}{\partial g_i} \right)^2 \Delta_{g_{i+}}^2} = \frac{\sqrt{\sum_i^h \Delta_{gi+}^2 / \left\langle \Delta g_i^2 \right\rangle^2}}{\sum_i^h 1 / \left\langle \Delta g_i^2 \right\rangle}, \tag{5.18a}$$

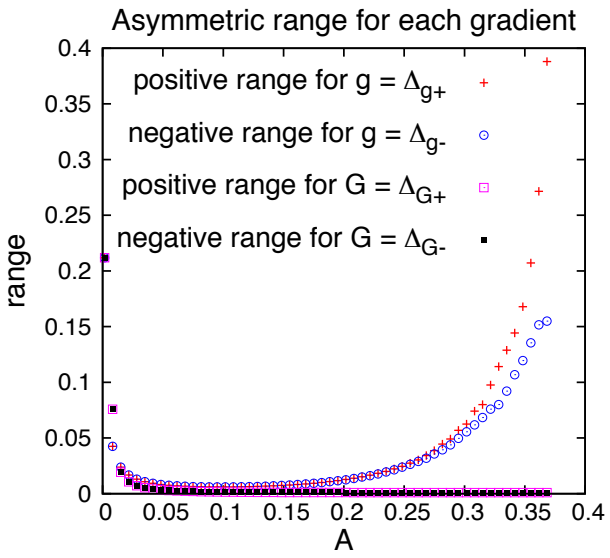

Figure 5.10: Range of the gradient, as given by the qualities specified by Eq. (5.17), for each pair of bins. Also shown is the range for the weighted average of the gradient, calculated in Eq. (5.18). This range was calculated using all pairs of histogram bins up to the value of A given on the x-axis. Note that these positive and negative ranges appear to overlap.

$$\Delta_{G-} = \sqrt{\sum_i^h \left(\frac{\partial G}{\partial g_i}\right)^2 \Delta_{g_{i-}}^2} = \frac{\sqrt{\sum_i^h \Delta_{gi-}^2 / \left\langle \Delta g_i^2 \right\rangle^2}}{\sum_i^h 1/\left\langle \Delta g_i^2 \right\rangle}. \tag{5.18b}$$

This range of values is included in Figure 5.10. The range decreases as the accuracy of G increases with increasing A. While the limits for g were asymmetric for the wings of the distribution, this asymmetry is not observable in the limits for G because of the low weight of these points. The errors given by Eq. (5.18) again are assumed linear, but here the errors are (except for small values of A) very small, so this approximation will be accurate.

5.7 Propagating Uncertainties to the NPI

As a first step towards extending this analysis to the NPI we will calculate the value of the NPI for each pair of histogram bins. We can show using the ES-FT that this is expected to have the same value as the full NPI,

$$\begin{aligned} \left\langle e^{-\bar{\Omega}_t t} \right\rangle_A &= \frac{\exp[-At]n(A) + \exp[At]n(-A)}{n(A) + n(-A)} \\ &= \frac{\exp[-At]Pr(A)W + \exp[At]Pr(-A)W}{n(A) + n(-A)} \\ &= \frac{W\left(Pr(-A) + Pr(A)\right)}{n(A) + n(-A)} = 1. \end{aligned} \tag{5.19}$$

We calculated this in the same system as before, but with a field strength of $F_{ex} = 0.29$, trajectory duration of $t = 18$, $W = 9 \times 10^7$ trials and histogram bin width of 0.004. This is plotted in Figure 5.11 as crosses. The error bars are constructed by splitting the data

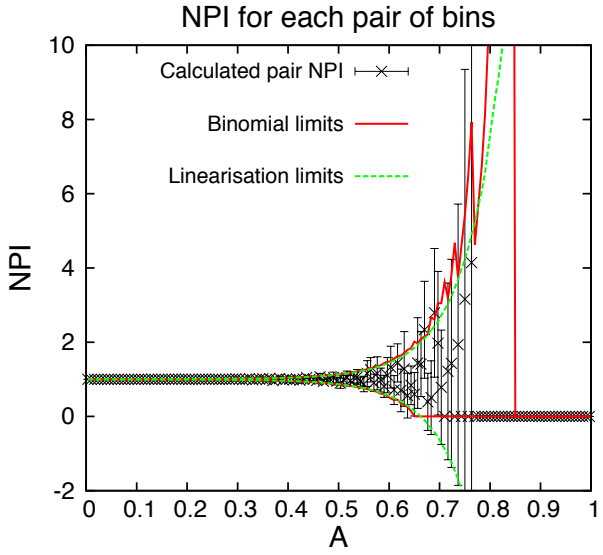

Figure 5.11: NPI calculated for each pair of histogram bins determined by A, shown as black crosses. The error bars are 2 times the standard error, from repeats of the simulation. The green dashed lines show the expected range of the pair NPI calculated from linearising the equation and using the variance of the binomial distribution describing the height of each bin. The limits calculated from the largest and smallest expected heights in each of the histogram bins are shown as the solid red line.

into 9 sets and calculating the standard error. This error analysis method consists simply of considering independent repetitions of the simulation, and is equivalent to the same method used when calculating the full NPI. For histogram bins close to the centre (small values of A), the NPI has a value within the error bars of unity, as expected. As the value of A increases the data becomes significantly noisier, though the error bars still overlap with the value of unity. However, in the wings of the distribution the NPI for a number of histogram bins drops to a value close to zero, with very small error bars. This is very clear for values of $A > 0.75$. In these cases, the histogram bin corresponding to $-A$ did not record any trajectories, and we can see that the standard error analysis method has failed. It is when these histogram bins make a significant contribution to the total NPI that its value appears to be significantly different to unity, as seen in Figure 5.3.

The measured pair NPI is given as

$$NPI_p(A) = \frac{\exp[-At]n_m(A) + \exp[At]n_m(-A)}{n_m(A) + n_m(-A)}. \tag{5.20}$$

We can now calculate the expected range for each pair NPI by linearising Eq. (5.20) and propagating the variance from the initial binomial distributions for each histogram bin. This is the standard error propagation method. Let $\Delta NPI_p(A) = NPI_p(A) - \langle NPI_p(A) \rangle$. Now

to linear order

$$\begin{aligned}\Delta NPI_p(A) &= \Delta n(A)\left\langle\frac{\partial NPI_p(A)}{\partial n(A)}\right\rangle + \Delta n(-A)\left\langle\frac{\partial NPI_p(A)}{\partial n(-A)}\right\rangle \\ &= \Delta n(A)\left\langle\frac{\exp[-At]}{n(A)+n(-A)} - \frac{\exp[-At]n(A)}{(n(A)+n(-A))^2} - \frac{\exp[At]n(-A)}{(n(A)+n(-A))^2}\right\rangle \\ &+ \Delta n(-A)\left\langle\frac{\exp[At]}{n(A)+n(-A)} - \frac{\exp[At]n(-A)}{(n(A)+n(-A))^2} - \frac{\exp[-At]n(A)}{(n(A)+n(-A))^2}\right\rangle.\end{aligned} \tag{5.21}$$

Using the ES-FT,

$$\begin{aligned}\Delta NPI_p(A) &= \Delta n(A)\left\langle\frac{\exp[-At]}{n(A)+n(-A)} - \frac{n(-A)}{(n(A)+n(-A))^2} - \frac{n(A)}{(n(A)+n(-A))^2}\right\rangle \\ &\quad +\Delta n(-A)\left\langle\frac{\exp[At]}{n(A)+n(-A)} - \frac{n(A)}{(n(A)+n(-A))^2} - \frac{n(-A)}{(n(A)+n(-A))^2}\right\rangle \\ &= \Delta n(A)(\exp[-At]-1)\left\langle\frac{1}{n(A)+n(-A)}\right\rangle \\ &\quad +\Delta n(-A)(\exp[At]-1)\left\langle\frac{1}{n(A)+n(-A)}\right\rangle\end{aligned} \tag{5.22}$$

which to linear order is

$$\Delta NPI_p(A) = \Delta n(A)\left[\frac{\exp[-At]-1}{\lambda(A)+\lambda(-A)}\right] + \Delta n(-A)\left[\frac{\exp[At]-1}{\lambda(A)+\lambda(-A)}\right]. \tag{5.23}$$

Since each histogram bin is statistically independent,

$$\begin{aligned}\left\langle\Delta NPI_p(A)^2\right\rangle &= \left\langle\Delta n(A)^2\right\rangle\left(\frac{(\exp[-At]-1)^2}{(\lambda(A)+\lambda(-A))^2}\right) \\ &\quad + \left\langle\Delta n(-A)^2\right\rangle\left(\frac{(\exp[At]-1)^2}{(\lambda(A)+\lambda(-A))^2}\right).\end{aligned} \tag{5.24}$$

This variance is used to calculate a range of two standard deviations around the expected value of the pair NPI, and is included in Figure 5.11, labelled as the linearisation limits. These limits show the increase in uncertainty as the value of A increases, and continues to increase after the error calculated using simple block averaging becomes unreliable.

We can also calculate the upper and lower limit for the pair NPI by using the extreme values for each histogram bin, with the limits that include 95% of the binomial distribution calculated in Eq. (5.12).These limits are included in Figure 5.11 as solid red lines. These limits correctly predict the increase in the noise of the pair NPI with A. The minimum possible value of the NPI of zero is also reflected by these limits. However, in the wings of the distribution the upper limit drops close to zero. This may be observed in the figure for all values of A that are larger than the value of $A = 0.85$, where the discontinuous drop of the line occurs. This sudden drop towards zero is because while the mean of the distribution describing the $-A$ histogram bin, $\lambda(-A)$, is still greater than zero, our 95% interval of the binomial distribution only includes the value zero. So, the upper and lower limits for the expected value of this histogram bin are both zero when the value $A > 0.85$. Obviously if we chose the interval to be larger than 95% this discontinuous drop would occur at a larger

value of A. This mirrors what happens with the actual simulation data, where the pair NPI goes to zero when A is larger than some *critical value*. If we sampled more data the value of A where this occurs would also be larger. The exponential nature of the ES-FT will mean that this increase in the *critical value* of A is extremely gradual with increased sampling.

We now turn our attention to what happens upon computing the full NPI rather than the pair NPI. To do this we have to sum up the pair NPI for each value of A as per,

$$\left\langle \exp[-\bar{\Omega}_t t] \right\rangle = \int_0^\infty dA \, \frac{n(A) + n(-A)}{N} \left\langle \exp[-\bar{\Omega}_t t] \right\rangle_A . \tag{5.25}$$

The pair NPI is not accurately estimated when the value of $|A|$ is too large and the value of $n(-A)$ becomes too small to get an accurate estimate. When the pair NPI with values of $|A|$ that are large enough to suffer from this problem make a significant contribution to the full NPI, it will not be accurately estimated. This happens when the trajectory duration the NPI is estimated at becomes large enough. If we increase the strength of the driving field, F_{ex}, this transition will occur at a shorter trajectory duration. At these sufficiently long durations the full NPI is consistently underestimated, as seen in Figure 5.3.

We can measure the significance of each histogram bin in calculating the value of the NPI by calculating the value of the integrand for that bin from writing the average as an integral

$$\left\langle \exp[-\bar{\Omega}_t t] \right\rangle = \int_{-\infty}^\infty dA P_m(A) \tag{5.26}$$

where $P_m(A) = \exp[-At] Pr(\bar{\Omega}_t = A)$. The integrand is actually the mirror of the probability distribution, as follows from the ES-FT, Eq. (2.37), i.e. $P_m(A) = Pr(-A)$, hence the subscript m for mirror.

This is plotted in Figure 5.12 for each histogram bin. We have also included a measure of the error in the calculated probability of each bin, the standard deviation of the bin height divided by the average height. This represents the relative error for each value of A. This data is from the same system as Figure 5.3, the colour conductivity system with a field strength of 2.0. The value of the probability distribution approximated from each histogram bin is given by $Pr(\bar{\Omega}_t = A) = \lambda(A)/W$ where $\lambda(A)$ is determined using the ES-FT in Eq. (5.9). The standard deviation is the square root of the variance for each histogram bin height, given by the binomial distribution, $\sigma(A) = \sqrt{\lambda(A)(1 - \lambda(A)/W)}$. Two trajectory durations are included, $t = 1$, where the calculated value for the NPI is as close to unity as expected, and $t = 4$ where the calculated value is far from unity. We can see that the most significant histogram bins in the first case have a much lower relative error than the most significant histogram bins at the latter time. This explains in detail why the NPI can be calculated in a numerical system for short times, but fails at later times.

5.8 Dirac-Delta Description of the NPI

We have seen that negative values of the dissipation function become less likely as the trajectory length increases. We expect at long time we can approximate the distribution of $\bar{\Omega}_t$ with a Dirac-delta distribution, with the value of the NPI given by Eq (5.6). From this

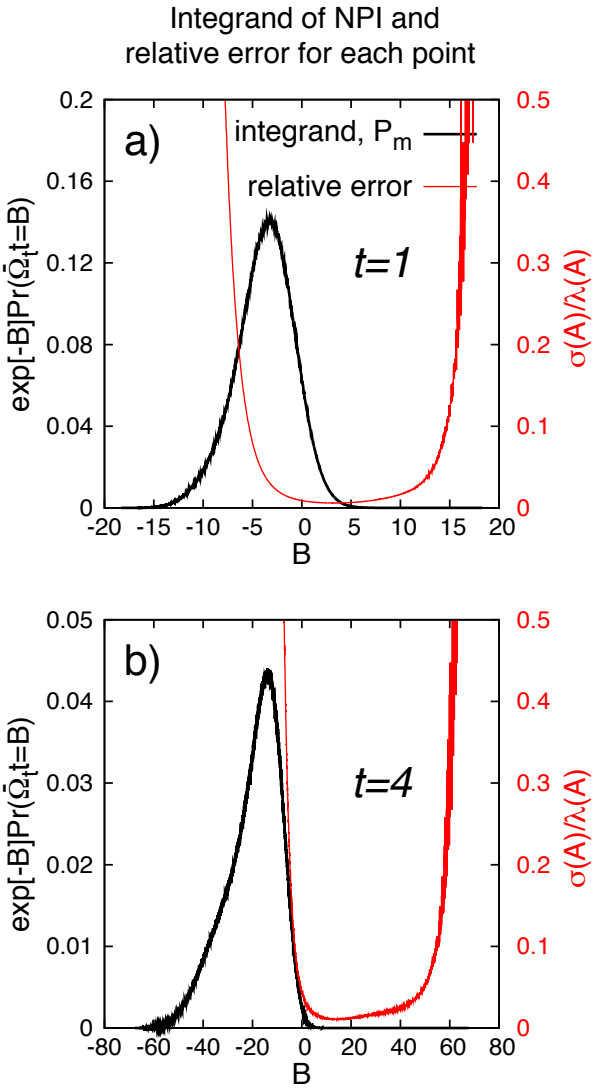

Figure 5.12: Integrand of the full NPI calculation shown for each histogram bin, labelled by At. Shown along side in red is the standard deviation of each bin height divided by the mean of that histogram bin, labelled as the relative error. This is plotted for the two trajectory durations, $t = 1$ on top and $t = 4$ below. Note: the dummy variable B is related to the previously used dummy variable A as per $B = At$. The histogram bin width used is 0.02.

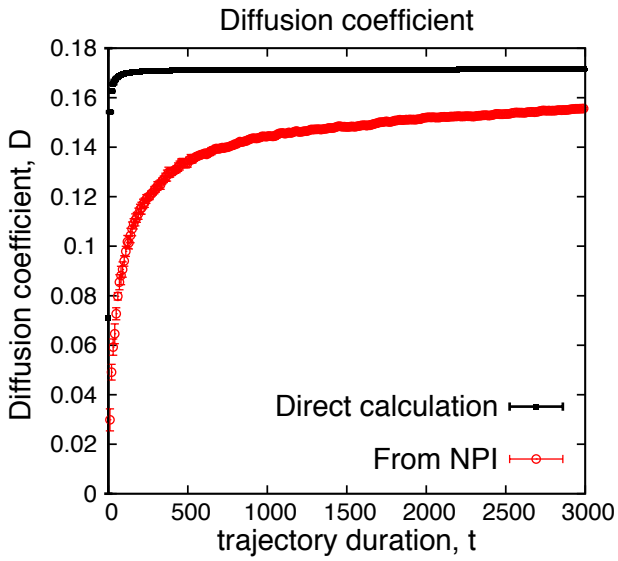

Figure 5.13: Long duration comparison between NPI derived diffusion coefficient, Eq. (5.27), and the more directly obtained diffusion coefficient, Eq. (5.28).

expression we will calculate the value of the self-diffusion coefficient as

$$D \approx \frac{N-1}{N} \frac{-\ln\left\langle e^{-\bar{\Omega}_t t}\right\rangle}{\beta^2 \rho t V F_{ex}^2}. \tag{5.27}$$

We can also calculate it directly as

$$D = \frac{N-1}{N} \frac{1}{\beta\rho} \lim_{t\to\infty} \lim_{F_{ex}\to 0} \frac{\langle J(t)\rangle}{F_{ex}} \tag{5.28}$$

where

$$J(t) = \frac{1}{V} \sum_{i=1}^{N} c_i \dot{x}_i \tag{5.29}$$

and

$$\langle J(t)\rangle \approx \frac{1}{t} \left\langle \int_0^t J(s) ds \right\rangle \tag{5.30}$$

which will become increasingly accurate as the duration is increased. The time dependent diffusion coefficient for each case is plotted in Figure 5.13. These simulations use the same system as Figure 5.3 with a field strength of 2.0, but using an ensemble of 10^5 trajectories. We can see that as the trajectory duration increases the value calculated from the NPI asymptotically approaches the direct calculation, which has become constant, demonstrating that the distribution of dissipation function values is approaching a Dirac-delta distribution. We note that significantly longer trajectories are needed to see this convergent behaviour than were necessary to see the ES-FT derived value of the NPI fail. Due to the large exponential functions being evaluated it was necessary to use quadruple precision in the numerical evaluation.

5.9 Truncated NPI

To avoid the problems caused by the lack of statistics at the negative edge of the probability distribution it is advantageous to calculate the NPI using only the positive half of distribution (values of A grater than zero). This half of the distribution can be mapped on to the negative side using the ES-FT. When this is done to calculate the NPI, it is known as the partial range NPI[44]. The partial range average shows better statistics than the ensemble average, but its value is much less sensitive to changes in the distribution of the dissipation function. This makes it much less appropriate for use as a diagnostic tool in experiments and simulations. This was discussed in Section 2.6.1.

Instead of using only the positive side of the distribution, but still avoiding the noisy negative wing of the distribution we can truncate the probability distribution symmetrically about zero. This is similar to the pair NPI, including many pairs in the average. We can prove that the NPI calculated over this truncated range has a value of unity. Writing out the truncated NPI as an integral we have

$$\langle e^{-\bar{\Omega}_t t}\rangle_{-R<\bar{\Omega}_t<R} = \int_{-R}^{R} \tilde{Pr}(\bar{\Omega}_t = A)e^{-At}dA \tag{5.31}$$

where the exponential average is now a conditional ensemble average. Only trajectories which have a value of the dissipation function within the truncated range, $-R$ to R, are included in the average. The probability distribution $\tilde{Pr}(\bar{\Omega}_t = A)$ is normalized over this truncated range. We can apply the fluctuation theorem to Eq. (5.31) resulting in

$$\langle e^{-\bar{\Omega}_t t}\rangle_{-R<\bar{\Omega}_t<R} = \int_{-R}^{R} \tilde{Pr}(\bar{\Omega}_t = -A)dA. \tag{5.32}$$

Preforming a change of variables to replace $-A$ with U we have

$$\langle e^{-\bar{\Omega}_t t}\rangle_{-R<\bar{\Omega}_t<R} = -\int_{R}^{-R} \tilde{Pr}(\bar{\Omega}_t = U)dU \tag{5.33}$$

and then swapping the limits of integrating gives

$$\langle e^{-\bar{\Omega}_t t}\rangle_{-R<\bar{\Omega}_t<R} = \int_{-R}^{R} \tilde{Pr}(\bar{\Omega}_t = U)dU. \tag{5.34}$$

Recognising that this is the integral over the entire truncated range of the probability distribution, which is normalized over this same range, we have the truncated form of the NPI

$$\langle e^{-\bar{\Omega}_t t}\rangle_{-R<\bar{\Omega}_t<R} = 1. \tag{5.35}$$

Using the same histogram of the dissipation function from simulation data calculated in Figure 5.1 we can calculate the value of the truncated NPI for a variety of range sizes. This is shown in Figure 5.14. Here we have used an applied colour field strength of 0.71 and trajectory length of 19,100 time steps. The error bars were calculated by splitting the data into 10 sets each containing 10^7 trajectories. The histogram of dissipation function values

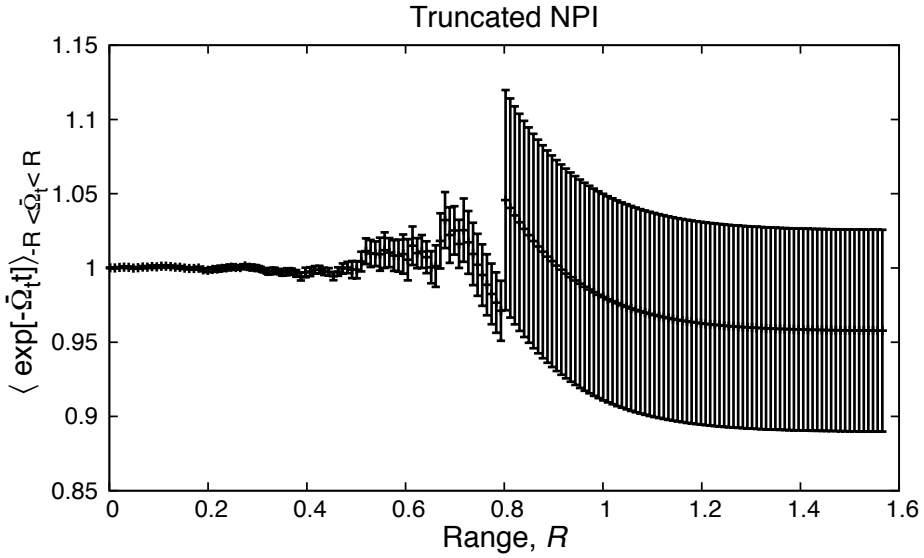

Figure 5.14: Truncated NPI, Eq. (5.31), calculated using data from the colour conductivity simulation. The range, R, corresponds to the value of A up to which the probability distribution in Figure 5.1 is included in the calculated average.

was constructed for each data set, and the truncated average calculated from that. The standard deviation of these data sets is used as the error bars in Figure 5.14.

We can see that initially the truncated ensemble average has the expected value of unity, demonstrating the new truncated NPI. As the range increases, the value of the average remains unity, with small error bars, until the range reaches $R = 0.5$ and the noise and error bars increase. This point corresponds roughly to the negative edge of the dissipation function histogram, with at least 16 trajectories in each histogram bin inside this range. The averages calculated with a smaller range than this show good statistics, with $\langle e^{-\bar{\Omega}_t t} \rangle_{-0.5<\bar{\Omega}_t<0.5} = 1.01 \pm 0.01$. This method is a viable way to more easily calculate the value of the NPI in computational and experimental systems. The method will only be effective when there is a portion of the negative side of the distribution of dissipation function values which has good statistics.

5.10 Conclusion

The properties of the subject of the NPI, the average $\langle \exp\left[-\bar{\Omega}_t t\right] \rangle$, have been studied in relation to the sampling in the system. The Evans-Searles Fluctuation Theorem predicts that given an infinite amount of sampling, the value of the ensemble average must be unity. If we take a fixed amount of sampling, but extend the duration of the trajectory, the NPI has a value of unity initially, but tends towards a value of less than unity. This is because the rare events become both rarer, and more significant in the calculation of the ensemble average. We have analysed the statistical sampling of errors to demonstrate in detail why the full ensemble average is realised at short trajectory durations but not long durations. To do this we first analysed the effects of rare events in demonstrating the ES-FT. For

trajectory durations significantly longer than those where the NPI starts to fail, we found that a Dirac-delta function was an accurate approximation to the distribution of dissipation function values. This is evidenced by the value of the self-diffusion coefficient calculated using this method converging to the directly calculated value. This approximation assumes no rare events are observed in the simulation, which at long times, for a fixed amount of sampling, becomes an accurate assumption. We expect that if we choose a fixed trajectory duration, and increased the amount of sampling, the rare events would eventually be sampled, and the ensemble average would approach a value of unity. We have also developed a truncated form of the ensemble average for the NPI which shows better statistics, provided some rare events are observed.

Chapter 6

Steady State NPI

Fluctuations in the dissipation function in steady state systems can be described by the Steady State Fluctuation Theorem[63, 40, 65, 34], discussed in Section 2.8. It is given by

$$\lim_{t\to\infty} \frac{1}{t} \ln \left[\frac{Pr(\bar{\Omega}_{ss,t} = A)}{Pr(\bar{\Omega}_{ss,t} = -A)} \right] = A \tag{6.1}$$

where $\bar{\Omega}_{ss,t}$ is the time average of the dissipation function calculated over a steady state trajectory of length t. These trajectories start from a point in the steady state. Since this equation has the same form as the ES-FT, from which the NPI can be derived, a similar relationship can be derived for steady state systems,

$$\langle e^{-\bar{\Omega}_{ss,t}t} \rangle = 1. \tag{6.2}$$

Because the Steady State Fluctuation Theorem, Eq. (6.1), is asymptotic we would expect the steady state NPI, Eq. (6.2), to hold as the length of the steady state trajectory gets longer.

To investigate the behaviour of the steady state NPI we will use a colour conductivity system where a colour field is applied to each of the particles. The equations of motion and thermostat are given in Section 2.3.2. To generate steady state trajectories, we start from an equilibrium isokinetic distribution, before applying a colour field of strength 0.29, and allowing the system to come to a steady state over 10,000 time steps. Steady state trajectories 30,000 time steps long are initiated from this point in series, each separated by 2,000 time steps of simulation to ensure statistical independence. The timestep used was 0.001, in a two dimensional 8 particle system with a density of 0.6. An ensemble of 10^7 trajectories was simulated. From this ensemble we can calculate the value of the steady state NPI given in Eq. (6.2) for a range of values of t. These results are presented in Figure 6.1. The uncertainty is calculated by splitting each ensemble into 10 sets and calculating the standard error.

The steady state NPI is not within the uncertainty of the expected value of unity. It also shows no improvement as the trajectory length increases, to within the precision of our calculations. This implies that this exponential average could show the same statistical

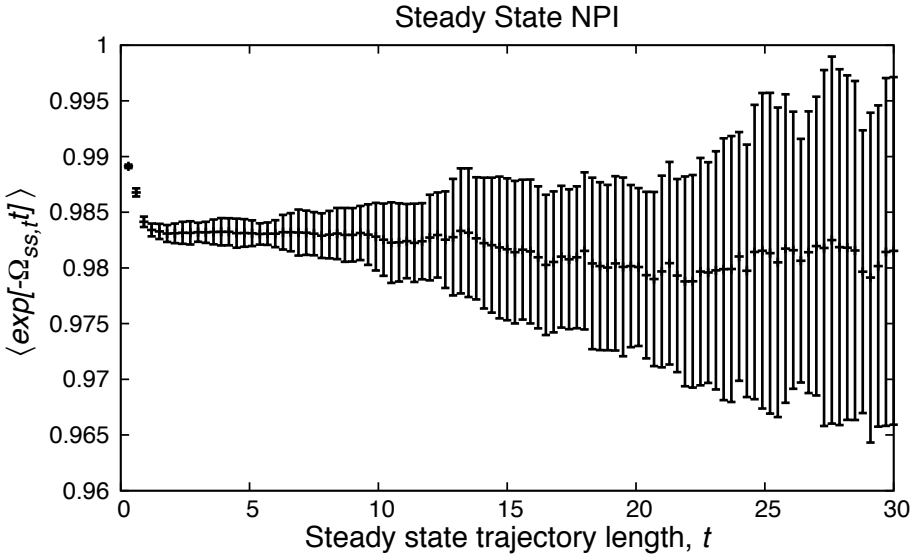

Figure 6.1: Value of the steady state NPI from the simulation of a colour conductivity system for a range of steady state trajectory lengths, t.

convergence issues as the transient NPI, discussed in Chapter 5.

6.1 Truncated Steady State NPI

To attempt to improve the statistics we can calculate a truncated version of the steady state NPI. Since the Steady State FT, Eq. (6.1), has the same form as the ES-FT, we can derive the truncated version of the NPI in the same way,

$$\langle e^{-\bar{\Omega}_{ss,t}t} \rangle_{-R<\bar{\Omega}_{ss,t}<R} = 1. \tag{6.3}$$

Using data from steady state simulations we can calculate the truncated NPI, Eq. (6.3), with the same method described in Section 5.9. The results are shown in Figure 6.2, for a selection of trajectory lengths. The error bars shown are the standard error from repeating the calculation with each ensemble split up into 10 sets.

For all trajectory lengths we see a very similar trend. While the truncated steady state NPI does initially have a value of unity, it drops quickly to the value of the untrunctated average. This is very different to the trend seen for transient systems, where the truncated NPI maintained a value of unity until the range reached the edge of the probability distribution on the negative side. Truncating the ensemble average does not allow us to calculate the steady state NPI with better statistics. This implies that the reason the steady state NPI relationship does not hold for this computational system is not primarily due to insufficient sampling.

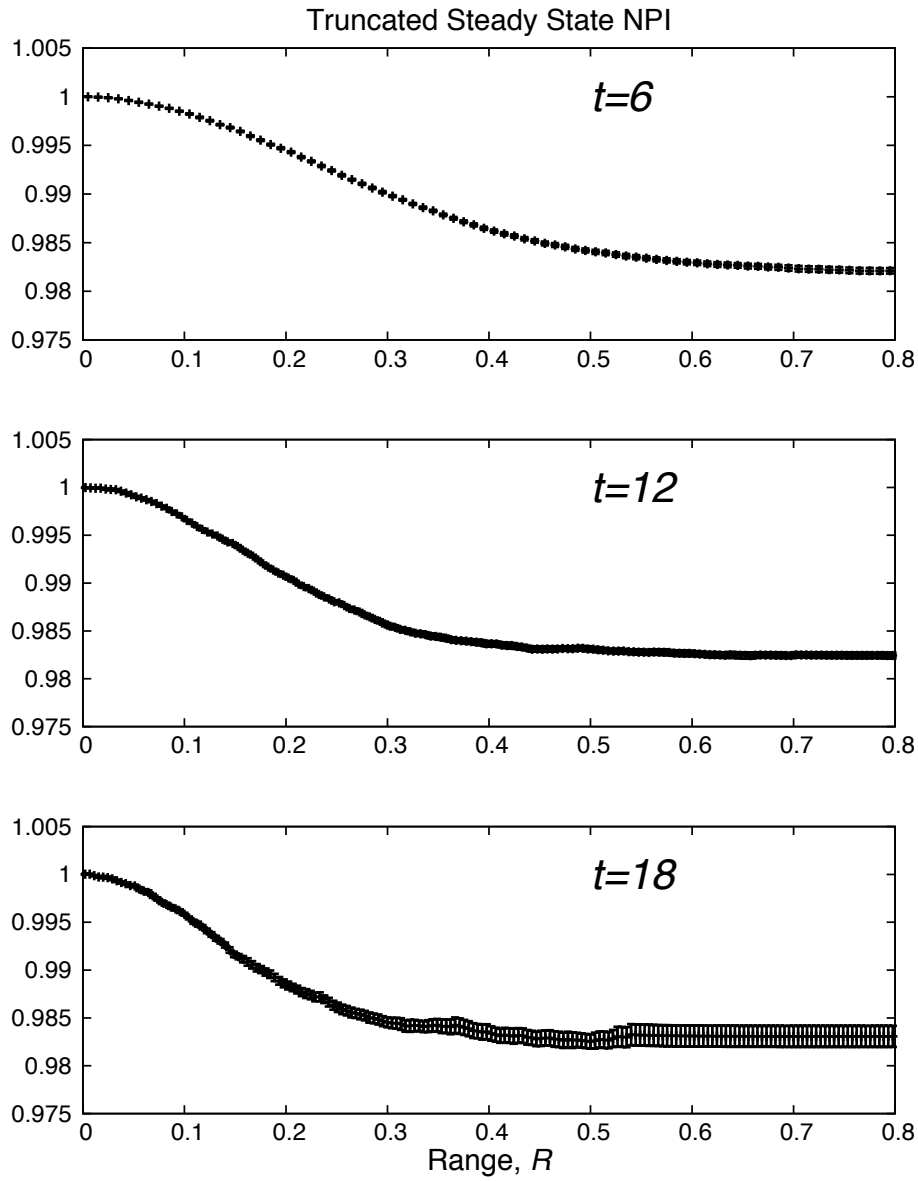

Figure 6.2: The steady state NPI calculated over a truncated range, given by the Eq. (6.3). Results are from the colour conductivity simulation, with trajectories initiated from the steady state. Three different trajectory lengths, t, are used. The range, R, indicates how much of the probability distribution of the dissipation function is included in the ensemble average. 10^8 trajectories were used in each of these simulations.

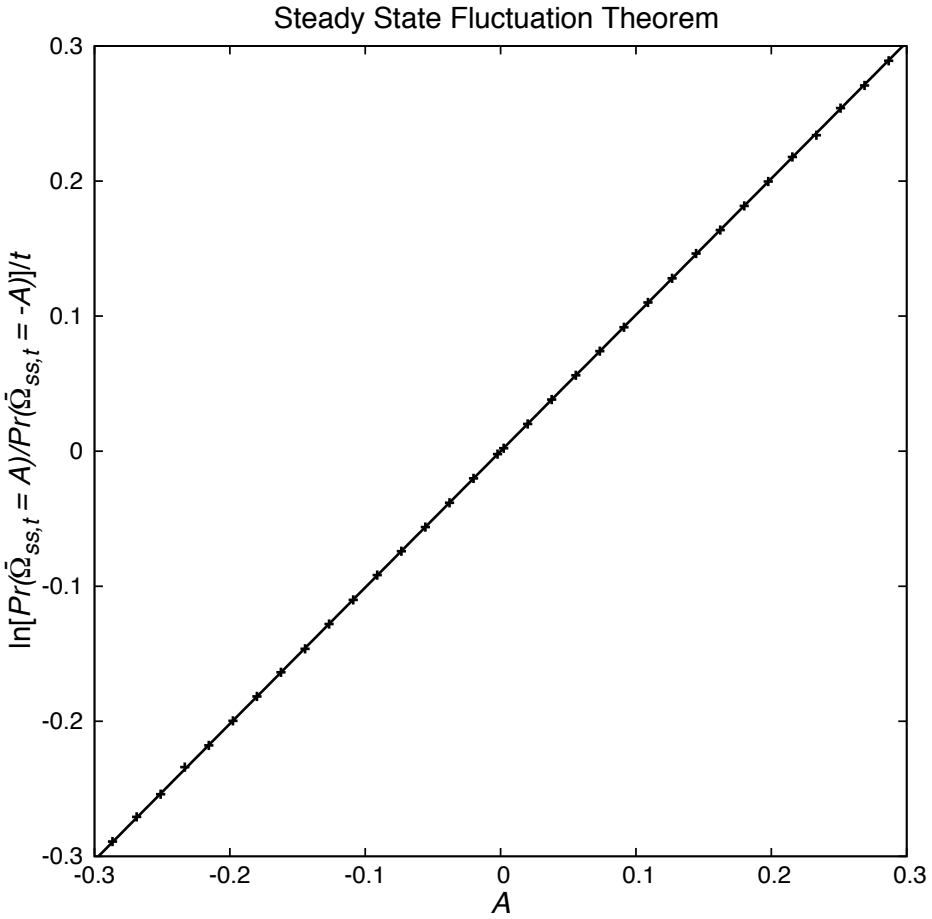

Figure 6.3: Test of the Steady State Fluctuation Theorem. Plot of the LHS of the Steady State FT, Eq. (6.4) against the RHS. Results are from the colour conductivity simulation using trajectory lengths of $t = 18$. Slope of the line of best fit is 1.0094±0.0002.

6.2 Gradient Corrected Steady State FT

The steady state NPI relies on the convergence of the Steady State Fluctuation Theorem. This fluctuation theorem converges quickly enough with the trajectory length to be observable[34], and can be verified to arbitrary accuracy. Since we saw no convergence of the steady state NPI with increasing trajectory length, in Figure 6.1, we can look at the behaviour of the Steady State FT in our system.

How well the Steady State FT holds can be tested by plotting the LHS of the FT against the RHS,

$$\frac{1}{t} \ln \left[\frac{Pr(\bar{\Omega}_{ss,t} = A)}{Pr(\bar{\Omega}_{ss,t} = -A)} \right] = A. \tag{6.4}$$

The relative probabilities can be computed for each histogram bin, generating a data point for each value of A. This was done for the $t = 18$ simulation, shown in Figure 6.3.

The slope of the line of best fit, 1.0094±0.0002, was calculated using a least squares fit to the data. While the slope is not unity, we can see that the data appears to be very

Trajectory length (t)	Slope of Steady State FT test (C)
6	1.030±0.004
12	1.015±0.001
18	1.0095±0.0005

Table 6.1: Calculated values for the gradient factor, C, described in Eq. (6.5) for the simulation with each trajectory length.

linear. To investigate how linear the data is, we can plot the slope of the graph in Figure 6.3 against the amount of data that is used in the slope calculation. This was done for the $t = 18$ simulation in the top plot of Figure 6.4, where all data points between $-R$ and R are included in the slope calculation.

We can see that the slope of the Steady State FT test is mostly constant. The noise initially is due to an insufficient number of data points used to calculate the slope, and the noise at large values of the range is due to a lack of statistics in calculating the relative probabilities in the wings of the distribution. Since this slope is constant, we can write an empirical version of Steady State FT,

$$\frac{1}{t}\ln\left[\frac{Pr(\bar{\Omega}_{ss,t} = A)}{Pr(\bar{\Omega}_{ss,t} = -A)}\right] = CA \tag{6.5}$$

where C is a constant that we will label the gradient factor. We will call Eq. (6.5) the gradient corrected steady state FT. When the LHS of the equation is plotted against A, the slope will be C. This is the same slope calculated in Figure 6.4. We can calculate the value of the gradient factor, C, and the linearity of the demonstration graph for the other simulation times in the same way as above. For the example lengths of $t = 6$ and $t = 12$, this can be seen in the second two plots of Figure 6.4, where the calculated slope is plotted against the amount of data used in the calculation. In both cases the calculated slope is not unity for all values of the range. Discounting the noisy initial and final sections, the slope of the Steady State FT test is roughly constant for $t = 12$. However, it is noisier than the $t = 18$ results. The results from the $t = 6$ simulation show that the slope is constantly increasing as the amount of data in the calculation is increased. This data is much less linear than the simulations that use longer trajectory lengths.

To calculate a value for the gradient factor, C, we will use the value of the slope in the middle of the approximately constant region, with the uncertainty given by the fluctuations within this region. In the case of the shortest trajectory length, $t = 6$, we will use a value for the slope in the middle of the calculated range, $R = 0.4$, with the uncertainty given by upper and lower values of the slope, excluding the noisy initial and final sections. These values are presented in Table 6.1.

For T-mixing systems the distribution of the dissipation function must become Gaussian asymptotically in time[117]. This implies that the Steady State FT will become linear for sufficiently long trajectory lengths, consistent with our observations from simulation seen in Figure 6.4.

To see the convergence of the Steady State Fluctuation Theorem we can graph the slope, C, against steady state trajectory length. These results are presented in Figure 6.5, and

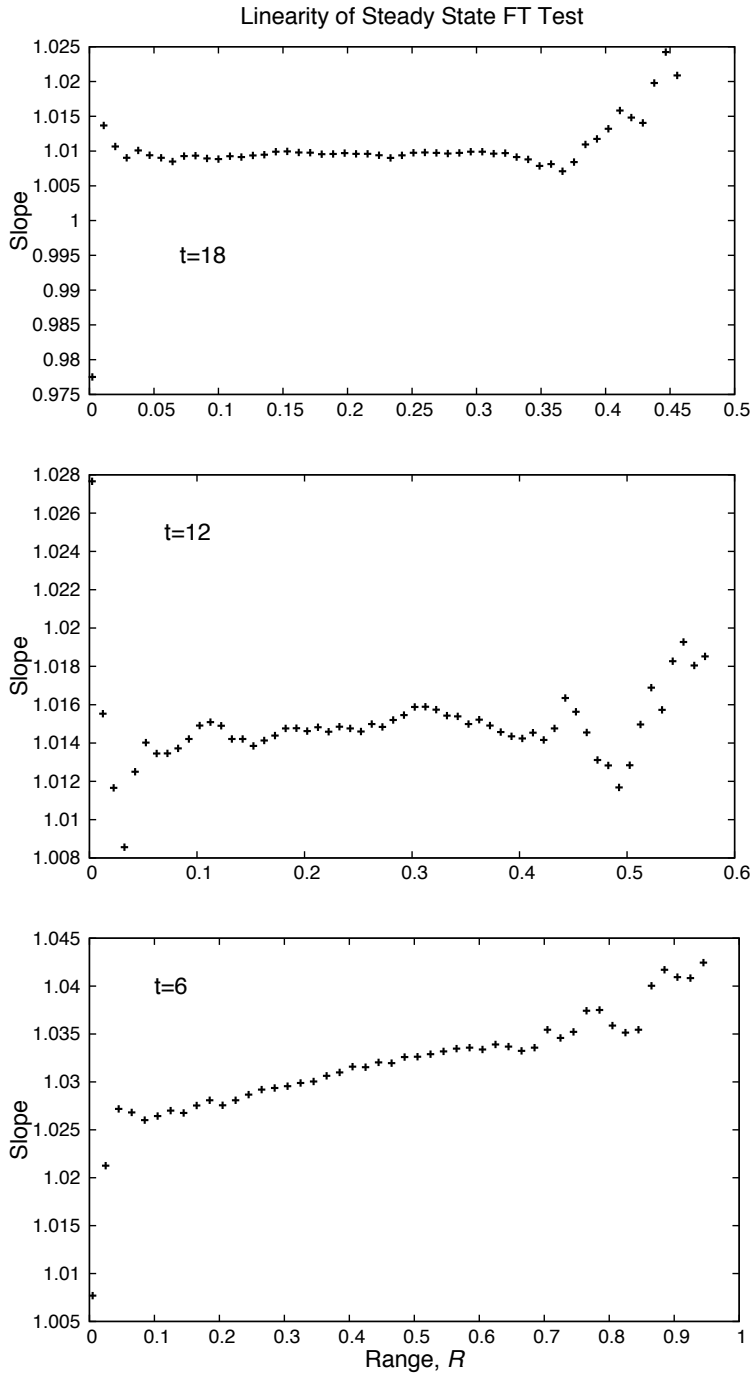

Figure 6.4: Slope of the LHS vs the RHS of the Steady State FT, Eq. (6.4), as the amount of data in the slope calculation is increased. All data points between the values of $A = R$ and $-R$ were included in the calculation. The range, R, is given by the $x-$axis. These results are shown for the colour conductivity simulation with a trajectory lengths of $t = 18$, 12 and 6.

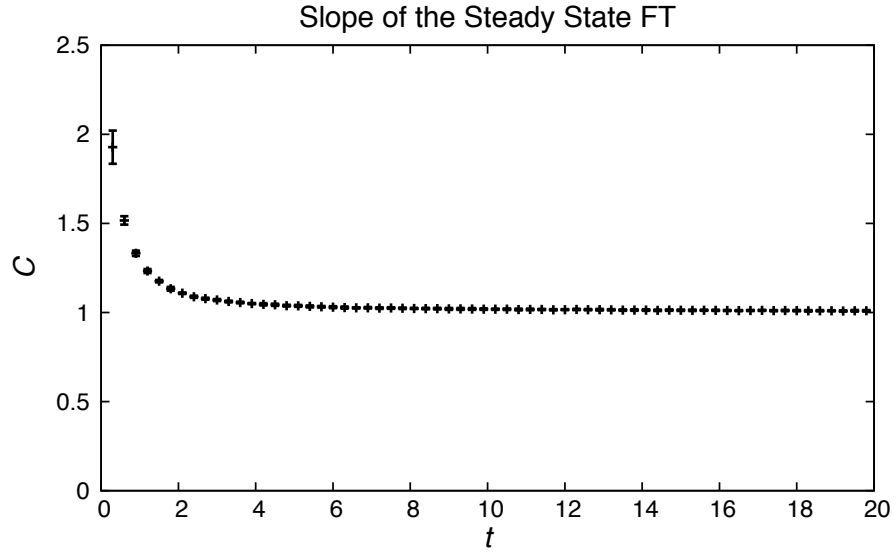

Figure 6.5: Convergence of the Steady State Fluctuation Theorem with trajectory length, t. Data is from the colour conductivity simulation where trajectories were initiated in the steady state.

we can see that for our computational system the Steady State FT is converging with time. The values of C used were calculated with a range that extended 2 standard deviations from the mean on the negative side of the distribution of dissipation function values. The error bars were calculated with 10 independent blocks in the simulation.

6.3 Gradient Corrected Steady State NPI

From the empirical gradient corrected steady state FT, Eq. (6.5), we can derive a corrected version of the NPI for steady state systems. This gradient corrected NPI will have the gradient factor contained within the exponential average,

$$\langle e^{-C\bar{\Omega}_{ss,t}t}\rangle_{-R<\bar{\Omega}_{ss,t}<R} = \int_{-R}^{R} \tilde{Pr}(\bar{\Omega}_{ss,t} = A)e^{-CAt}dA. \tag{6.6}$$

Substituting in the gradient corrected steady state FT gives

$$\langle e^{-C\bar{\Omega}_{ss,t}t}\rangle_{-R<\bar{\Omega}_{ss,t}<R} = \int_{-R}^{R} \tilde{Pr}(\bar{\Omega}_{ss,t} = -A)dA \tag{6.7}$$

which after a change of variables can be rewritten as

$$\langle e^{-C\bar{\Omega}_{ss,t}t}\rangle_{-R<\bar{\Omega}_{ss,t}<R} = \int_{-R}^{R} \tilde{Pr}(\bar{\Omega}_{ss,t} = A)dA = 1, \tag{6.8}$$

recognising that the probability distribution is normalized over the range $-R$ to R. This truncated gradient corrected steady state NPI was calculated with the simulation data for

a range of values of R. The results are presented in Figure 6.6 for a selection of trajectory lengths.

For all lengths the gradient corrected NPI is within the error bars of unity, the expected value. The corrected version is a significant improvement over the uncorrected version. We can also note that truncating the gradient corrected steady state NPI has little effect on the calculated value, though the error bars tend to increase with increasing range. Since the corrected version of the NPI works while truncated the NPI does not, we can infer that the lack of convergence of the steady state NPI is not due to a lack of statistics but a failure of the Steady State FT to converge quickly enough. The regular version of the steady state NPI is not equal to the expected value of unity, and the corrected version can only be calculated after first empirically determining how well the FT has converged, so the steady state NPI will not be useful as a diagnostic tool in simulation and experiment.

6.4 Convergence of the Steady State NPI

To investigate the convergence of the steady state NPI further we can study its behaviour using model Gaussian distributions for the dissipation function. For long trajectory lengths, the distribution must become Gaussian around the mean according to the Central Limit Theorem[117]. From the corrected form of the steady state FT, Eq. (6.5), we can construct a Gaussian distribution that would satisfy this relationship. We saw in Figure 6.4 that it is reasonable to assume a linear relationship for the steady state FT for long enough trajectory lengths. Substituting the equation for a Gaussian distribution,

$$Pr(\bar{\Omega}_{ss,t} = A) = \frac{1}{\sigma\sqrt{2\pi}} \exp\left[-\frac{(A-\mu)^2}{2\sigma^2}\right] \tag{6.9}$$

into the gradient corrected FT gives

$$\exp[CAt] = \frac{\exp\left[-\frac{(A-\mu)^2}{2\sigma^2}\right]}{\exp\left[-\frac{(-A-\mu)^2}{2\sigma^2}\right]} \tag{6.10}$$

$$CAt = \ln\left[\exp\left[-\frac{(A-\mu)^2}{2\sigma^2} + \frac{(-A-\mu)^2}{2\sigma^2}\right]\right] \tag{6.11}$$

$$CAt = \frac{4A\mu}{2\sigma^2} \tag{6.12}$$

$$\sigma^2 = \frac{2\mu}{Ct}. \tag{6.13}$$

The variance of the distribution of the time averaged dissipation function, σ^2, is twice the mean of the dissipation function, μ, divided by the gradient factor, C and trajectory duration, t. This specifies the Gaussian distribution that satisfies the corrected form of the steady state FT, where the value of C determines how close it is to converging. The probability distribution of the time average of the dissipation function is now given by

$$Pr(\bar{\Omega}_{ss,t} = A) = \frac{1}{\sqrt{4\mu\pi/Ct}} \exp\left[-\frac{Ct(A-\mu)^2}{4\mu}\right]. \tag{6.14}$$

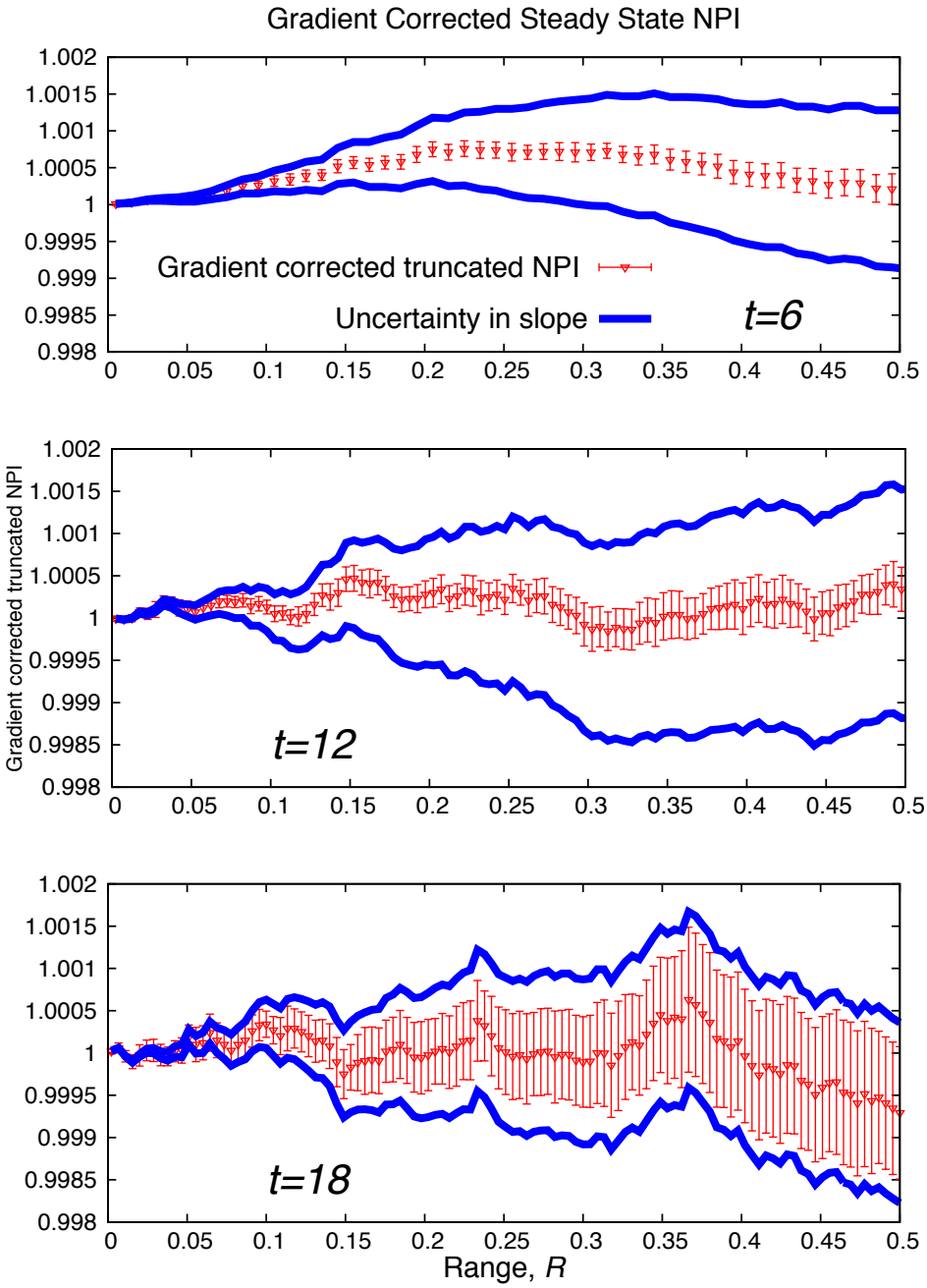

Figure 6.6: The gradient corrected steady state NPI, Eq. (6.5), calculated for each trajectory length, t, used in the colour conductivity simulations. The values used for C to calculate the gradient corrected NPI are given in Table 6.1. This data is represented by the red triangles, with the error bars calculated from the data being split into 10 sets. The blue dotted line corresponds to the uncertainty in the gradient corrected NPI due to the uncertainty in C.

We can use this to calculate the value of the NPI

$$\begin{aligned}\langle e^{-\bar{\Omega}_{ss,t}t}\rangle &= \int_{-\infty}^{\infty} Pr(\bar{\Omega}_t = A)\exp[-At]dA &(6.15)\\ &= \int_{-\infty}^{\infty} \frac{1}{\sqrt{4\mu\pi/Ct}}\exp\left[-\frac{Ct(A-\mu)^2}{4\mu}\right]\exp[-At]dA &(6.16)\\ &= \frac{1}{\sqrt{4\mu\pi/Ct}}\exp\left[\frac{-Ct\mu}{4}\right]\int_{-\infty}^{\infty}\exp\left[\frac{-CtA^2}{4\mu}-\left(1-\frac{C}{2}\right)At\right]dA. &(6.17)\end{aligned}$$

Recognising that this is the definite integral over a Gaussian distribution we have

$$\langle e^{-\bar{\Omega}_{ss,t}t}\rangle = \frac{1}{\sqrt{4\mu\pi/Ct}}\exp\left[\frac{-Ct\mu}{4}\right]\times\sqrt{\frac{4\pi\mu}{Ct}}\exp\left[\frac{\mu t\left(1-\frac{C}{2}\right)^2}{C}\right] \quad (6.18)$$

for $Ct/4\mu > 0$. Now,

$$\langle e^{-\bar{\Omega}_{ss,t}t}\rangle = \exp\left[-\mu t\left(1-\frac{1}{C}\right)\right]. \quad (6.19)$$

This equation shows how the value of the steady state NPI will change with the mean of the time averaged dissipation function, the trajectory duration and the slope of the Steady State FT, C. It is displayed graphically in Figure 6.7. Substituting in the calculated values from the simulation system for $t = 18$ of $\mu = 0.0994$ and $C = 1.0095$ we can calculate the expected value of the NPI, if the data was Gaussian. This gives a value for the exponential average of 0.983, which agrees with the simulation result of 0.983 ± 0.001.

From Eq. (6.19) we can see that when C=1 the NPI has a value of unity for all values of the mean because the distribution of dissipation function values satisfies the regular fluctuation theorem. Also, when $\mu = 0$, corresponding to an equilibrium system, the NPI has a value of unity. As the mean of the distribution increases, the value of the NPI drops faster with an increasing gradient factor.

The Steady State Fluctuation Theorem, Eq. (6.1), converges as the trajectory length, t, approaches infinity. The mean of the distribution of the time averaged dissipation function $\bar{\Omega}_{ss,t}$ will be constant with trajectory length. Thus, from Eq. (6.19), to keep the NPI constant with t

$$\begin{aligned} t &\propto \frac{1}{1-\frac{1}{C}}\\ \frac{1}{t} &\propto \frac{C-1}{C}. \end{aligned} \quad (6.20)$$

In order for the value of the NPI to converge as $t \to \infty$ the difference between the slope of the Steady State FT and unity, divided by the slope, must converge to zero faster than $1/t$.

Using the steady state simulation data we can examine the convergence of the Steady State FT. Figure 6.8 shows $(C-1)/C$ plotted against $1/t$ for a range of steady state trajectory lengths. We can see that to within the uncertainty the relationship is linear. This is consistent with the observation in Figure 6.1 that the steady state NPI does not converge with increasing trajectory length.

To further examine the behaviour of the NPI calculated using the Gaussian distribution

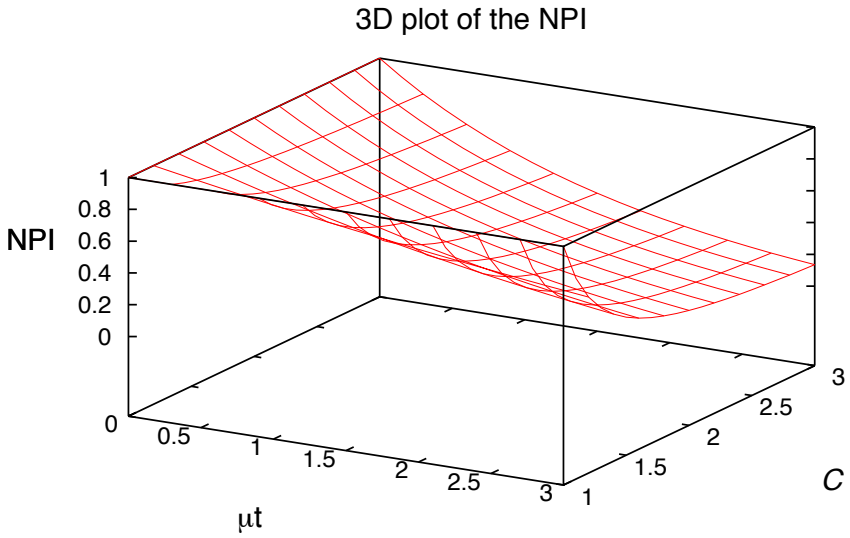

Figure 6.7: The value of the steady state NPI, Eq. (6.19), calculated from a Gaussian distribution for the dissipation function that satisfies the gradient corrected steady state FT, Eq. (6.5). It varies depending on μ, the mean of the time averaged dissipation function, t, the trajectory duration and C, the gradient factor and slope of the Steady State Fluctuation Theorem.

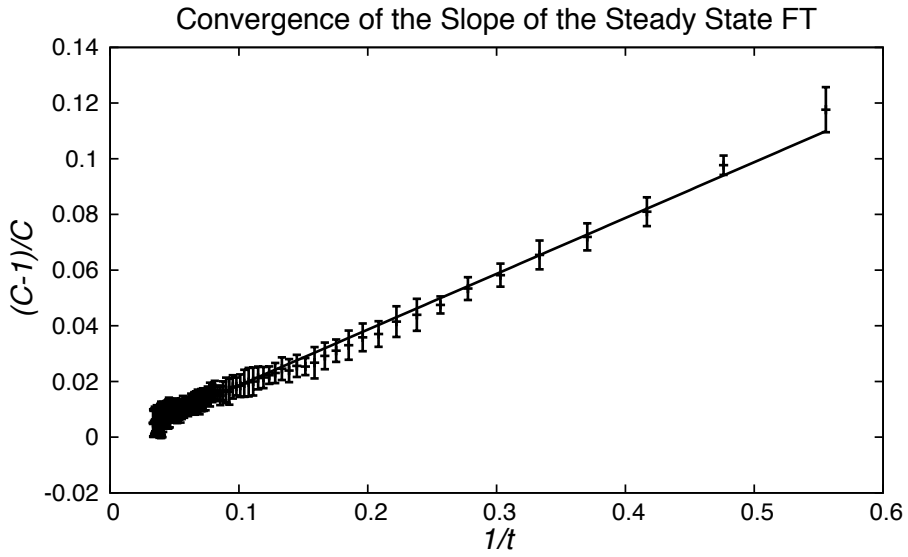

Figure 6.8: Graph showing the relationship between the slope of the Steady State FT, C, and the length of the steady state trajectory, t.

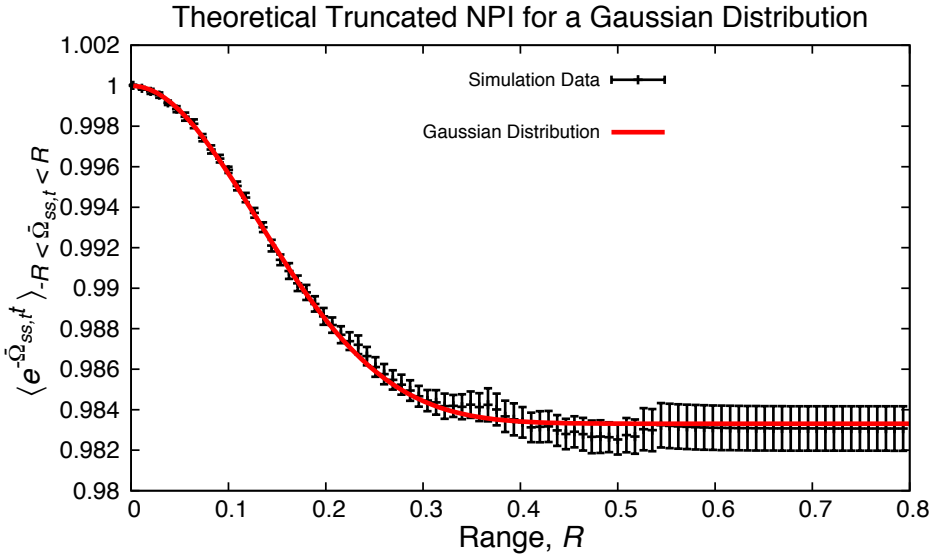

Figure 6.9: The truncated NPI calculated for a Gaussian distribution of the path integral of the dissipation function, over the truncated range, R. The same quantity calculated using the simulation data is shown for comparison.

we can calculate the truncated form of the NPI, given by

$$\left\langle e^{-\bar{\Omega}_{ss,t}t} \right\rangle_{-R<\bar{\Omega}_{ss,t}<R} = \frac{\int_{-R}^{R} Pr(\bar{\Omega}_{ss,t} = A) \exp[-At] dA}{\int_{-R}^{R} Pr(\bar{\Omega}_{ss,t} = A) dA}. \tag{6.21}$$

Substituting in the Gaussian distribution for the probability of the time average of the dissipation function, Eq. (6.14) we have

$$\left\langle e^{-\bar{\Omega}_{ss,t}t} \right\rangle_{-R<\bar{\Omega}_{ss,t}<R} = \frac{\exp\left[\frac{\mu t\left(1-(C/2)^2\right)}{C}\right]\left(\mathrm{erf}\left[\frac{CR/2\mu+(1-C/2)}{\sqrt{C/\mu t}}\right] - \mathrm{erf}\left[\frac{-CR/2\mu+(1-C/2)}{\sqrt{C/\mu t}}\right]\right)}{\exp\left[\frac{\mu t C}{4}\right]\left(\mathrm{erf}\left[\frac{CR/2\mu-C/2}{\sqrt{C/\mu t}}\right] - \mathrm{erf}\left[\frac{-CR/2\mu-C/2}{\sqrt{C/\mu t}}\right]\right)}. \tag{6.22}$$

Selecting values for C and μ corresponding to the colour conductivity simulation at time $t = 18$ we can plot the truncated NPI against the truncated range, R. This can be seen in Figure 6.9. We can see that this result from the Gaussian distribution has the same shape and is within the error bars of the truncated NPI calculated from the simulation data. Since the Gaussian distribution is effectively perfectly sampled, the shape of this truncated NPI with increasing range is a property of the function. The observed difference between the value of the truncated steady state NPI and unity is not a result of limited statistics in our computational system.

6.4.1 Linear Response Regime

In the linear response regime the mean and variance of the steady state dissipative flux, J_t, are known. The dissipation function of the system can be written in terms of the dissipative

flux. We will assume the distribution of dissipation function values is Gaussian, which will allow us to calculate the value of the steady state NPI for systems in the linear response regime.

The variance of the time integral of the dissipative flux[13, 32] is defined to be

$$\begin{aligned}
\left\langle J_t^2 \right\rangle_{eq} &\equiv \left\langle \left(\int_0^t J(s) ds \right)^2 \right\rangle_{eq} && (6.23)\\
&= \int_0^t ds' \int_0^t ds \langle J(s) J(s') \rangle_{eq} && (6.24)\\
&= \int_0^t ds' \int_0^t ds \langle J(s-s') J(0) \rangle_{eq} && (6.25)
\end{aligned}$$

since we can shift the equilibrium autocorrelation function in time. Making the substitution $u = s - s'$,

$$\left\langle J_t^2 \right\rangle_{eq} = \int_0^t ds' \int_{-s'}^{t-s'} du \langle J(u) J(0) \rangle_{eq}. \tag{6.26}$$

Changing the order of integration we have

$$\begin{aligned}
\left\langle J_t^2 \right\rangle_{eq} &= \int_{-t}^0 du \int_{-u}^t ds' \langle J(u) J(0) \rangle_{eq} + \int_0^t du \int_0^{t-u} ds' \langle J(u) J(0) \rangle_{eq} && (6.27)\\
&= \int_{-t}^0 du (t+u) \langle J(u) J(0) \rangle_{eq} + \int_0^t du (t-u) \langle J(u) J(0) \rangle_{eq} && (6.28)\\
&= 2t \int_0^t ds \langle J(s) J(0) \rangle_{eq} - 2 \int_0^t s \langle J(s) J(0) \rangle_{eq} ds. && (6.29)
\end{aligned}$$

The equilibrium variance will be the same as the steady state and transient variance in the weak field limit. The dissipation function is given by[63]

$$\bar{\Omega}_t = -\frac{1}{t} \beta J_t V F_{ex}, \tag{6.30}$$

so the variance of the time averaged dissipation function in the steady state, σ_{ss}^2, is given by

$$\sigma_{ss}^2 = \sigma_{Tr}^2 = \left(\frac{1}{t} \beta V F_{ex} \right)^2 \left(2t \int_0^t ds \langle J(s) J(0) \rangle_{eq} - 2 \int_0^t s \langle J(s) J(0) \rangle_{eq} ds \right). \tag{6.31}$$

This is the same as the variance in the transient, σ_{Tr}^2. In the transient case the distribution of $\bar{\Omega}_t$ satisfies the ES-FT, which allows us to calculate mean of the transient dissipation function from the variance[113],

$$\begin{aligned}
\mu_{Tr} &= \frac{t \sigma_{Tr}^2}{2} && (6.32)\\
&= (\beta V F_{ex})^2 \left(\int_0^t ds \langle J(s) J(0) \rangle_{eq} - \frac{1}{t} \int_0^t s \langle J(s) J(0) \rangle_{eq} ds \right). && (6.33)
\end{aligned}$$

The mean of the dissipative flux for steady state systems is given by the Green-Kubo[68,

67] relation,

$$\langle \bar{J}_t \rangle_{Fe} = -\beta V F_{ex} \int_0^\infty \langle J(0)J(s)\rangle_{eq} ds \tag{6.34}$$

and so the mean of the time averaged dissipation function in the steady state, μ_{ss}, is given by

$$\mu_{ss} = (\beta V F_{ex})^2 \int_0^\infty \langle J(0)J(s)\rangle_{eq} ds. \tag{6.35}$$

As $t \to \infty$ the integral $\int_0^t s\langle J(s)J(0)\rangle_{eq} ds$ in Eq. (6.33) converges and approaches a constant value. As time increases we can see that

$$\lim_{t\to\infty} \mu_{ss} = \mu_{Tr} + \frac{k}{t} \tag{6.36}$$

where $k = \lim_{t\to\infty}(\beta V Fe)^2 \int_0^t s\langle J(s)J(0)\rangle_{eq} ds$.

In order to calculate the value of the steady state NPI, Eq. (6.19), we need to know the slope of the Steady State FT, C. For a Gaussian distribution of dissipation function values, the natural log of the relative probabilities is given by

$$\ln\left[\frac{Pr(\bar{\Omega}_{ss,t} = A)}{Pr(\bar{\Omega}_{ss,t} = -A)}\right] = \frac{2\mu_{ss}}{\sigma_{ss}^2} A. \tag{6.37}$$

The slope of the Steady State FT is then $C = 2\mu_{ss}/t\sigma_{ss}^2 = \mu_{ss}/\mu_{Tr}$. Substituting this into the equation for the steady state NPI, Eq. (6.19) we have

$$\langle e^{-\bar{\Omega}_{ss,t}t} \rangle \quad = \quad \exp\left[-k\right].$$

In the linear response regime the steady state NPI is a constant whose value depends on the autocorrelation function of the dissipative flux. In the delta correlated case this reduces to a value of unity. That is, when there is no time correlation for the value of J. In the low field limit we have $\langle \exp[-\bar{\Omega}_{ss,t}t]\rangle = 1 - k + \frac{1}{2}k^2 + \cdots$ so the steady state NPI decays from unity as $O(F_{ex}^2)$.

6.5 Conclusion

The nonequilibrium partition identity can be more easily calculated in transient systems using its truncated form. The truncated from is not useful in calculating the value of the steady state NPI. Although the Steady State Fluctuation Theorem converges with time, we have shown that for systems where the distribution of dissipation function values is Gaussian, the steady state NPI only converges to unity if the Steady State FT converges sufficiently quickly. That is, the difference between the slope of the Steady State FT and unity, divided by the slope, must converge to zero faster than one over the trajectory length. In the linear response regime the FT converges at precisely this rate, so the value of the steady state NPI is simply a constant with respect to the length of the steady state trajectory. Its value is dependent on the field strength and the autocorrelation function of the dissipative flux, and is unity in delta correlated systems.

Chapter 7

The Instantaneous Fluctuation Theorem

Fluctuation relations typically provide information about path integrals of phase functions in time-reversible dynamical systems[4, 10, 71, 72, 118, 119, 120, 121, 122, 123, 77, 124, 125, 126, 127, 113]. In this chapter we will present a fluctuation relation that gives the relative probability that the instantaneous values of a phase function take on opposite values, $\pm A$, in terms of the well known path integral of the dissipation function.

This new theorem is closely related to a key result by Evans *et. al.*[70] which gives the form of the covariant dissipation function. An overview of the covariant dissipation function is provided in Section 2.11. Evans *et. al.* introduce new notation useful in the derivation we present. The dissipation function is a function of the dynamics of the system and a distribution. Typically the distribution function used is the known initial distribution of the system. The covariant dissipation function is defined with respect to the time dependent distribution function as the system evolves.

To represent this situation exactly we will use this more detailed notation. The distribution function used will be defined by the point in time, t_b, at which the system takes on this distribution. To fully specify the dissipation function we also need the variables τ, the time interval the dissipation function is integrated over, and t_a, the starting point of this interval. We assume the dynamics are autonomous. We will use the notation set out in the previous work[70] for the integrated dissipation function,

$$\Omega_\tau(S^{t_a}\mathbf{\Gamma};t_b) \equiv \int_{t_a}^{t_a+\tau} \Omega(S^s\mathbf{\Gamma};t_b)ds \equiv \ln\left(\frac{f(S^{t_a}\mathbf{\Gamma};t_b)}{f(M^TS^\tau S^{t_a}\mathbf{\Gamma};t_b)}\right) - \int_{t_a}^{t_a+\tau}\Lambda(S^s\mathbf{\Gamma})ds \quad (7.1)$$

where $\mathbf{\Gamma}$ is the phase space position at time 0, S^t is the phase space evolution operator acting for a time t, M^T is the time reversal operator, $\Omega(\mathbf{\Gamma};t)$ is the instantaneous dissipation function defined with respect to the distribution function at time t, $f(\mathbf{\Gamma};t)$ is the phase space density at position $\mathbf{\Gamma}$ of the system at time t and $\Lambda = \frac{\partial}{\partial\mathbf{\Gamma}}\cdot\dot{\mathbf{\Gamma}}$ is the phase space expansion factor.

7.1 Derivation

To derive the new relation we consider a deterministic system initially at equilibrium at time 0 that then undergoes a transient when a constant force is applied. We are interested in the instantaneous probability of a phase function at some particular time, t_1, during this transient.

The Evans-Searles Fluctuation Theorem[63] involves a quantity now known as dissipation. The ES-FT gives the probability of observing a set of trajectories in some small volume of phase space $\delta V_{\mathbf{\Gamma}}$ centered on some phase space vector compared to the conjugate set of antitrajectories,

$$\frac{p(\delta V_{\mathbf{\Gamma}}(\mathbf{\Gamma});0)}{p(\delta V_{\mathbf{\Gamma}}(M^T S^{2t_1}\mathbf{\Gamma});0)} = \exp[\Omega_{2t_1}(\mathbf{\Gamma};0)] \tag{7.2}$$

where $M^T(\mathbf{q},\mathbf{p}) \equiv (\mathbf{q},-\mathbf{p})$ is the time reversal mapping[128], $\delta V_{\mathbf{\Gamma}}(\mathbf{\Gamma})$ is the infinitesimal volume around the phase space position $\mathbf{\Gamma}$ and $p(\delta V_{\mathbf{\Gamma}}(\mathbf{\Gamma});0) = f(\mathbf{\Gamma},0)\delta V_{\mathbf{\Gamma}}(\mathbf{\Gamma})$ is the relative number of ensemble members inside this volume at time 0. The length of the trajectory in this case is $2t_1$. Conservation of phase space trajectories means that

$$p(\delta V_{\mathbf{\Gamma}}(\mathbf{\Gamma});0) = p(\delta V_{\mathbf{\Gamma}}(S^{t_1}\mathbf{\Gamma});t_1) \tag{7.3}$$

and

$$p(\delta V_{\mathbf{\Gamma}}(M^T S^{2t_1}\mathbf{\Gamma});0) = p(\delta V_{\mathbf{\Gamma}}(S^{t_1} M^T S^{2t_1}\mathbf{\Gamma});t_1) \tag{7.4}$$

because the volumes are defined such that they contain a fixed number of ensemble members. Those ensemble members that are located within $\delta V_{\mathbf{\Gamma}}(\mathbf{\Gamma})$ at $t=0$ also flow through $\delta V_{\mathbf{\Gamma}}(S^{t_1}\mathbf{\Gamma})$ at time t_1. This allows us to write the ES-FT in terms of phase space volumes at time t_1.

$$\frac{p(\delta V_{\mathbf{\Gamma}}(S^{t_1}\mathbf{\Gamma});t_1)}{p(\delta V_{\mathbf{\Gamma}}(S^{t_1} M^T S^{2t_1}\mathbf{\Gamma});t_1)} = \exp[\Omega_{2t_1}(\mathbf{\Gamma};0)]. \tag{7.5}$$

Let us consider an arbitrary phase function, $B(S^t\mathbf{\Gamma})$, that is odd under a time reversal transformation. We can write the probability of particular values of the phase function, $B(S^t\mathbf{\Gamma}) = A$, in terms of the probability of infinitesimal volumes around particular phase space positions. Summing each of these volumes gives the relative probability distribution of such values,

$$\frac{Pr(B(S^{t_1}\mathbf{\Gamma}) = A)}{Pr(B(S^{t_1}\mathbf{\Gamma}) = -A)} = \frac{\sum_{\delta V_{\mathbf{\Gamma}}(S^{t_1}\mathbf{\Gamma})|_{B=A}} p(\delta V_{\mathbf{\Gamma}}(S^{t_1}\mathbf{\Gamma});t_1)}{\sum_{\delta V_{\mathbf{\Gamma}}(S^{t_1}\mathbf{\Gamma})|_{B=-A}} p(\delta V_{\mathbf{\Gamma}}(S^{t_1}\mathbf{\Gamma});t_1)}. \tag{7.6}$$

Substituting in Eq. (7.5) gives

$$\frac{Pr(B(S^{t_1}\mathbf{\Gamma}) = A)}{Pr(B(S^{t_1}\mathbf{\Gamma}) = -A)} = \frac{\sum_{\delta V_{\mathbf{\Gamma}}(S^{t_1}\mathbf{\Gamma})|_{B=A}} p(\delta V_{\mathbf{\Gamma}}(S^{t_1}\mathbf{\Gamma});t_1)}{\sum_{\delta V_{\Gamma}(S^{t_1}\mathbf{\Gamma})|_{B=-A}} \exp[\Omega_{2t_1}(\mathbf{\Gamma};0)] p(\delta V_{\mathbf{\Gamma}}(S^{t_1} M^T S^{2t_1}\mathbf{\Gamma});t_1)}. \tag{7.7}$$

To understand this sum over volumes defined by phase space points $S^{t_1}\mathbf{\Gamma}$, where the prob-

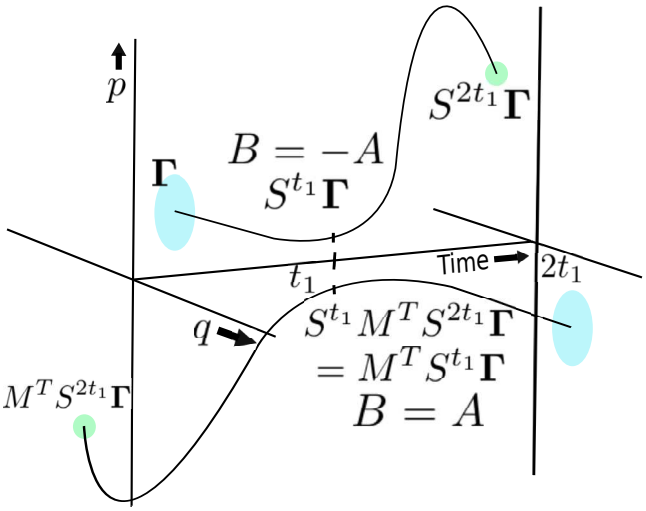

Figure 7.1: A trajectory starting from $\mathbf{\Gamma}$ with $B{=}\ -A$ at time $t = t_1$, along with its antitrajectory which begins from the time reversed map of $S^{2t_1}\mathbf{\Gamma}$.

ability in the argument is defined by the point $S^{t_1}M^TS^{2t_1}\mathbf{\Gamma}$ we need to understand the relationship between the trajectory and antitrajectory pair. This is represented visually in Figure 7.1.

It is easy to see from Figure 7.1 why the dissipation function needs to be defined over the time interval 0 to $2t_1$; at the mid point of the interval the position in phase space that the trajectory has evolved to is the time reverse map of the position reached by the antitrajectory. Since $B(\mathbf{\Gamma})$ is odd under the time reversal transformation, for each trajectory where $B(S^{t_1}\mathbf{\Gamma}) = -A$, the antitrajectory has $B(S^{t_1}M^TS^{2t_1}\mathbf{\Gamma}) = B(M^TS^{t_1}\mathbf{\Gamma}) = A$. This allows us to rewrite the denominator of Eq. (7.7) in terms of the conjugate antitrajectory volumes,

$$\frac{Pr(B(\mathbf{\Gamma}(t_1)) = A)}{Pr(B(\mathbf{\Gamma}(t_1)) = -A)} = \frac{\sum_{\delta V_{\mathbf{\Gamma}}(S^{t_1}\mathbf{\Gamma})|_{B=A}} p(\delta V_{\mathbf{\Gamma}}(S^{t_1}\mathbf{\Gamma}); t_1)}{\sum_{\delta V_{\mathbf{\Gamma}}(S^{t_1}M^TS^{2t_1}\mathbf{\Gamma})|_{B=A}} \exp[\Omega_{2t_1}(\mathbf{\Gamma}; 0)]p(\delta V_{\mathbf{\Gamma}}(S^{t_1}M^TS^{2t_1}\mathbf{\Gamma}); t_1)}. \quad (7.8)$$

Using the definition of the dissipation function, Eq. (2.33), $\exp[\Omega_{2t_1}(\mathbf{\Gamma}; 0)] = \exp[-\Omega_{2t_1}(M^TS^{2t_1}\mathbf{\Gamma}; 0)]$. The initial distribution function is always assumed to be even in the momenta. Eq. (7.8) now becomes

$$\begin{aligned} &\frac{Pr(B(\mathbf{\Gamma}(t_1)) = A)}{Pr(B(\mathbf{\Gamma}(t_1)) = -A)} \\ = \ &\frac{\sum_{\delta V_{\mathbf{\Gamma}}(S^{t_1}\mathbf{\Gamma})|_{B=A}} p(\delta V_{\mathbf{\Gamma}}(S^{t_1}\mathbf{\Gamma}); t_1)}{\sum_{\delta V_{\mathbf{\Gamma}}(S^{t_1}M^TS^{2t_1}\mathbf{\Gamma})|_{B=A}} \exp[-\Omega_{2t_1}(M^TS^{2t_1}\mathbf{\Gamma}; 0)]p(\delta V_{\mathbf{\Gamma}}(S^{t_1}M^TS^{2t_1}\mathbf{\Gamma}); t_1)}. \end{aligned} \quad (7.9)$$

Recognising that the sums in both the numerator and the denominator are over all phase space volumes defined by some $\mathbf{\Gamma}'$, where $B(S^{t_1}\mathbf{\Gamma}') = A$, Eq. (7.9) can be rewritten as a

conditional average,

$$\frac{Pr(B(S^{t_1}\mathbf{\Gamma})=A)}{Pr(B(S^{t_1}\mathbf{\Gamma})=-A)}=\frac{1}{\left\langle e^{-\Omega_{2t_1}(\mathbf{\Gamma};0)}\right\rangle_{B(S^{t_1}\mathbf{\Gamma})=A}}. \tag{7.10}$$

Similarly

$$\frac{Pr(B(S^{t_1}\mathbf{\Gamma})=A)}{Pr(B(S^{t_1}\mathbf{\Gamma})=-A)}=\left\langle e^{-\Omega_{2t_1}(\mathbf{\Gamma};0)}\right\rangle_{B(S^{t_1}\mathbf{\Gamma})=-A}. \tag{7.11}$$

This relationship is the Instantaneous Fluctuation Theorem, written in terms of conditional ensemble averages of exponentials of the dissipation function path integrals. These path integrals are symmetrically extended both before and after the time at which the instantaneous fluctuation relation is required. This instantaneous fluctuation relation is non-local in time. This is a standard feature of fluctuation relations that are required over time intervals that do not begin at the initial known distribution[70]. Another example is the steady state Evans-Searles fluctuation relation[63, 34].

We can look at the behaviour of the relative probabilities of opposite values of A as a function of time, t_1. Initially, when $t_1 = 0$ the dissipation function, $\Omega_{2t_1}(\mathbf{\Gamma};0) = 0$, and so the RHS of Eq. (7.11) is equal to 1 and both values of A are equally probable. At later times the value of the dissipation function changes, meaning the opposite values of A are not equally probable, corresponding to the irreversibility of the system growing.

The dissipation function in our new result can be written as a covariant dissipation function[70] from Eq. (2.85) in Section 2.11,

$$\Omega_{2t_1}(\mathbf{\Gamma};0)=\Omega_0(S^{t_1}\mathbf{\Gamma};t_1). \tag{7.12}$$

To those not used to the mathematical definition of dissipation the fact that $\Omega_0(S^{t_1}\mathbf{\Gamma};t_1)\neq 0$ may seem strange. It is due to the fact that in our work we always assume that the initial distribution is even in the momenta. This guarantees that the average velocity of the system is zero with respect to the observer and it also guarantees that $\Omega_0(\mathbf{\Gamma};0)=0$, $\forall\mathbf{\Gamma}$ because $f(\mathbf{\Gamma};0)/f(M^T\mathbf{\Gamma};0)=1$. At later times, $f(\mathbf{\Gamma};t)/f(M^T\mathbf{\Gamma};t)\neq 1$.

Clearly the right hand side of Eq. (7.10) is more involved to calculate, the simulation needs to be run for twice as long. However, in certain circumstances this new fluctuation relation may be the only way to calculate the value of the left hand side of the equation. For example, it is often the case that the probability of a particular value of $B=-A$ is be very low, while the probability of $B=A$ is substantial. In this case, calculating $Pr(B=-A)$ directly could be challenging and require a huge number of statistics, where as calculating the other terms in the instantaneous fluctuation theorem may be straightforward, particularly if care is taken to select the form of the equation which includes the conditional average with the more probable trajectories. This is one possible direct application of the new theorem to real problems.

7.2 Restricted Phase Space NPI

We may obtain an obvious summing rule from Eq. (7.10) and Eq. (7.11). Upon setting $A = 0$ we obtain

$$\left\langle e^{-\Omega_{2t_1}(\mathbf{\Gamma};0)} \right\rangle_{B(S^{t_1}\mathbf{\Gamma})=0} = 1. \tag{7.13}$$

This may be understood in terms of ergodic consistency. When $B(S^{t_1}\mathbf{\Gamma}) = 0$ the set of trajectories used to form the above average is the exact same set as the conjugate antitrajectories and thus we have ergodic consistency over this restricted set of phase space. The phase space volume at time 0 coincides with the phase space volume at time $2t_1$, since the effect of B being odd under time reversal symmetry is lost when we set $B(S^{t_1}\mathbf{\Gamma}) = 0$. Because of this ergodic consistency the above summing rule may be viewed as an application of the NPI to this restricted set of phase space. The ES-FT can also be applied to this subset of phase space.

7.3 Numerical Results

To get a better understanding of the convergence and nature of the new instantaneous fluctuation relation we studied it numerically with a simple system. We modeled shear flow in a constant kinetic energy system that started from the equilibrium isokinetic ensemble. We chose to look at this in a two-dimensional 32 particle system. An isokinetic thermostat was used to obtain the desired starting conditions and keep a constant kinetic energy throughout the simulation. The system is subject to a constant shear at time $t > 0$ using the SLLOD equations of motion[27, 129] and square unit cell Lees-Edwards periodic boundary conditions[102]. Particle interactions were modeled using the WCA potential[87]. The temperature used was $T = 1$, the density was $\rho = 0.6$ and the time step used was $dt = 0.001$. Transient trajectories of length $t_1 = 0.1$ were initiated from positions found in the equilibrium system and were propagated using the SLLOD equations of motion, Eq. (2.13) and (2.14) in Section 2.3.1, with an applied strain rate of $\dot{\gamma} = 0.1$. An ensemble of 5×10^6 trajectories were simulated.

7.3.1 Derivation of Dissipation Function

To demonstrate the new theorem we need to know the form of the dissipation function for our numerical system[4]. From the definition of the dissipation function we have

$$\Omega_t = \ln\left(\frac{f(\mathbf{\Gamma},0)}{f(S^t\mathbf{\Gamma},0)}\right) - \int_0^t \Lambda(S^s\mathbf{\Gamma})ds \tag{7.14}$$

$$= \beta(H_0(t) - H_0(0)) + \int_0^t 2N\alpha(S^s\mathbf{\Gamma})ds \tag{7.15}$$

since our system starts in the canonical distribution. $H_0(t)$ is the internal energy of the system at time t. So, Eq. (7.15) is the change in internal energy less that due to the thermostat.

$$\Omega_t = \int_0^t \beta\dot{H}_0(s) + 2N\alpha(S^s\mathbf{\Gamma})ds. \tag{7.16}$$

The change in internal energy can be split into the kinetic, KE, and potential energy, Φ, components

$$\dot{H}_0(t) = \frac{\partial KE}{\partial t} + \frac{\partial \Phi}{\partial t} \tag{7.17}$$

$$= \frac{\partial}{\partial \mathbf{p}}\left(\frac{\mathbf{p}^2}{2m}\right)\cdot\frac{\partial \mathbf{p}}{\partial t} + \frac{\partial \Phi}{\partial \mathbf{q}}\cdot\frac{\partial \mathbf{q}}{\partial t} \tag{7.18}$$

$$= \sum_i^N \frac{\mathbf{p}_i\cdot\dot{\mathbf{p}}_i}{m} - \sum_i^N \mathbf{F}_i\cdot\dot{\mathbf{q}}_i. \tag{7.19}$$

Substituting in the SLLOD equations of motion, Eq. (2.13) and (2.14), we have

$$\dot{H}_0(t) = \sum_i^N\left(\frac{\mathbf{F}_i\cdot\mathbf{p}_i}{m} - \frac{\dot{\gamma}p_{yi}p_{xi}}{m} - \frac{\alpha(S^t\mathbf{\Gamma})\mathbf{p}_i\cdot\mathbf{p}_i}{m} - \frac{\mathbf{F}_i\cdot\mathbf{p}_i}{m} - \dot{\gamma}F_{xi}y_i\right) \tag{7.20}$$

$$= -\dot{\gamma}\sum_i^N\left(\frac{p_{yi}p_{xi}}{m} + F_{xi}y_i\right) - 2\alpha(S^t\mathbf{\Gamma})KE \tag{7.21}$$

$$= \dot{H}_0^{(ad)}(t) - \frac{2N\alpha(S^t\mathbf{\Gamma})}{\beta} \tag{7.22}$$

where

$$\dot{H}_0^{(ad)}(t) = -\dot{\gamma}\sum_i^N\left(\frac{p_{yi}p_{xi}}{m} + F_{xi}y_i\right) \tag{7.23}$$

is the adiabatic in energy. The dissipation function is given by combing Eq (7.16) and Eq (7.22),

$$\Omega_t = \beta\int_0^t \dot{H}_0^{(ad)}(s)ds \tag{7.24}$$

$$= -\beta\int_0^t \dot{\gamma}VP_{xy}(S^s\mathbf{\Gamma})ds. \tag{7.25}$$

where P_{xy} is the xy component of the pressure tensor, V is the area of the unit cell, p_{yi} and p_{xi} are the components of the peculiar momenta of particle i, F_{xi} is the x component of force on particle i and y_i is the y component of the position.

The computer simulation is run using periodic boundary conditions, so it is easier to calculate the value of the dissipation function when it is rewritten in terms of pairs of particles. Writing the total potential in terms of the potential of pairs of particles, ϕ_{ij}, we have

$$\Phi = \frac{1}{2}\sum_{i=1}^N\sum_{j=1}^N(1-\delta_{ij})\phi_{ij}. \tag{7.26}$$

Taking the force term in Eq. (7.23) we have

$$F_{xi} \equiv -\frac{\partial\Phi}{\partial x_i} = -\sum_{j=1}^N(1-\delta_{ij})\frac{\partial\phi_{ij}}{\partial x_i}. \tag{7.27}$$

Let us define $\Delta x_{ij} = x_j - x_i$ and $\Delta y_{ij} = y_j - y_i$. So,

$$\frac{\partial \phi_{ij}}{\partial x_i} = -\frac{\partial \phi_{ij}}{\partial \Delta x_{ij}} = \frac{\partial \phi_{ij}}{\partial \Delta x_{ji}}. \tag{7.28}$$

Now,

$$\sum_{i=1}^{N} F_{xi} y_i = \sum_{i=1}^{N}\sum_{j=1}^{N}(1-\delta_{ij})\frac{\partial \phi_{ij}}{\partial x_i} y_i \tag{7.29}$$

$$= -\frac{1}{2}\sum_{i=1}^{N}\sum_{j=1}^{N}(1-\delta_{ij})\frac{\partial \phi_{ij}}{\partial \Delta x_{ij}}\Delta y_{ij}. \tag{7.30}$$

Let $F_{xij} \equiv \frac{\partial \phi_{ij}}{\partial \Delta x_{ij}}$, the force on particle i due to j. So,

$$\sum_{i=1}^{N} F_{xi} y_i = -\frac{1}{2}\sum_{i=1}^{N}\sum_{j=1}^{N}(1-\delta_{ij}) F_{xij}\Delta y_{ij} \tag{7.31}$$

$$= -\sum_{i=1}^{N}\sum_{j=i+1}^{N} F_{xij}\Delta y_{ij}. \tag{7.32}$$

Substituting this into Eq. (7.23) gives the adiabatic change in energy

$$\dot{H}_0^{(ad)} = -\dot{\gamma}\left(\sum_{i}^{N}\frac{p_{yi}p_{xi}}{m} - \sum_{i=1}^{N}\sum_{j=i+1}^{N} F_{xij}\Delta y_{ij}\right) \tag{7.33}$$

which leads to the integrated dissipation function from Eq. (7.24),

$$\Omega_t = -\beta\dot{\gamma}\int_0^t ds \sum_{i}^{N}\frac{p_{yi}p_{xi}}{m} - \sum_{i=1}^{N}\sum_{j=i+1}^{N} F_{xij}\Delta y_{ij}. \tag{7.34}$$

7.3.2 Phase Function Selection

In the analysis above we generate the antitrajectories using a time reversal map of the final point in a trajectory, and then evolve this point in time using the equations of motion. A time reversal map in our chosen system would change the sign of the strain rate, $\dot{\gamma}$. It is inconvenient and unnecessary to run the simulation with two values of $\dot{\gamma}$ because we can instead use a different trajectory mapping. The appropriate mapping is known as the Kawasaki mapping[27], $(x, y, p_x, p_y, \dot{\gamma}) \rightarrow (x, -y, -p_x, p_y, \dot{\gamma})$. Evolving the new point generated from this mapping forward in time using a strain rate $\dot{\gamma}$ generates the same antitrajectory as evolving a time reversed map point forward in time with the strain rate $-\dot{\gamma}$. The analysis of this system is otherwise identical to the general case above.

In order to demonstrate the new fluctuation relation we need to select a phase function of the system that is odd under the Kawasaki mapping. We can then numerically calculate the relative probabilities of particular values of the phase function at a given time, and compare this to the integrated dissipation function calculated over twice this time. A convenient

phase function to use is the dissipative flux,

$$VP_{xy}(\mathbf{\Gamma}) = \sum_{i=1}^{N} \left[\frac{p_{yi} p_{xi}}{m} + F_{xi} y_i \right]. \tag{7.35}$$

Although $VP_{xy}(\mathbf{\Gamma})$ is even under the time reversal mapping it is odd under the Kawasaki mapping, hence $VP_{xy}(\mathbf{\Gamma})$ is a suitable phase function to investigate the Instantaneous FT. Rewritten for easier computation in a system which has periodic boundary conditions this becomes

$$VP_{xy}(\mathbf{\Gamma}) = \sum_{i=1}^{N} \frac{p_{yi} p_{xi}}{m} - \sum_{i=1}^{N} \sum_{j=i+1}^{N} F_{xij} \Delta y_{ij}. \tag{7.36}$$

7.3.3 Demonstration of the Instantaneous Fluctuation Theorem

To demonstrate the new fluctuation relation we need to calculate the relative probability of positive and negative values of $VP_{xy}(S^t\mathbf{\Gamma})$ at each time we are interested in for a system undergoing planar shear at constant shear rate $\dot{\gamma}$. This was done by constructing frequency histograms from an ensemble of trajectories, dividing the values of $VP_{xy}(S^{t_1}\mathbf{\Gamma})$ into discrete bins and taking the ratio of frequencies for a positive valued bin to the corresponding negative bin. The integrated dissipation function, $\Omega_{2t_1}(\mathbf{\Gamma}; 0)$, was calculated for each time interval $2t_1$.

We calculated the conditional average, $\left\langle e^{-\Omega_{2t_1}(\mathbf{\Gamma};0)} \right\rangle^{-1}_{VP_{xy}(S^{t_1}\mathbf{\Gamma})=A}$, based on the value of $VP_{xy}(S^{t_1}\mathbf{\Gamma})$. The relative probability was plotted against the conditional average, seen in Figure 7.2(a). The uncertainties given in the equations in Figure 7.2 are the standard errors from the least squares fit of the data. To the order of the standard error, the slope of this graph is unity, demonstrating the new fluctuation relation. It was observed that the slope of (a) trended upwards towards unity with an increasing number of ensemble members used in the average. The system displays non-Gaussian statistics, a common feature in other nonequilibrium systems[130, 37, 75, 84, 116, 131] and nonequilibrium averages such as the Nonequilibrium Partition Identity[27], and it is not straightforward to accurately determine the uncertainty in these calculations. In Figure 7.2 (a) and (b) we also demonstrated the equivalence of the two forms of the Instantaneous Fluctuation Theorem, Eq. (7.10) and Eq. (7.11).

Since the form of this new fluctuation relation is not necessarily intuitive, it is instructive to look at the behaviour of an altered form of the relation. We can consider the case where the dissipation function is integrated only up to the time where the relative probabilities of the phase functions are measured, i.e. over the time interval 0 to t_1. This simulation was conducted in the same manner as above and the results are included in Figure 7.2(c). The fluctuation relation is clearly not satisfied in this case as the slope of the curve is not 1. This demonstrates that the use of conjugate sets of trajectories and antitrajectories is essential in this fluctuation relation, as it is in the original Evans-Searles fluctuation relation[33].

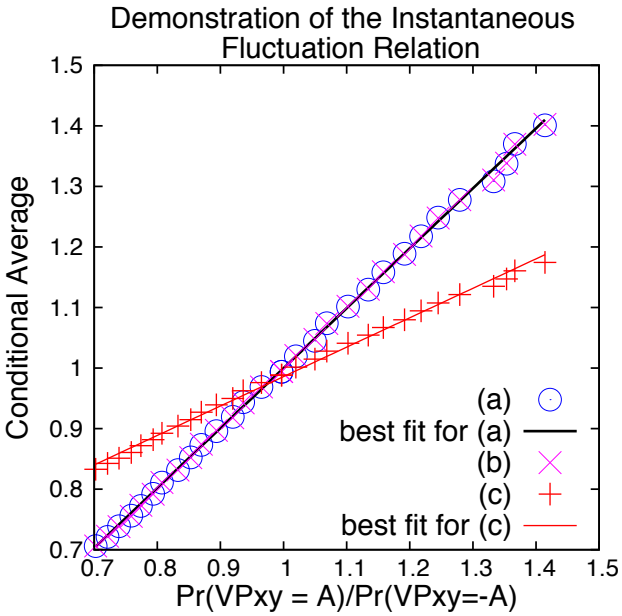

Figure 7.2: (a) $\left\langle e^{-\Omega_{2t_1}(\mathbf{\Gamma};0)}\right\rangle^{-1}_{VP_{xy}(S^{t_1}\mathbf{\Gamma})=A}$, demonstration of Eq. (7.10) with a line of best fit $y = (0.994 \pm 0.001)x + (0.006 \pm 0.001)$. (b)$\left\langle e^{-\Omega_{2t_1}(\mathbf{\Gamma};0)}\right\rangle_{VP_{xy}(S^{t_1}\mathbf{\Gamma})=-A}$, demonstration of Eq. (7.11), the second equivalent form of the relation. Note that the $\times$'s are falling on top of the circles. (c) $\left\langle e^{-\Omega_{t_1}(\mathbf{\Gamma};0)}\right\rangle_{VP_{xy}(S^{t_1}\mathbf{\Gamma})=-A}$, test of altered form of the relation with a line of best fit $y = (0.488 \pm 0.003)x + (0.497 \pm 0.003)$.

7.3.4 Additional Phase Function Demonstrations

To prove that this result is not unique to the dissipative flux we demonstrated the new theorem using the phase functions $\sum_{i=1}^{N} p_{yi}p_{xi}/m$ and $-\sum_{i}^{N}\sum_{j=i+1}^{N} F_{xij}y_{ij}$. These functions are the kinetic and configurational components of the dissipative flux, and so are clearly different from it. In both cases the new instantaneous fluctuation relation is satisfied, seen in Figure 7.3.

7.3.5 Demonstration of the ES-FT in Ergodic Subsets of Phase Space

Subsets of phase space defined by $B(S^{t_1}\mathbf{\Gamma}) = 0$ are ergodic over the time interval t_1, and as such the ES-FT can be applied to them.

$$\frac{Pr(\Omega_{2t_1}(\mathbf{\Gamma};0) = A)_{B(S^{t_1}\mathbf{\Gamma})=0}}{Pr(\Omega_{2t_1}(\mathbf{\Gamma};0) = -A)_{B(S^{t_1}\mathbf{\Gamma})=0}} = \exp[A] \tag{7.37}$$

where the trajectories included in the probability calculation are only those with $B(S^{t_1}\mathbf{\Gamma}) = 0$. Using the same computational system as above, and the phase function $B = VP_{xy}$ we can demonstrate the Evans-Searles FT in this subset of phase space.

Trajectories satisfying the criteria $VP_{xy}(S^{t_1}\mathbf{\Gamma}) = 0$ were selected, and the dissipation function was calculated over the interval $(0, 2t_1)$. We demonstrated the FT in the usual

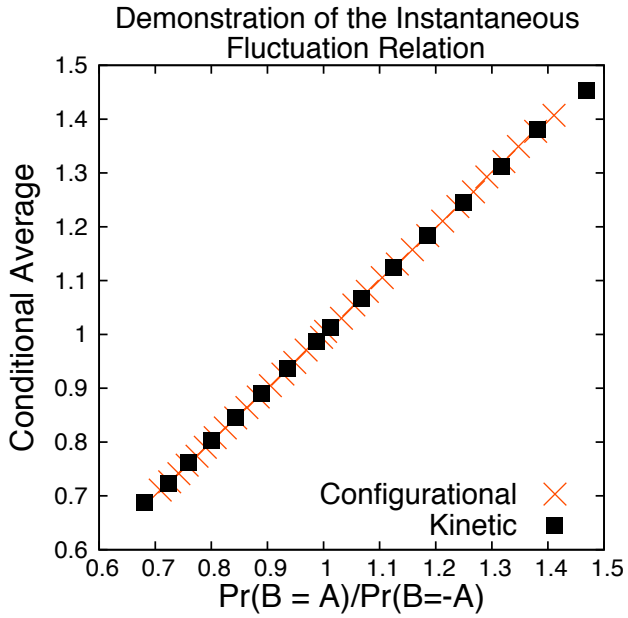

Figure 7.3: Demonstration of the Instantaneous Fluctuation Theorem using the kinetic ($B = \sum_{i=1}^{N} p_{yi} p_{xi}/m$) and configurational ($B = -\sum_{i}^{N} \sum_{j=i+1}^{N} F_{xij} y_{ij}$) components of the dissipative flux. The equations of best fit are $y = (0.981 \pm 0.002)x + (0.019 \pm 0.002)$ and $y = (0.996 \pm 0.001)x + (0.004 \pm 0.001)$ respectively.

way, by plotting the LHS of Equation (7.37) against the RHS, seen in Figure 7.4. This linear curve with a slope of unity demonstrates the fluctuation theorem. To demonstrate that the FT is not applicable to all subsets of phase space, we carried out the procedure using trajectories where $VP_{xy}(S^{t_1}\mathbf{\Gamma}) = -5$ and plotted this in the same graph. This value for the dissipative flux was selected because it has a similar probability to $VP_{xy}(S^{t_1}\mathbf{\Gamma}) = 0$ and so comparable statistics will be obtained. The attempted demonstration curve is clearly not linear, so the ES-FT is not applicable to this non-ergodic subset of phase space.

7.4 Conclusion

We have derived and demonstrated computationally a new fluctuation relation applicable to physical systems which gives different information to those studied in the past. The instantaneous fluctuation relation is similar in form to other fluctuation relations, except it considers path integrals of dissipation that are symmetrically extended both before and after the time at which the relative probabilities are compared. This work confirms the non time-local nature of dissipation. We also demonstrated that time reversibility for the trajectory/antitrajectory sets is a necessary condition for the fluctuation relation to hold. The instantaneous fluctuation relation shows how in driven, thermostatted systems, irreversibility (as manifest in the relative probabilities of odd phase functions taking on opposite values) grows as the system leaves equilibrium.

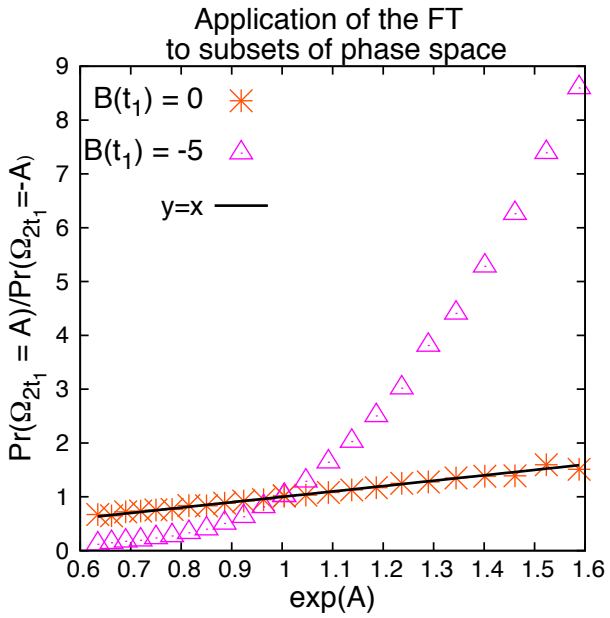

Figure 7.4: Evans-Searles FT applied to two subsets of phase space, defined by $VP_{xy}(S^{t_1}\mathbf{\Gamma}) = 0$ and $VP_{xy}(S^{t_1}\mathbf{\Gamma}) = -5$.

Chapter 8

The Integrated Instantaneous Fluctuation Theorem and its Behaviour as the Steady State is Approached

The Evans-Searles Fluctuation Theorem was one of the first exact results in far from equilibrium statistical mechanics. It quantifies the probability of fluctuations of the dissipation function with complimentary values. From this theorem an integrated form was derived to make it more directly comparable with the Second Law of Thermodynamics[4]. This integrated form gives the probability of positive fluctuations in the time averaged dissipation function relative to the probability of negative fluctuations. More of phase space is included in calculating the relative probability, so this form of the theorem displays better statistics making it valuable in computational and experimental demonstrations[37, 15, 40].

8.1 Derivation of the Integrated Form

Like the ES-FT, we can derive an integrated form of the Instantaneous Fluctuation Theorem. That is, we can compare the probability of all positive values of the phase function to all negative values. The derivation below follows the same method as the derivation of the Evans-Searles Integrated FT[4]. We define $p_+(t_1) \equiv p(B(S^{t_1}\mathbf{\Gamma}) > 0)$ and $p_-(t_1) \equiv p(B(S^{t_1}\mathbf{\Gamma}) < 0)$, the probability of positive and negative values of B respectively. We can write

$$\frac{p_-(t_1)}{p_+(t_1)} = \frac{\int_0^\infty dA Pr(B(S^{t_1}\mathbf{\Gamma}) = -A)}{\int_0^\infty dA Pr(B(S^{t_1}\mathbf{\Gamma}) = A)}. \tag{8.1}$$

Using one of the forms of the Instantaneous Fluctuation Theorem[132], Eq. (7.10), we can rewrite this as

$$\frac{p_-(t_1)}{p_+(t_1)} = \frac{\int_0^\infty dA \langle e^{-\Omega_{2t_1}(\mathbf{\Gamma};0)}\rangle_{B(S^{t_1}\mathbf{\Gamma})=A} Pr(B(S^{t_1}\mathbf{\Gamma})=A)}{\int_0^\infty dA Pr(B(S^{t_1}\mathbf{\Gamma})=A)}. \tag{8.2}$$

Recognising that this is an ensemble average calculated over all trajectories with a positive value of A gives

$$\frac{p_-(t_1)}{p_+(t_1)} = \langle \langle e^{-\Omega_{2t_1}(\mathbf{\Gamma};0)}\rangle_{B(S^{t_1}\mathbf{\Gamma})=A}\rangle_{A>0} = \langle e^{-\Omega_{2t_1}(\mathbf{\Gamma};0)}\rangle_{B(S^{t_1}\mathbf{\Gamma})>0}. \tag{8.3}$$

Similarly, from the other form of the Instantaneous Fluctuation Theorem, Eq. (7.11), it can be shown that

$$\frac{p_+(t_1)}{p_-(t_1)} = \langle e^{-\Omega_{2t_1}(\mathbf{\Gamma};0)}\rangle_{B(S^{t_1}\mathbf{\Gamma})<0}. \tag{8.4}$$

This new integrated fluctuation relation gives the relative probability of positive instantaneous values of an arbitrary phase function in terms of the dissipation function over the symmetric interval surrounding the time in question. We can use $p_+(t_1) + p_-(t_1) = 1$ to write

$$p_+ = \frac{1}{1 + \langle e^{-\Omega_{2t_1}(\mathbf{\Gamma};0)}\rangle_{B(S^{t_1}\mathbf{\Gamma})>0}}, \tag{8.5}$$

the probability of a value of B being positive.

The integrated form of the instantaneous fluctuation relation will display better statistics than the original form since it includes more values in the conditional average. This makes it more applicable to computer simulations and experimental systems, particularly in the case of long trajectories where rare events, which have a significant effect on the exponential average, are much less common.

The ability to use longer trajectories allows us to apply the new integrated instantaneous fluctuation relation to a numerical system on the approach to the steady state. The theorem is now written in terms of a single value at each point in time, which makes monitoring the system's behaviour with time easier.

8.2 Demonstration of the Integrated Instantaneous Fluctuation Theorem

To demonstrate this theorem we need to choose a nonequilibrium system to study. We consider using the shear flow system used to demonstrate the original version of the Instantaneous Fluctuation Theorem in Chapter 7, however we would need to reduce the number of particles in the system to be able to extend the trajectories into the steady state. The Couette flow model is not well suited to systems with few particles because the equations of motion become non-autonomous, as discussed in Section 3.1.5. The limitations of the SLLOD equations of motion for this case are discussed below.

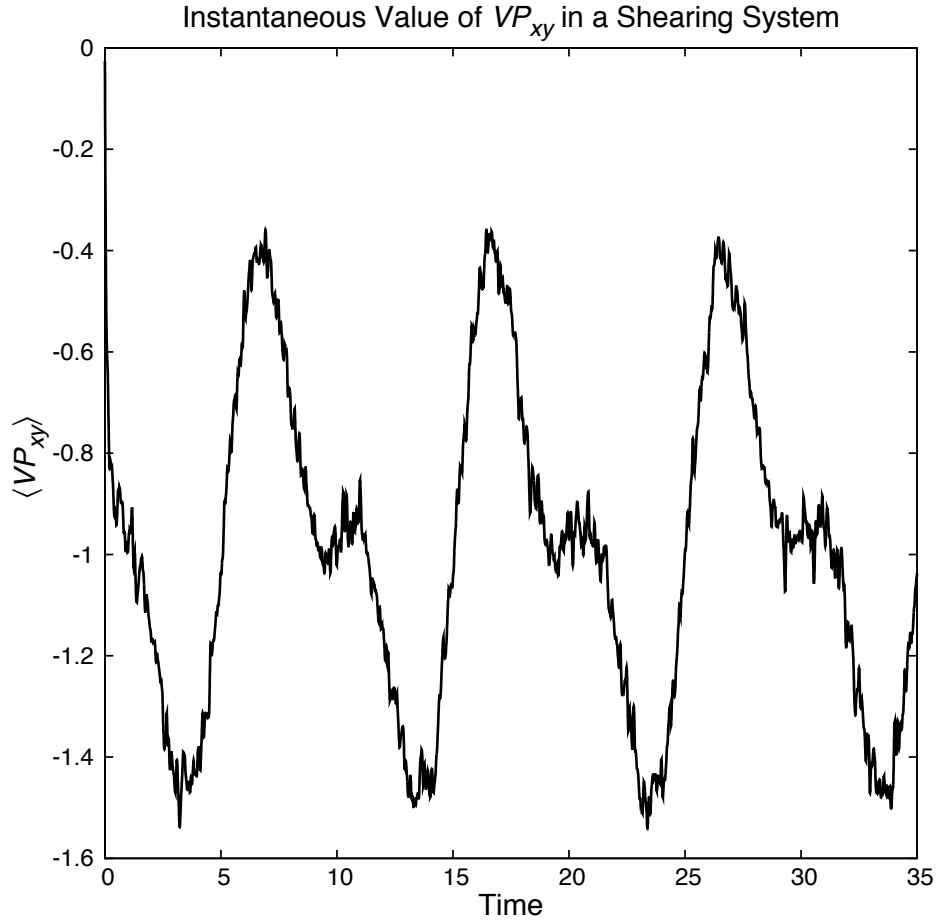

Figure 8.1: Behaviour of the ensemble average of the instantaneous value of the phase function VP_{xy} as a function of the time since the system began to shear.

8.2.1 Limitations of the Couette Flow System

A shear flow system relaxes to an unphysical periodic state rather than a steady state when a small number of particles are used in the simulation. This behaviour has been observed for two-particle planar-couette flow systems[133, 134], and is because the periodic boundary conditions used are not autonomous[105].

As an example, we can simulate a system similar to what was used in Chapter 7. We will use SLLOD equations of motion, Eq. (2.13) and (2.14), in a system with temperature $T = 1$, density $\rho = 0.6$ and a time step of $dt = 0.001$. The system starts in an equilibrium canonical ensemble and 10^5 trajectories are simulated. We will use a two dimensional system of 8 WCA particles, and a trajectory length long enough that the system should be approaching a steady state. Selecting the phase function $B = VP_{xy}$, we can investigate its instantaneous value as the system moves away from equilibrium. This was done in Figure 8.1, where the average instantaneous value of VP_{xy} is plotted against time.

We can see that the value of VP_{xy} is time dependent and periodic. This is a consequence of the periodic boundary conditions used and is unphysical. Clearly this system can not be

used to study the Integrated Instantaneous Fluctuation Theorem on the approach to a steady state, as the relative probability of positive to negative values of the phase function VP_{xy} is meaningless, and the system does not approach a steady state.

8.2.2 Colour Conductivity System

Instead, we choose a system that starts in the equilibrium isokinetic ensemble, then progresses towards a steady state when a colour field is applied. This is described in Section 2.3.2, with the equations of motion given by Eq. (2.18) and (2.19) The kinetic energy of the system is kept constant by the thermostat[34] given by Eq. (2.20). We will use a system of $N = 8$ particles. The simulations used a temperature of $T = 1$, a density of $\rho = 0.6$ and a time step of $dt = 0.001$. Transient trajectories were initiated from random positions taken from the equilibrium ensemble and then propagated using the equations of motion with a constant colour field applied in the x direction, $\mathbf{F}_e = (F_{ex}, 0) = (0.5, 0)$. An ensemble of 10^8 trajectories was used.

We can demonstrate the new theorem using a phase function which is odd under the time reversal mapping. A convenient phase function to use is

$$B(\mathbf{\Gamma}) = -\mathbf{J}(\mathbf{\Gamma})V \cdot \mathbf{F}_e = \sum_{i=1}^{N} c_i \frac{\mathbf{p}_i}{m} \cdot \mathbf{F}_e = F_{ex} \sum_{i=1}^{N} c_i \frac{p_{xi}}{m} \tag{8.6}$$

where $\mathbf{J}$ is the dissipative flux, p_{xi} is the $x-$component of the peculiar momenta of particle i and in our 2D system V is the area of the unit cell.

We would expect that the conditional average with more members will give better statistics, so will use Eq. (8.3) as positive values of $-\mathbf{J}(\mathbf{\Gamma})V \cdot \mathbf{F}_e$ are more probable in this system. To demonstrate this new integrated fluctuation relation we need to calculate the relative probability of all negative values of $B(\mathbf{\Gamma})$ to all positive values, $p_-(t_1)/p_+(t_1)$. This was done by taking an ensemble of trajectories and calculating the relative frequency of negative to positive values. The form of the dissipation function for this system is well known[34], and is given by

$$\Omega_{2t_1}(\mathbf{\Gamma}; 0) = -\int_0^{2t_1} ds\beta \mathbf{J}(\mathbf{\Gamma})V \cdot \mathbf{F}_e = \int_0^{2t_1} ds\beta F_{ex} \sum_{i=1}^{N} c_i \frac{p_{xi}}{m}. \tag{8.7}$$

Its value was calculated over the interval $(0, 2t_1)$ for each trajectory and was included in the conditional average $\langle e^{-\Omega_{2t_1}(\mathbf{\Gamma};0)} \rangle_{B(S^{t_1}\mathbf{\Gamma})>0}$ when the value of $-\mathbf{J}(\mathbf{\Gamma})V \cdot \mathbf{F}_e$ was positive at time t_1. To look at how the behaviour of the system changes with time we calculate $p_-(t_1)/p_+(t_1)$ and $\langle e^{-\Omega_{2t_1}(\mathbf{\Gamma};0)} \rangle_{B(S^{t_1}\mathbf{\Gamma})>0}$ for a range of values of t_1 along each trajectory as it moves towards a steady state.

8.2.3 Numerical Results

The behaviour of the LHS and RHS of Equation (8.3) as a function of the trajectory length, t_1, is plotted in Figure 8.2. We can see that as the length of the trajectory increases and the system is closer to being in a steady state, the relative probability of positive and

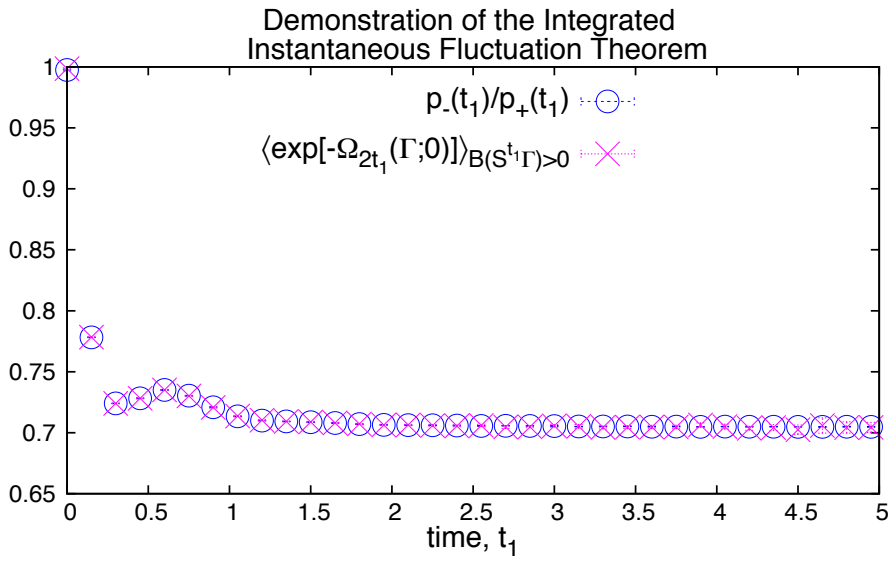

Figure 8.2: The LHS($p_-(t_1)/p_+(t_1)$) in circles, and the RHS($\langle e^{-\Omega_{2t_1}(\mathbf{\Gamma};0)}\rangle_{B(S^{t_1}\mathbf{\Gamma})>0}$) in crosses of Eq. (8.3) against t_1, the time at the midpoint of the trajectory. Note that the crosses are falling on top of the circles, and the error bars are not visible on this scale.

negative fluctuations approaches a constant value, as expected. This trend is matched by the conditional average. We can see that the LHS and RHS appear equivalent, but the error bars are not visible on the scale shown.

The error bars were calculated by splitting the ensemble of trajectories into 10 groups and calculating both sides of the equation in each one, then using these values to calculate the standard error. Twice the standard error, the 95% confidence interval, was used as the error bars in Figure 8.2. The error bars on both variables were summed to give the error bar range, which is compared to the difference between the variables in Figure 8.3. We can see that the difference is within the 95% confidence interval for all times, demonstrating the new relation.

8.3 Derivation of the Steady State Form

We can look at the behaviour of the Integrated Instantaneous FT in the steady state. We will start by assuming the value of the dissipation function is delta correlated. That is, there is no serial correlation in the time series data for the instantaneous dissipation function, nor any between the instantaneous dissipation function and the phase function B. This allows us to rewrite Eq. (8.3) as

$$\frac{p_-(t_1)}{p_+(t_1)} = \langle e^{-\Omega_{t_1}(\mathbf{\Gamma};0)}\rangle \langle e^{-\Omega_0(S^{t_1}\mathbf{\Gamma};0)}\rangle_{B(S^{t_1}\mathbf{\Gamma})>0} \langle e^{-\Omega_{t_1}(S^{t_1}\mathbf{\Gamma};0)}\rangle. \tag{8.8}$$

From the Nonequilibrium Partition Identity we have $\langle e^{-\Omega_{t_1}(\mathbf{\Gamma};0)}\rangle = 1$ and $\langle e^{-\Omega_{t_1}(S^{t_1}\mathbf{\Gamma};0)}\rangle = 1$ (since $\langle e^{-\Omega_{2t_1}(\mathbf{\Gamma};0)}\rangle = \langle e^{-\Omega_{t_1}(\mathbf{\Gamma};0)}\rangle \langle e^{-\Omega_{t_1}(S^{t_1}\mathbf{\Gamma};0)}\rangle = 1$ for delta correlated systems).

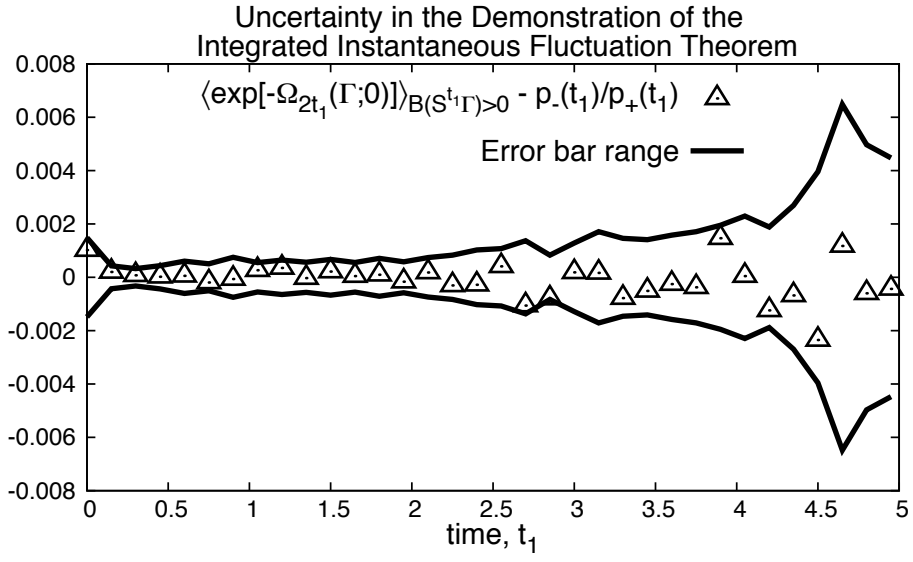

Figure 8.3: The difference between the LHS and the RHS of Eq. (8.3), the Integrated Instantaneous Fluctuation Theorem, as a function of t_1. The error bar range is the sum of the 95% confidence intervals of both variables.

Now,

$$\frac{p_-(t_1)}{p_+(t_1)} = \langle e^{-\Omega_0(S^{t_1}\mathbf{\Gamma};0)}\rangle_{B(S^{t_1}\mathbf{\Gamma})>0} \tag{8.9}$$

which in the steady state is constant, as expected.

For systems which are not delta correlated the condition on the average will affect more than just one instant in time. For a T-mixing system the correlations of the dissipation function will decay to an arbitrarily fine tolerance after some cut off time, $c\tau_M$ (a multiple of the Maxwell time τ_M). So, if we split the conditional average into three parts, the part containing the condition must include the interval $(t_1 - c\tau_M, t_1 + c\tau_M)$. This means the parts of the trajectory affected by the condition will be included in the conditional average. There will be some error introduced due to the correlation between each of the sections that have been split up in the average, as well as an error introduced in assuming delta correlation to give the value of $\langle e^{-\Omega_{t_1}(S^{t_1}\mathbf{\Gamma};0)}\rangle = 1$. We can write the approximate form of the Integrated Instantaneous FT as

$$\frac{p_-(t_1)}{p_+(t_1)} = \langle e^{-\Omega_{2c\tau_M}(S^{t_1-c\tau_M}\mathbf{\Gamma};0)}\rangle_{B(S^{t_1}\mathbf{\Gamma})>0}. \tag{8.10}$$

If this interval is in the steady state then the relative probability of positive to negative values of B will be constant with respect to t_1, as expected. This relationship will only be valid for dissipation function integrals over a large enough range around the point in time at which we are computing the relative probability. We will call this the steady state trajectory length, $\tau = 2c\tau_M$. We can use computer simulations to investigate the trajectory length required.

We saw in Section 6.4 that for non-delta correlated systems the steady state NPI is not

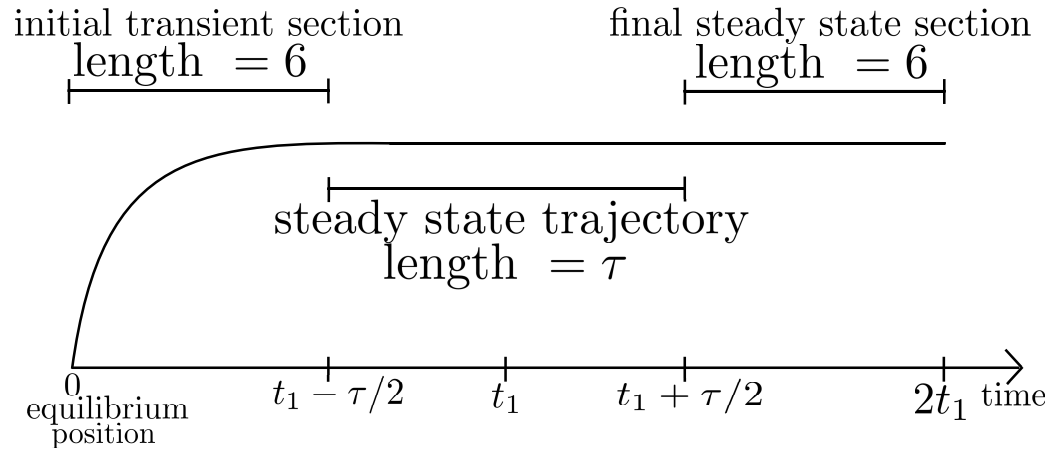

Figure 8.4: Schematic diagram illustrating the computational procedure to generate an ensemble of steady state trajectories. Each ensemble member is initiated from a different position in the equilibrium ensemble.

equal to unity. The third section in Eq. (8.8) is the steady state NPI, and will not have a value of unity. This demonstrates that assuming delta correlation to split up the exponential averages introduces an error. We can use computer simulations to further investigate the behaviour of these exponential averages and test the approximations made in arriving at Eq. (8.10).

8.4 Numerical Test of the Steady State Form

To test the steady state form of the relation computationally we need to initiate our trajectories from within the steady state. We use the same colour conductivity system described in Section 8.2.2, but don't start recording the path integral of the dissipation function until after the system has reached a steady state. Each trajectory was generated by initiating the system from a different equilibrium position, and running a transient trajectory for a length of 6 (i.e., $t_1 - \tau/2 = 6$). After this time the system was assumed to be in a steady state, and the steady state trajectory is recorded. The simulation is then continued for an additional time of 6 to allow for the calculation of averages in the final steady state trajectory. This computational procedure is illustrated in Figure 8.4. The simulation parameters are the same as described in Section 8.2.2.

The LHS and the RHS of Eq. (8.10) are both plotted against the steady state trajectory length in Figure 8.5. We can see that the relative probability of negative values of B to positive values is constant as expected. While the conditional average converges to a constant value with increasing trajectory length, this value is not within the uncertainty of the relative probability.

The value of the conditional average (at $\tau = 10$) and the relative probabilities were calculated for a range of field strengths, presented in Table 8.1. In each case, the steady state form of the new FT is not satisfied. The difference between the LHS and RHS of Eq. (8.10) increases with field strength. The shape of the trend of the conditional average

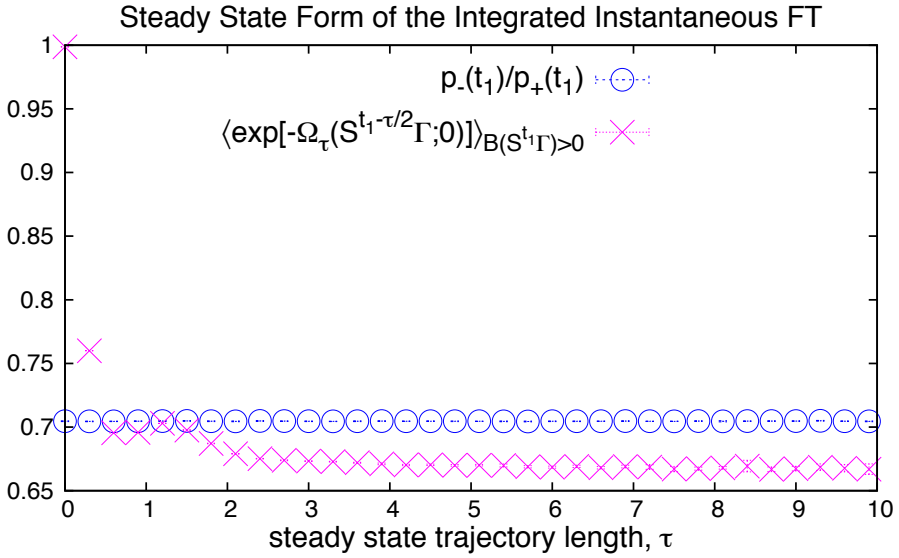

Figure 8.5: Test of the steady state form of the Instantaneous Fluctuation Theorem, Eq. (8.10), with field strength 0.5. The LHS of the equation, the relative probability of negative to positive values of the phase function B is plotted in blue circles, and the RHS of the equation, the conditional average of the exponential of the dissipation function is plotted in pink crosses. Note that the error bars in both quantities are not visible on this scale.

with trajectory length is not presented, but was the same as observed in Figure 8.5 for all field strengths.

To understand the source of this deviation between the LHS and RHS of Eq. (8.10) we can consider the approximations made in deriving this steady state form of the FT. The transient ensemble average was split into three segments; the unconditional average of the initial transient section, the conditional average of the middle steady state section (plotted in Figure 8.5), and the unconditional average of the steady state section. This involved assuming that the condition does not affect the first and last section when the middle steady state section is sufficiently long. We can test this assumption by calculating each of the sections using the simulated system, with the condition applied. This condition, $B > 0$, will be applied at time t_1, with the distance between the condition and the outer

F_{ex}	$\frac{p_-(t_1)}{p_+(t_1)}$	$\langle e^{-\Omega_\tau(S^{t_1-\tau/2}\mathbf{\Gamma};0)}\rangle_{B(S^{t_1}\mathbf{\Gamma})>0}$	Percentage difference
0.71	0.606	0.536	12%
0.5	0.705	0.667	5.4%
0.29	0.817	0.803	1.7%
0.17	0.888	0.883	0.6%
0.043	0.971	0.970	0.1%

Table 8.1: The conditional average in the steady state form of the Integrated Instantaneous Fluctuation Theorem, Eq. (8.10), and its expected value, the relative probability of negative values of the phase function at time t_1. The time t_1 is in the steady state. The percentage difference between these values are calculated. Results are from the colour conductivity simulation, conducted with a range of applied field strengths, F_{ex}.

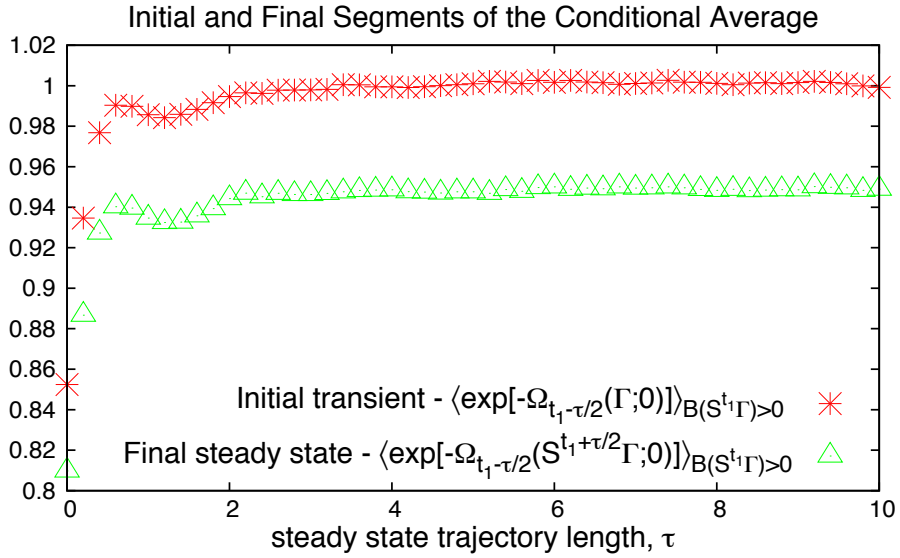

Figure 8.6: Values of the average over the initial transient trajectory, and the average over the final steady state trajectory (following the steady state trajectory which contains the time where the condition is applied, t_1). The x-axis shows the steady state trajectory length, which is a measure of how far the applied condition is from the trajectories used to calculate the averages shown.

sections determined by the length of the steady state trajectory, τ. The value of both of these conditional averages is plotted against the steady state trajectory length in Figure 8.6. As the length of the steady state trajectory grows, and there is a sufficiently long distance between the trajectory used in the average and the applied condition, both of these averages approach a constant value. This implies that at this time the averages are uncorrelated from the condition. The initial transient average approaches a value of unity, as expected from the transient NPI. The steady state average approaches a value that is not equal to unity, consistent with what was observed for the steady state NPI in Section 6.4.

The other approximation used in deriving the steady state form of this FT was assuming that the conditional average could be written as three separate averages. To test this assumption we can multiply each of the calculated sections together, and compare it to the value of the conditional average calculated over the entire transient trajectory, which includes the steady state sections. Both of these functions are plotted in Figure 8.7, along with the value of the relative probabilities. The conditional average calculated over the full length of the trajectory is equal to the probability of negative values of the phase function relative to the probability of positive values, as expected. We can clearly see that the product of the conditional averages from the first, middle and final trajectory segments is not equal of the conditional average for the full length of the trajectory.

These two approximations made in deriving the steady state form of the fluctuation theorem mean that the value of the steady state conditional average is not equal to the value of the relative probability.

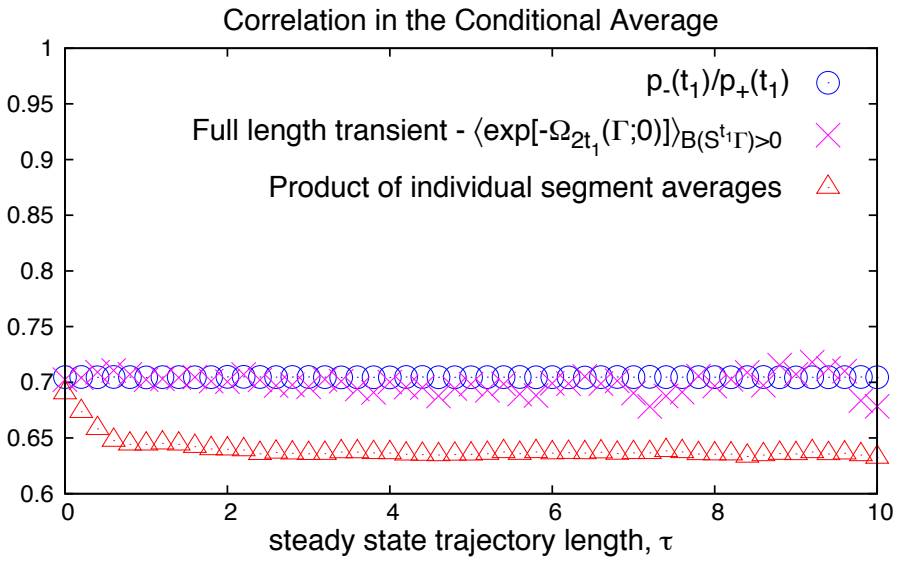

Figure 8.7: The conditional average in the transient Integrated Instantaneous FT, Eq. (8.3), compared to the product of three segment averages. The product of the individual segment averages $= \langle e^{-\Omega_{t_1-\tau/2}(\mathbf{\Gamma};0)}\rangle_{B(S^{t_1}\mathbf{\Gamma})>0} \times \langle e^{-\Omega_\tau(S^{t_1-\tau/2}\mathbf{\Gamma};0)}\rangle_{B(S^{t_1}\mathbf{\Gamma})>0} \times \langle e^{-\Omega_{t_1-\tau/2}(S^{t_1+\tau/2}\mathbf{\Gamma};0)}\rangle_{B(S^{t_1}\mathbf{\Gamma})>0}$. Each of these averages is plotted individually in Figures 8.5 and 8.6. The relative probabilities of the negative to positive values of B are shown to demonstrate that the full length transient conditional average satisfies the transient version of the Integrated Instantaneous FT.

8.4.1 Truncated Steady State Form

We can attempt to improve the statistics of the calculation of the conditional average in Eq. (8.10) by truncating the distribution symmetrically around zero, as was done in calculating the truncated NPI in Section 5.9. The truncated average,

$$\langle e^{-\Omega_\tau(S^{t_1-\tau/2}\mathbf{\Gamma};0)}\rangle_{B(S^{t_1}\mathbf{\Gamma})>0,-R<\Omega_\tau<R} \tag{8.11}$$

is plotted against the truncation range in Figure 8.8. A steady state trajectory length of $\tau = 6$ was used for these results.

The truncated form of the average starts at a value of unity when a very small range is used, then quickly falls to the untrunctated value. Truncating the range of dissipation function values used does not bring the average any closer to the value of the relative probability, and is not a viable method for calculating this nonequilibrium exponential average.

8.4.2 Renormalized Steady State Form

We have established that both of the approximations made in deriving the steady state form contribute to the deviation of the value of the conditional average from the relative probability. The percentage difference between the value of the conditional average and the relative probability is dependent on the field strength in the system. We can note from Table 8.2 that this difference appears to be the same as the percentage difference between

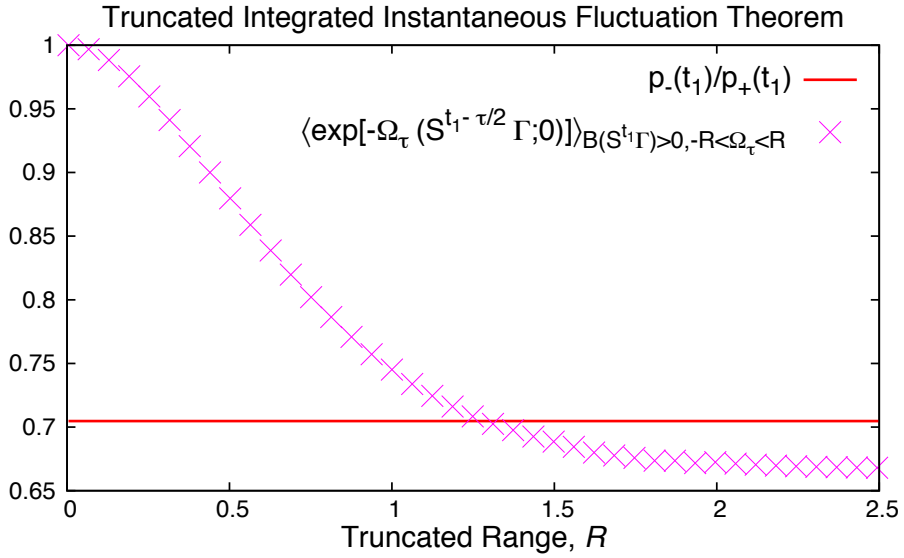

Figure 8.8: The ensemble average from the steady state Integrated Instantaneous FT, Eq. (8.10), calculated using only values of the dissipation function within the truncated range. The relative probability of negative values of the phase function to positive values is shown as a solid line for comparison.

the value of the steady state NPI and unity. The steady state NPI is the same average as the conditional average, calculated over the full ensemble. To exploit this we will calculate the value of

$$\frac{\langle e^{-\Omega_\tau(S^{t_1-\tau/2}\mathbf{\Gamma};0)}\rangle_{B(S^{t_1}\mathbf{\Gamma})>0}}{\langle e^{-\Omega_\tau(S^{t_1-\tau/2}\mathbf{\Gamma};0)}\rangle} \tag{8.12}$$

and compare its value to $\frac{p_-(t_1)}{p_+(t_1)}$. This is effectively renormalising the conditional average by the steady state NPI. The relative probabilities and the explicitly renormalized average are plotted in Figure 8.9 for a range of trajectory lengths.

As the length of the steady state trajectory increases, the renormalized conditional average in Eq. (8.12) approaches the relative probability. Renormalising the conditional average

F_{ex}	Difference in LHS and RHS of the Steady State Integrated Instantaneous FT, Eq. (8.10)	Steady state NPI	Difference between NPI and unity
0.71	12%	0.896	10%
0.5	5.4%	0.949	5.1%
0.29	1.7%	0.982	1.8%
0.17	0.6%	0.994	0.6%
0.043	0.1%	0.9996	0.04%

Table 8.2: Relationship between the conditional average of the Steady State Integrated Instantaneous Fluctuation Theorem, $\langle e^{-\Omega_\tau(S^{t_1-\tau/2}\mathbf{\Gamma};0)}\rangle_{B(S^{t_1}\mathbf{\Gamma})>0}$, and its expected value, the relative probability, given for a range of field strengths used in the simulation. The percentage difference between the steady state NPI and unity is also given for comparison.

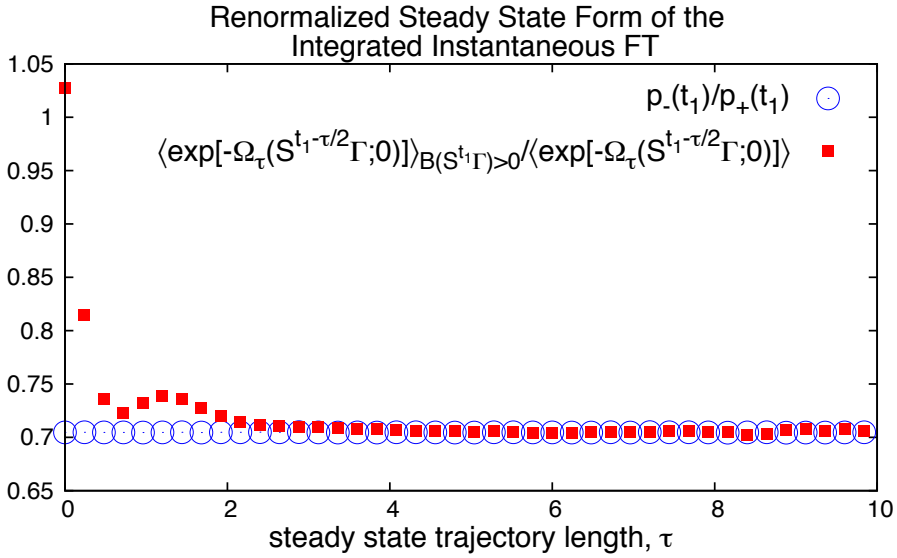

Figure 8.9: Test of the renormalized conditional average, shown as red squares, plotted against the relative probability, shown as blue circles. The simulation data is plotted for a range of steady state trajectory lengths. The simulation used a field strength of 0.5.

has corrected its value to what was expected from the delta correlated derivation, for sufficiently long trajectory lengths.

When the trajectory is long enough, the applied condition only affects parts of the trajectory that are included in the middle steady state average. In this simulated system that time is approximately 3, meaning the condition is a time of 1.5 from the edge of the steady state trajectory on each side.

8.5 Conclusion

We have derived an integrated form of the Instantaneous Fluctuation Theorem. This form shows better statistics than the original, and so it could be demonstrated computationally in a system approaching a steady state. A new form of the theorem applicable to systems that start in the steady state was investigated. This form of the theorem was derived exactly for the delta correlated case. For non-delta correlated systems we observed that the assumptions made in deriving the relationship resulted in a deviation between the value of the conditional average in the steady state and the relative probability. This error could be corrected by renormalising the conditional average with the steady state NPI.

Chapter 9

Conclusions

This thesis has examined the significance of the dissipation function in a number of applications in nonequilibrium statistical mechanics. Chapter 1 introduced the problems provoking the need for the fluctuation theorems. In Chapter 2 the dissipation function was introduced, a critical part of the Evans-Searles Fluctuation Theorem. The most significant results involving the dissipation function to date were also covered. Chapter 3 outlined the computer simulation techniques necessary for the investigations in this thesis.

In Chapter 4 we applied a number of the significant results involving the dissipation function to systems relaxing monotonically and non-monotonically towards equilibrium. We used these systems to demonstrate the Second Law Inequality and the Dissipation Theorem. For systems undergoing field free relaxation from a colour gradient, the dissipation function relaxes monotonically, while the colour density distribution decayed to a sine curve of fundamental wavelength, which decayed conformally towards a uniform distribution. The dissipation function was also monitored in systems relaxing from a density gradient affecting all particles, and non-monotonic relaxation was observed. The density distribution function did not relax conformally, and at times appeared to be moving away from a uniform distribution.

The Nonequilibrium Partition Identity is discussed in Chapter 5. While the value of this average involving the dissipation function is simply derived from the ES-FT, it can also be derived to have a different value when other approximations are made. We show that both of these values are observable, under different simulation conditions.

Calculating the average which is the subject of the NPI proves difficult in computational and experimental systems. We first approach this problem by examining the uncertainty and asymmetry in data arising from demonstrating the fluctuation theorem. We used the fluctuation theorem itself to model the range of values we expect to measure for the frequency of each value of the dissipation function. This was done by modeling each histogram bin with a binomial distribution. This allowed us to see the asymmetry involved in the wings of the distribution of dissipation function values when demonstrating the ES-FT. We also constructed a method for sensibly weighting the data when demonstrating the fluctuation theorem, which will be useful for many experimental and computational studies. We extend this process to calculate the expected range of values for the NPI when it is calculated using

only one pair of histogram bins from the distribution of the dissipation function, providing valuable insight into the mechanism of the difficulty in calculating the value of the full NPI. A new truncated form of ensemble average is derived, which eliminates some of the problems caused by a lack of statistics, and can be calculated more easily than the full average.

Chapter 6 extends this work to the less studied steady state form of the NPI. We show that while the asymptotic steady state FT from which it is derived converges, the steady state NPI never reaches the expected value of unity. This was observed in computer simulations and proven for the linear response regime, where the distribution of dissipation function values is Gaussian. The value of the NPI is dependent on the autocorrelation function of the dissipative flux, and in the special delta correlated case it is equal to unity.

A new result involving the dissipation function was derived and demonstrated in Chapter 7. This new Instantaneous Fluctuation Theorem has the same form as previous fluctuation relations, but provides different information. It considers path integrals of the dissipation function that are symmetrically extended both before and after the time at which the relative probabilities are compared. We demonstrated computationally that time reversibility for the trajectory/antitrajectory sets is a necessary condition for this fluctuation theorem to hold.

In Chapter 8 this work was extended by deriving an integrated form of the Instantaneous Fluctuation Theorem. This was demonstrated in a system approaching a steady state. We also investigated a form of the theorem applicable to systems already in the steady state. This is a desirable class of systems to study because they are more accessible experimentally. The steady state form of the theorem was derived exactly for delta correlated systems, but for realistic non-delta correlated systems it was found that the assumptions made in the derivation resulted in a deviation between the value of the conditional average in the steady state and the relative probability. This systematic error could be corrected by renormalising the average by the steady state NPI.

We have seen that the dissipation function can be useful in studying nonequilibrium systems since it is the argument in a number of exact results, such as the ES-FT, the Relaxation Theorem and the Dissipation Theorem. Ensemble averages of the exponential of the negative dissipation function have been studied in this thesis in the form of the conditional average encountered in the Instantaneous Fluctuation Theorem, the NPI and the steady state NPI. We have seen that these quantities can be difficult to calculate computationally, and looked into the mechanism of this difficulty and approaches to resolve it.

Bibliography

[1] Loschmidt, J. *J. Sitzungsber. der kais. Akad. d. W. Math. Naturw. II* **73**, 128 (1876).

[2] Cercignani, C. *Ludwig Boltzmann : The Man Who Trusted Atoms* (Oxford University Press, Oxford, 2006).

[3] Ehrenfest, P. & Ehrenfest, T. *The Conceptual Foundations of the Satistical Approach in Mechanics* (Cornell University Press, Ithica, New York, 1959).

[4] Evans, D. J. & Searles, D. J. The Fluctuation Theorem. *Advances in Physics* **51**, 1529–1585 (2002).

[5] Broda, E. & Gay, L. *Ludwig Boltzmann: Man, Physicist, Philosopher* (Ox Bow Press, Woodbridge, 1983).

[6] Boltzmann, L. *Rejoinder to the heat theoretical considerations of Mr. E. Zermelo* (1896).

[7] Maxwell, J. C. On Boltzmann's theorem on the average distribution of energy in a system of material points. *Transactions of the Cambridge Philosophical Society* **12**, 547 (1879).

[8] Klein, M. The Development of Boltzmann's Statistical Ideas. In Cohen, E. G. D. & Thirring, W. (eds.) *The Boltzmann Equation: Theory and Applications*, 53–106 (Springer Vienna, 1973).

[9] Reid, J. C., Brookes, S. J., Evans, D. J. & Searles, D. J. The Dissipation Function: Its Relationship to Entropy Production, Theorems for Nonequilibrium Systems and Observations on Its Extrema. In Dewar, R. C., Lineweaver, C. H., Niven, R. K. & Regenauer-Lieb, K. (eds.) *Beyond the Second Law*, 31–47 (Springer Berlin Heidelberg, Heidelberg, 2014).

[10] Sevick, E. M., Prabhakar, R., Williams, S. R. & Searles, D. J. Fluctuation Theorems. *Annual Review of Physical Chemistry* **59**, 603–33 (2008).

[11] Evans, D. J. & Searles, D. J. Equilibrium microstates which generate second law violating steady states. *Physical Review E* **50**, 1645 (1994).

[12] Searles, D. J. & Evans, D. J. Fluctuations Relations for Nonequilibrium Systems. *Australian Journal of Chemistry* **57**, 1119–1123 (2004).

[13] Searles, D. J. & Evans, D. J. The fluctuation theorem and Green-Kubo relations. *The Journal of Chemical Physics* **112**, 9727 (2000).

[14] Mittag, E. & Evans, D. J. Time-dependent fluctuation theorem. *Physical Review E* **67**, 026113 (2003).

[15] Wang, G. M., Sevick, E. M., Mittag, E., Searles, D. J. & Evans, D. J. Experimental Demonstration of Violations of the Second Law of Thermodynamics for Small Systems and Short Time Scales. *Physical Review Letters* **89**, 050601 (2002).

[16] Carberry, D. M., Baker, M. A. B., Wang, G. M., Sevick, E. M. & Evans, D. J. An optical trap experiment to demonstrate fluctuation theorems in viscoelastic media. *Journal of Optics A: Pure and Applied Optics* **9**, S204–S214 (2007).

[17] Evans, D. J., Searles, D. J. & Williams, S. R. On the fluctuation theorem for the dissipation function and its connection with response theory. *The Journal of Chemical Physics* **128**, 014504 (2008).

[18] Evans, D. J., Searles, D. J. & Williams, S. R. Erratum: "On the fluctuation theorem for the dissipation function and its connection with response theory" [J. Chem. Phys. 128, 014504 (2008)]. *The Journal of Chemical Physics* **128**, 249901 (2008).

[19] Evans, D. J., Searles, D. J. & Williams, S. R. Dissipation and the relaxation to equilibrium. *Journal of Statistical Mechanics: Theory and Experiment* **2009**, P07029 (2009).

[20] Evans, D. J., Searles, D. J. & Williams, S. R. A Simple Mathematical Proof of Boltzmann's Equal a priori Probability Hypothesis. In Chmelik, C., Kanellopoulos, N., Karger, N. & Doros, T. (eds.) *Diffusion Fundamentals III* (Leipziger Universitatsverlag, Leipzig, 2009).

[21] Carberry, D. M., Williams, S. R., Wang, G. M., Sevick, E. M. & Evans, D. J. The Kawasaki identity and the Fluctuation Theorem. *The Journal of chemical physics* **121**, 8179 (2004).

[22] Gibbs, J. W. *Elementary Principles in Statistical Mechanics* (Dover Publications, Inc., New York, 1960).

[23] Boltzmann, L. Weitere Studien über das Wärmegleichgewicht unter Gasmolekülen. *Sitzungsberichte der mathematisch-naturwissenschlaftlichen Classe der kaiserlichen Akademic der Wissenschaften Wien* **66**, 275–370 (1872).

[24] Feynman, R. P. *Statistical Mechanics: A Set Of Lectures* (W. A. Denjamin, Inc., Reading, Massachusetts, 1972).

[25] Landau, L. D. & Lifshitz, E. M. *Statistical Physics* (Pergamon Press Ltd., Oxford, 1969), second edn.

[26] Szász, D. Boltzmann's Ergodic Hypothesis, a Conjecture for Centuries? In Szasz, D. (ed.) *Hard Ball Systems and the Lorentz Gas*, chap. Appendix, 421–446 (Springer Berlin Heidelberg, Berlin, 2000).

[27] Evans, D. J. & Morriss, G. P. *Statistical Mechanics of Nonequilibrium Liquids* (Academic Press, London, 1990), 1st edn.

[28] Williams, S. R., Searles, D. J. & Evans, D. J. Independence of the transient fluctuation theorem to thermostatting details. *Physical Review E* **70**, 066113 (2004).

[29] Brown, D. & Clarke, J. H. R. Constant-stress nonequilibrium molecular dynamics: Shearing of the soft-sphere crystal and fluid. *Physical Review A* **34**, 2093 (1986).

[30] Evans, D. J. & Morriss, G. P. Isothermal-isobaric molecular dynamics. *Chemical Physics* **77**, 63–66 (1983).

[31] Evans, D. J. & Morriss, G. P. Nonlinear-response theory for steady planar Couette flow. *Physical Review A* **30**, 1528 (1984).

[32] Evans, D. J. & Searles, D. J. Steady states, invarient meaures, and resposne theory. *Physical Review E* **52**, 5839 (1995).

[33] Mittag, E., Evans, D. J. & Williams, S. R. Verification of time-reversibility requirement for systems satisfying the Evans-Searles fluctuation theorem. *Pure and Applied Chemistry* **79**, 1361–1368 (2007).

[34] Searles, D. J., Johnston, B. M., Evans, D. J. & Rondoni, L. Time reversibility, Correlation Decay and the Steady State Fluctuation Relation for Dissipation. *Entropy* **15**, 1503–1515 (2013).

[35] Searles, D. J. & Evans, D. J. Ensemble dependence of the transient fluctuation theorem. *The Journal of Chemical Physics* **113**, 3503 (2000).

[36] Evans, D. J., Searles, D. J. & Mittag, E. Fluctuation theorem for Hamiltonian Systems: Le Chatelier's principle. *Physical Review E* **63**, 051105 (2001).

[37] Reid, J. C. *et al.* Reversibility in nonequilibrium trajectories of an optically trapped particle. *Physical Review E* **70**, 016111 (2004).

[38] Reid, J. C., Evans, D. J. & Searles, D. J. Communication: Beyond Boltzmann's H-theorem: demonstration of the relaxation theorem for a non-monotonic approach to equilibrium. *The Journal of Chemical Physics* **136**, 021101 (2012).

[39] Ayton, G., Evans, D. J. & Searles, D. J. A local fluctuation theorem. *The Journal of Chemical Physics* **115**, 2033 (2001).

[40] Wang, G. M. *et al.* Experimental study of the fluctuation theorem in a nonequilibrium steady state. *Physical Review E* **71**, 046142 (2005).

[41] Wang, G. M., Carberry, D. M., Reid, J. C., Sevick, E. M. & Evans, D. J. Demonstration of the steady-state fluctuation theorem from a single trajectory. *Journal of Physics: Condensed Matter* **17**, S3239–S3244 (2005).

[42] Garnier, N. & Ciliberto, S. Nonequilibrium fluctuations in a resistor. *Physical Review E* **71**, 060101 (2005).

[43] Carberry, D. M. *et al.* Fluctuations and Irreversibility: An Experimental Demonstration of a Second-Law-Like Theorem Using a Colloidal Particle Held in an Optical Trap. *Physical Review Letters* **92**, 140601 (2004).

[44] Reid, J. C., Cunning, B. V. & Searles, D. J. Different approaches for evaluating exponentially weighted nonequilibrium relations. *Journal of Chemical Physics* **133**, 154108 (2010).

[45] Chong, S.-H., Otsuki, M. & Hayakawa, H. Generalized Green-Kubo relation and integral fluctuation theorem for driven dissipative systems without microscopic time reversibility. *Physical Review E* **81**, 041130 (2010).

[46] Liu, F., Luo, Y.-P., Huang, M.-C. & Ou-Yang, Z.-c. A generalized integral fluctuation theorem for general jump processes. *Journal of Physics A: Mathematical and Theoretical* **42**, 332003 (2009).

[47] Seifert, U. Stochastic thermodynamics, fluctuation theorems and molecular machines. *Reports on Progress in Physics* **75**, 126001 (2012).

[48] Speck, T. & Seifert, U. Integral fluctuation theorem for the housekeeping heat. *Journal of Physics A: Mathematical and General* **38**, L581–L588 (2005).

[49] Seifert, U. Entropy Production along a Stochastic Trajectory and an Integral Fluctuation Theorem. *Physical Review Letters* **95**, 040602 (2005).

[50] Seifert, U. Fluctuation theorem for birth-death or chemical master equations with time-dependent rates. *Journal of Physics A: Mathematical and General* **37**, L517–L521 (2004).

[51] Liphardt, J., Dumont, S., Smith, S. B., Tinoco Jr., I. & Bustamante, C. Equilibrium Information from Nonequilibrium Measurements in an Experimental Test of Jarzynski's Equality. *Science* **296**, 1832 (2002).

[52] Douarche, F., Ciliberto, S., Petrosyan, A. & Rabbiosi, I. An experimental test of the Jarzynski equality in a mechanical experiment. *Europhysics Letters* **70**, 593–599 (2005).

[53] Bena, I., Van den Broeck, C. & Kawai, R. Jarzynski equality for the Jepsen gas. *Europhysics Letters* **71**, 879–885 (2005).

[54] Jayannavar, A. M. & Sahoo, M. Charged particle in a magnetic field: Jarzynski equality. *Physical Review E* **75**, 032102 (2007).

[55] West, D. K., Olmsted, P. D. & Paci, E. Free energy for protein folding from nonequilibrium simulations using the Jarzynski equality. *Journal of Chemical Physics* **125**, 204910 (2006).

[56] Jarzynski, C. Nonequilibrium work relations: foundations and applications. *The European Physical Journal B* **64**, 331–340 (2008).

[57] Gore, J., Ritort, F. & Bustamante, C. Bias and error in estimates of equilibrium free-energy differences from nonequilibrium measurements. *PNAS* **100**, 12564–12569 (2003).

[58] Williams, S. R. & Evans, D. J. The rheology of solid glass. *Journal of Chemical Physics* **132**, 184105 (2010).

[59] Evans, D. J., Williams, S. R. & Rondoni, L. A mathematical proof of the zeroth "law" of thermodynamics and the nonlinear Fourier "law" for heat flow. *The Journal of Chemical Physics* **137**, 194109 (2012).

[60] Ayton, G. & Evans, D. J. On the Asymptotic Convergence of the Transient and Steady-State Fluctuation Theorems. *Journal of Statistical Physics* **97**, 811 (1999).

[61] Evans, D. J., Cohen, E. G. D. & Morriss, G. P. Probability of Second Law Violations in Shearing Steady States. *Physical Review Letters* **71**, 2401 (1993).

[62] Evans, D. J., Cohen, E. G. D. & Morriss, G. P. Errata: Probability of Second Law Violations in Shearing Steady States. *Physical Review Letters* **71**, 3616 (1993).

[63] Searles, D. J., Rondoni, L. & Evans, D. J. The Steady State Fluctuation Relation for the Dissipation Function. *Journal of Statistical Physics* **128**, 1337–1363 (2007).

[64] Marconi, U. M. B., Puglisi, A., Rondoni, L. & Vulpiani, A. Fluctuation-dissipation: Response theory in statistical physics. *Physics Reports* **461**, 111–195 (2008).

[65] Williams, S. R., Searles, D. J. & Evans, D. J. Numerical study of the steady state fluctuation relations far from equilibrium. *The Journal of Chemical Physics* **124**, 194102 (2006).

[66] Searles, D. J. & Evans, D. J. Fluctuation theorem for stochastic systems. *Physical Review E* **60**, 159 (1999).

[67] Kubo, R. Statistical-Mechanical Theory of Irreversible Processes. I. General Theory and Simple Applications to Magnetic and Conduction Problems. *Journal of the Physical Society of Japan* **12**, 570 (1957).

[68] Green, M. S. Markoff Random Processes and the Statistical Mechanics of Time-Dependent Phenomena. II. Irreversible Processes in Fluids. *Journal of Chemical Physics* **22**, 398 (1954).

[69] Dorfman, J. R. *An Introduction to Chaos in Nonequilibrium Statistical Mechanics.* Cambridge Lecture Notes in Physics (Cambridge University Press, 1999).

[70] Evans, D. J., Searles, D. J. & Williams, S. R. The covariant dissipation function for transient nonequilibrium states. *The Journal of Chemical Physics* **133**, 054507 (2010).

[71] Crooks, G. E. Nonequilibrium Measurements of Free Energy Differences for Microscopically Reversible Markovian Systems. *Journal of Statistical Physics* **90**, 1481 (1998).

[72] Crooks, G. E. Entropy production fluctuation theorem and the nonequilibrium work relation for free energy differences. *Physical Review E* **60**, 2721 (1999).

[73] Jarzynski, C. Equilibrium free-energy differences from nonequilibrium measurements: A master-equation approach. *Physical Review E* **56**, 5018 (1997).

[74] Jarzynski, C. Nonequilibrium Equality for Free Energy Differences. *Physical Review Letters* **78**, 2690 (1997).

[75] Collin, D. *et al.* Verification of the Crooks fluctuation theorem and recovery of RNA folding free energies. *Nature* **437**, 231 (2005).

[76] Crooks, G. E. Path-ensemble averages in systems driven far from equilibrium. *Physical Review E* **61**, 2361–2366 (2000).

[77] Kurchan, J. Fluctuation theorem for stochastic dynamics. *Journal of Physics A: Mathematical and General* **31**, 3719 (1998).

[78] Sekimoto, K. Kinetic Characterization of Heat Bath and the Energetics of Thermal Ratchet Models. *Journal of Physical Society of Japan* **66**, 1234–1237 (1997).

[79] Ritort, F. Nonequilibrium fluctuations in small systems: From physics to biology. *Advances in chemical physics* **137**, 31 (2008).

[80] Seifert, U. Stochastic thermodynamics : principles and perspectives. *The European Physical Journal B* **64**, 423–431 (2008).

[81] Bustamante, C. *et al.* The Nonequilibrium Thermodynamics of Small Systems. *Physics Today* **58**, 43 (2005).

[82] Saha, A. & Jayannavar, A. M. Nonequilibrium work distributions for a trapped Brownian particle in a time-dependent magnetic field. *Physical Review E* **77**, 022105 (2008).

[83] Jiménez-Aquino, J. I., Velasco, R. M. & Uribe, F. J. Fluctuation relations for a classical harmonic oscillator in an electromagnetic field. *Physical Review E* **79**, 061109 (2009).

[84] Blickle, V., Speck, T., Helden, L., Seifert, U. & Bechinger, C. Thermodynamics of a Colloidal Particle in a Time-Dependent Nonharmonic Potential. *Physical Review Letters* **96**, 070603 (2006).

[85] Falcón, C. & Falcon, E. Fluctuations of energy flux in a simple dissipative out-of-equilibrium system. *Physical Review E* **79**, 041110 (2009).

[86] Bonaldi, M. *et al.* Nonequilibrium Steady-State Fluctuations in Actively Cooled Resonators. *Physical Review Letters* **103**, 010601 (2009).

[87] Weeks, J. D., Chandler, D. & Andersen, H. C. Role of repulsive forces in determining the equilibrium structure of simple liquids. *The Journal of Chemical Physics* **54**, 5237 (1971).

[88] Rapaport, D. C. *The Art of Molecular Dynamics Simulation* (Cambridge University Press, Cambridge, UK, 2004), second edn.

[89] Allen, M. P. & Tildesley, D. J. (eds.) *Computer Simulation in Chemical Physics* (Klewer Academic Publishers, Dordrecht, Netherlands, 1993).

[90] Jones, J. E. On the Determination of Molecular Fields.-II. From the Equation of State of a Gas. *Proceedings of the Royal Society A* **106**, 463 (1924).

[91] Jones, J. E. Cohesion. *The Proceedings of the Physical Society* **43**, 461 (1931).

[92] Axilrod, B. M. & Teller, E. Interaction of the van der Waals Type Between Three Atoms. *Journal of Chemical Physics* **11**, 299 (1943).

[93] Axilrod, B. M. The Triple-Dipole Interaction between Atoms and Cohesion in Crystals of the Rare Gases. *Journal of Chemical Physics* **17**, 1349 (1949).

[94] Barker, J. A. & Henderson, D. Theories of Liquids. *Annual Review of Physical Chemistry* **23**, 439–484 (1972).

[95] Guggenheim, E. A. & McGlashan, M. L. Interaction between argon atoms. *Proceedings of the Royal Society of London. A* **255**, 456–476 (1960).

[96] Mcglashan, M. L. Effective Pair Interaction Energy in Crystalline. *Discussions of the Faraday Society* **40**, 59–68 (1965).

[97] Barker, J. A., Fisher, R. A. & Watts, R. O. Liquid argon: Monte Carlo and molecular dynamics calculations. *Molecular Physics* **21**, 657–673 (1971).

[98] Hoover, W. G. *Computational Statistical Mechanics* (Elsevier, Amsterdam, 1991).

[99] Baranyai, A. & Evans, D. J. New algorithm for constrained molecular-dynamics simulation of liquid benzene and naphthalene. *Molecular Physics* **70**, 53–63 (1990).

[100] Zhang, F., Searles, D. J., Evans, D. J., den Toom Hansen, J. S. & Isbister, D. J. Kinetic energy conserving integrators for Gaussian thermostatted SLLOD. *Journal of Chemical Physics* **111**, 18 (1999).

[101] Frenkel, D. & Smit, B. *Understanding Molecular Simulation: From Algorithms to Applications* (Academic Press, Amsterdam, 2001), second edn.

[102] Lees, A. W. & Edwards, S. F. The computer study of transport processes under extreme conditions. *Journal of Physics C: Solid State Physics* **5**, 1921 (1972).

[103] Petravic, J. Influence of strain on transport in dense Lennard-Jones systems. *Journal of Chemical Physics* **120**, 7041 (2004).

[104] Bernardi, S., Brookes, S. J. & Searles, D. J. System size effects on calculation of the viscosity of extended molecules. *Chemical Engineering Science* **121**, 236–244 (2015).

[105] Petravic, J. & Evans, D. J. Approach to the non-equilibrium time-periodic state in a 'steady' shear flow model. *Molecular Physics* **95**, 219–231 (1998).

[106] Petravic, J. & Evans, D. J. Nonlinear Response for Time-Dependent External Fields: Shear Flow and Color Conductivity. *International Journal of Thermophysics* **19**, 1049 (1998).

[107] Metropolis, N., Rosenbluth, A. W., Rosenbluth, M. N., Teller, A. H. & Teller, E. Equation of State Calculations by Fast Computing Machines. *Journal of Chemical Physics* **21**, 1087 (1953).

[108] Mountain, R. D. & Thirumalai, D. Quantative measure of efficiency of Monte Carlo simulations. *Physica A: Statistical Mechanics and its Applications* **210**, 453–460 (1994).

[109] Sundararajan, D. *The Discrete Fourier Transform: theory, algorithms and applications* (World Scientific, Singapore, 2001).

[110] Dalton, B. A., Glavatskiy, K. S., Daivis, P. J., Todd, B. D. & Snook, I. K. Linear and nonlinear density response functions for a simple atomic fluid. *Journal of Chemical Physics* **139**, 044510 (2013).

[111] Weisberg, S. *Applied Linear Regression* (John Wiley & Sons, Inc, Hoboken, New Jersey, 2014), fourth edn.

[112] Crank, J. *The Mathematics of Diffusion.* Oxford science publications (Clarendon Press, 1979).

[113] van Zon, R. & Cohen, E. G. D. Extended heat-fluctuation theorems for a system with deterministic and stochastic forces. *Physical Review E* **69**, 056121 (2004).

[114] Mittag, E., Searles, D. J. & Evans, D. J. Isobaric-isothermal fluctuation theorem. *The Journal of Chemical Physics* **116**, 6875 (2002).

[115] Wang, G. M. & Sevick, E. M. Optical Tweezers manipulation of colloids and biopolymers: non-equilibrium processes. *NanoScience+ Engineering. International Society for Optics and Photonics* 70380L (2008).

[116] Feitosa, K. & Menon, N. Fluidized Granular Medium as an Instance of the Fluctuation Theorem. *Physical Review Letters* **92**, 164301 (2004).

[117] Evans, D. J., Searles, D. J. & Rondoni, L. Application of the Gallavotti-Cohen fluctuation relation to thermostated steady states near equilibrium. *Physical Review E* **71**, 056120 (2005).

[118] Gallavotti, G. & Cohen, E. G. D. Dynamical Ensembles in Nonequilibrium Statistical Mechanics. *Physical Review Letters* **74**, 2694 (1995).

[119] Gallavotti, G. & Cohen, E. G. D. Dynamical Ensembles in Stationary States. *Journal of Statistical Physics* **80**, 931 (1995).

[120] Gallavotti, G. Reversible Anosov diffeomorphisms and large deviations. *Mathematical Physics Electronic Journal* **1**, 1 (1995).

[121] Gallavotti, G. Dynamical ensembles equivalence in fluid mechanics. *Physica D: Nonlinear Phenomena* **105**, 163–184 (1997).

[122] Gallavotti, G. A local fluctuation theorem. *Physica A: Statistical Mechanics and its Applications* **263**, 39–50 (1999).

[123] Gallavotti, G., Rondoni, L. & Segre, E. Lyapunov spectra and nonequilibrium ensembles equivalence in 2D fluid mechanics. *Physica D: Nonlinear Phenomena* **187**, 338–357 (2004).

[124] Lebowitz, J. L. & Spohn, H. A Gallavotti-Cohen-Type Symmetry in the Large Deviation Functional for Stochastic Dynamics. *Journal of Statistical Physics* **95**, 333 (1999).

[125] Maes, C. The Fluctuation Theorem as a Gibbs property. *Journal of Statistical Physics* **95**, 367 (1999).

[126] Rondoni, L., Tél, T. & Vollmer, J. Fluctuation theorems for entropy prduction in open systems. *Physical Review E* **61**, 4679 (2000).

[127] van Zon, R. & Cohen, E. G. D. Extension of the Fluctuation Theorem. *Physical Review Letters* **91**, 110601 (2003).

[128] Hoover, W., Kum, O. & Posch, H. Time-reversible dissipative ergodic maps. *Physical Review E* **53**, 2123 (1996).

[129] Daivis, P. J. & Todd, B. D. A simple, direct derivation and proof of the validity of the SLLOD equations of motion for generalized homogeneous flows. *The Journal of Chemical Physics* **124**, 194103 (2006).

[130] Rondoni, L. & Segre, E. Fluctuations in two-dimensional reversibly damped turbulence. *Nonlinearity* **12**, 1471–1487 (1999).

[131] Ciliberto, S. & Laroche, C. An experimental test of the Gallavotti-Cohen fluctuation theorem. *Le Journal de Physique IV* **8**, 215 (1998).

[132] Petersen, C. F., Evans, D. J. & Williams, S. R. The instantaneous fluctuation theorem. *The Journal of Chemical Physics* **139**, 184106 (2013).

[133] Hoover, W. G. & Moran, B. Phase-space singularities in atomistic planar diffusive flow. *Physical Review A* **40**, 5319 (1989).

[134] Morriss, G. P. Phase-space singularities in planar Couette flow. *Physical Review A* **39**, 4811 (1989).